A HIGH ORDER METHOD FOR ANALYZING THE ELECTROMAGNETIC RESPONSE OF AN ARRAY OF THIN WIRES

QUN XING XUE

A THESIS SUBMITTED TO THE FACULTY OF GRADUATE STUDIES
IN PARTIAL FULFILMENT OF THE REQUIREMENTS
FOR THE DEGREE OF

MASTER OF SCIENCE

GRADUATE PROGRAM IN DEPARTMENT OF MATHEMATICS AND STATISTICS
YORK UNIVERSITY
TORONTO, ONTARIO
MAY 2019

Abstract

The problem of evaluating the electromagnetic response of wire-antenna systems by means of integral equations is one of great importance and significant mathematical complexity. The literature on this subject is extensive, including contributions from the 19th century work of Pocklington [8], the classic works of King [9], to some of the most recent work by Davies *et. al.* [10], Bruno and Haslam [11] and others [12], [13]. In this thesis, we develop a new high order numerical method to treat the problem corresponding to a parallel array of thin straight wires. A number of significant difficulties arise in this problem as a result of certain singularities and near-singularities that are inherent in its integral equation formulation. In particular, no satisfactory quadrature methods exist for the high-order evaluation of the integrals which arise from the thin wire equations when two wires in an array are separated by a small distance but finite distance. Such a configuration requires the evaluation of integrals whose integrands are logarithmically singular not only at a point inside the domain of integration, but also at a point just outside of the domain integration. The quadrature formulas we derive as a main contribution of this thesis explicitly treat both of these cases. A full numerical implementation of our algorithm was developed and results corresponding to high, moderate and low excitation frequencies are presented.

Table of Contents

List of Tables

List of Figures

1 Introduction

The problem of evaluating the electromagnetic response of a thin straight wire by means of integral equations is one of great importance and significant mathematical complexity. The literature on this subject is extensive, starting with the 19th century work of Pocklington [8]. There was a significant amount of activity in studying the theoretical problem in the mid 20th century. While the number of contributions is vast given the fundamental nature of the problem, many of the main results are summarized in the classic book of King [9]. Many other notable papers appeared mid century, including the contributions of Hallén [16], Mei [15] and Wu [12] which proposed early numerical schemes to handle the problem. Excellent surveys of late 20th century work in developing computational algorithms to treat the problem can be found in the articles [31] and [24], as well as the modern reference text by Balanis [13]. More recently there has been interest in developing high order algorithms to treat the problem, including the works by Davies *et. al.* [10], Champagne *et. al.* [32] and Bruno and Haslam [11].

The goal of this thesis is to extend the theoretical approaches in these previous works (and in particular the contribution [11]) and develop an efficient high order solver for an array of parallel straight wires. To accomplish this goal, we produce a new high order computational approach to the problem which requires specialized numerical quadrature techniques. The new quadrature formulas required for our solver are of significant mathematical complexity, and are derived from first principles in this thesis as one of its main contributions. In what follows, we will attempt to outline in broad terms the main mathematical problems that arise in developing efficient numerical algorithms to treat this problem.

1.1 Mathematical Challenges

While we carefully develop the mathematical model for the problem of scattering from thin straight wires in later chapters, it is useful to detail here in broad terms the main challenges a numerical implementation of such a model will face. In the early work [8], Pocklington presented the first mathematical description for the surface fields on a thin straight wire of radius a lying on the interval $z \in [-1, 1]$ excited by an external time-harmonic electromagnetic field with wave number k. The Pocklington integro-differential equation governing the current excited on the surface of the wire has the form

$$\left(\frac{\partial^2}{\partial z^2} + k^2\right) \int_{-1}^{1} G(z - z')\phi(z')\, dz' = \eta(z) \qquad z \in [-1, 1], \tag{1.1}$$

where $\phi(z)$ is the unknown density to be found and $\eta(z)$ is a known external field. The so-called exact kernel of the integro-differential equation (1.1) represented by $G(z)$ given by

$$G(z) = \frac{1}{\pi} \int_0^{\pi} \frac{\mathrm{e}^{ik\sqrt{z^2+4a^2\sin^2\psi}}}{\sqrt{z^2 + 4a^2 \sin^2\psi}}\, d\psi, \tag{1.2}$$

Another kernel for the Pocklington integro-differential equation which results from use of approximations additional to those implicit in equation (1.1) is the so-called reduced kernel

$$G_{red}(z) = \frac{\mathrm{e}^{ik\sqrt{z^2+a^2}}}{\sqrt{z^2 + a^2}}. \tag{1.3}$$

While this form of the kernel has been used extensively in the engineering literature (see for example the classic reference [9]) some difficulties may arise in this case, especially when a delta source is present on the wire. Indeed, as pointed out in [33] solutions to the problem with a delta driving source formally do not exist when the reduced kernel is used in place of the exact kernel. In order to produce stable algorithms that converge to high order accuracy, we therefore confine our attention to the so-called exact kernel in this work.

It has been known for some time that the kernel (1.2) has the form

$$G(z) = -\frac{1}{a\pi} \ln|z| + G_1(z), \tag{1.4}$$

where the function $G_1(z)$ is continuous, it has a bounded derivative and an unbounded second derivative; see [17, p.115], [34]. The logarithmic behavior of the function $G(z)$ can be easily grasped by consideration of the expression

$$G(z) = \frac{2}{\pi\sqrt{z^2+4a^2}}\,K\!\left(\frac{2a}{\sqrt{z^2+4a^2}}\right) - \frac{1}{\pi}\int_0^{\pi} \frac{1-\mathrm{e}^{ik\sqrt{z^2+4a^2\sin^2\psi}}}{\sqrt{z^2+4a^2\sin^2\psi}}\,d\psi, \tag{1.5}$$

where K, the complete elliptic integral of the first kind [35], contains the leading-order singularity. Equations (1.4) and (1.5) have been used as the basis for many numerical solvers for the Pocklington problem [10, 36]. Numerical integration schemes for integrands containing such singularities which, based on polynomial interpolation, do not explicitly account for the singularity of the second derivative of the integrand, typically exhibit low-order convergence. Indeed, the leading singular term in $G_1(z)$ is of the form $z^2\ln|z|$ [36]. Due to the unbounded second derivative, a typical integration scheme applied to this problem will have an error limited to order $\mathcal{O}(h^3)$ where h is the integration step size.

A full understanding of the singular nature of the straight wire kernel leading to high order integration algorithms for the straight wire problem was finally presented in the more recent article [11]. In that paper, the authors showed that the kernel could be decomposed as

$$G(z) = F_1(z)\ln|z| + F_2(z) \tag{1.6}$$

where $F_1(z)$ and $F_2(z)$ are analytic on the real line. Integrators to explicitly treat the logarithmic singularity to high order were also developed in [11] for the single straight wire. The resulting quadrature formulas presented were mathematically correct, but a direct implementation of those formulas is ill-conditioned due to large subtractive cancelations that arise in their evaluation. The authors dealt with this problem by pre-computing tables of values using symbolic software, storing them to file to be read in for each execution of their code.

In addition to singularities that arise in the kernel, another mathematical issue that arises in the design of a numerical solver for the straight wire problem is the singular nature of the solution itself. It has been known since the work of Jones [17] and Rynne [34] that solutions to the Pocklington integro-differential equation (1.1) have the form $\phi(z) = I(z)/\sqrt{1-z^2}$; i.e., the solution contains square-root end-point singularities. The

papers [34] and [11] relate the regularity of the unknown function $I(z)$ to the known data $\eta(z)$. In particular, in [11] it is shown that if $\eta(z)$ is infinitely differentiable, then the function $I(z)$ is infinitely differentiable as well. A carefully-designed high-order solver must therefore explicitly account for these end-point singularities as part of the integrators.

1.2 Outline of the Thesis

The remainder of this thesis is organized as follows. In Chapter 2 we review the basic formulation of electromagnetic problems via Maxwell's equations and the conditions that need to be applied at any material boundary. We then introduce the time harmonic version of the equations and use these to derive the classic integral formulations used in the study of radiation and scattering problems, and in particular the electric field integral equation.

In Chapter 3 we show how the electric field integral equation can be further reduced to obtain thin wire equations. We then specialize these thin wire equations to parallel arrays of straight wires. A numerical high order numerical implementation for the problem using a collocation method is then designed around the straight wire equations.

In Chapter 4 localized integrators for the wire array problem are designed. While these integrators are based on a similar domain decomposition to that presented in [11], results are extended to not only account for logarithmic singularity that arises in a single straight wire problem, but they also account for a near singularity that arises when two wires in the array are spaced at small distances. As one of the main contributions of this thesis, new numerical quadrature formulas that are useful in treating both the singularities and near singularities are derived. In contrast to the formulas presented in [11] which are unstable in floating point arithmetic, our new formulas can be used to easily generate integration weights to full accuracy, thus eliminating the need for stored tables.

In Chapter 5 we provide several examples detailing the performance of our numerical implementation for cases of high, moderate and low frequencies. Finally in Chapter 6 we summarize our results are propose how this work can be extended in future directions.

2 Maxwell's Equations and Integral Formulations

The purpose of this chapter is connect the framework exploited in the description of electromagnetic scattering from bodies, to basic electromagnetic theory through Maxwell's equations. We present a general description of electromagnetic phenomena inside material media, and later specialize to perfect conductors, and a time-harmonic dependence in the fields. This of course represents a summary of well-understood material which we include for completeness. For more information and detail, the reader is referred to the classic works of Jackson [2], Stratton [3], and many others [25],[4],[7].

2.1 Field Equations and Boundary Conditions

The macroscopic Maxwell equations in the Gaussian system of units take the form [1][2]

$$\nabla \times \mathbf{E}(\mathbf{r},t) + \frac{1}{c}\frac{\partial}{\partial t}\mathbf{B}(\mathbf{r},t) = \mathbf{0} \tag{2.1}$$

and

$$\nabla \times \mathbf{H}(\mathbf{r},t) - \frac{1}{c}\frac{\partial}{\partial t}\mathbf{D}(\mathbf{r},t) = \frac{4\pi}{c}\mathbf{J}(\mathbf{r},t)\,, \tag{2.2}$$

where $\mathbf{r}$ is a 3-dimensional position vector and t is time. We denote $\mathbf{E}$ as the electric field intensity, $\mathbf{H}$ as the magnetic field intensity, $\mathbf{D}$ as the electric displacement field, $\mathbf{B}$ as the magnetic induction field, and $\mathbf{J}$ as the electric current density. The speed of light in a vacuum is $c \simeq 2.998 \times 10^8$ m/s. Equation (2.1) is Faraday's law for the induction of an electric field by a time-varying magnetic flux. Equation (2.2) is Ampere's law for the magnetic field resulting from a distribution of current. Continuity of the magnetic induction and electric displacement fields give, respectively

$$\nabla \cdot \mathbf{B}(\mathbf{r},t) = 0 \tag{2.3}$$

and

$$\nabla \cdot \mathbf{D}(\mathbf{r}, t) = 4\pi\rho(\mathbf{r}, t)\,, \tag{2.4}$$

where ρ is the electric charge density. Conservation of charge/current may be expressed as

$$\frac{\partial}{\partial t}\rho(\mathbf{r}, t) + \nabla \cdot \mathbf{J}(\mathbf{r}, t) = 0, \tag{2.5}$$

which follows simply from taking the divergence of (2.2) and using the continuity equation (2.4).

If $\hat{\mathbf{n}}$ is a unit normal vector to an interface between two distinct regions of space, then the jump conditions for the electromagnetic fields across the surface are

$$\hat{\mathbf{n}}(\mathbf{r}) \cdot \mathcal{J}\{\mathbf{B}(\mathbf{r}, t)\} = 0 \qquad \hat{\mathbf{n}}(\mathbf{r}) \times \mathcal{J}\{\mathbf{H}(\mathbf{r}, t)\} = \frac{4\pi}{c}\mathbf{K}(\mathbf{r}, t) \tag{2.6}$$

and

$$\hat{\mathbf{n}}(\mathbf{r}) \cdot \mathcal{J}\{\mathbf{D}(\mathbf{r}, t)\} = 4\pi\sigma(\mathbf{r}, t) \qquad \hat{\mathbf{n}}(\mathbf{r}) \times \mathcal{J}\{\mathbf{E}(\mathbf{r}, t)\} = \mathbf{0} \tag{2.7}$$

where $\mathbf{K}$ is the surface current, and σ is the surface charge density. Both $\mathbf{K}$ and σ are nonzero only for a perfect conductor. The relations are used for matching across boundaries to connect solutions in different regions of space Here $\mathcal{J}\{\cdot\}$ represents the jump in the enclosed quantity across the surface with outward unit normal vector $\hat{\mathbf{n}}$. In particular, if we consider the a scattering body occupying region $\mathcal{V}_1$ which lies inside the larger region $\mathcal{V}_0$ then the jump in some vector field $\mathbf{A} = \mathbf{A}(\mathbf{r}, t)$ is

$$\mathcal{J}\{\mathbf{A}\} = \mathbf{A}_0 - \mathbf{A}_1, \tag{2.8}$$

where the unit normal vector points into the region $\mathcal{V}_0$, i.e. that which contains the vector field $\mathbf{A}_0$.

2.2 Constitutive Relations

We now discuss the constitutive relations, which are used to describe the electromagnetic fields in the presence of matter. From equations (2.1) through (2.4), we may eliminate the electric displacement field and the magnetic induction field with the help of the following universal definitions:

$$\mathbf{D}(\mathbf{r}, t) = \mathbf{E}(\mathbf{r}, t) + 4\pi\mathbf{P}(\mathbf{r}, t) \tag{2.9}$$

and

$$\mathbf{H}(\mathbf{r},t) = \mathbf{B}(\mathbf{r},t) - 4\pi\mathbf{M}(\mathbf{r},t)\,. \tag{2.10}$$

Here $\mathbf{P}$ and $\mathbf{M}$ are the electric and magnetic polarization fields respectively. We relate the electric polarization field to the electric field strength through the constitutive relation. The constitutive relation corresponding to a linear, homogeneous, isotropic dielectric is

$$\mathbf{P}(\mathbf{r},t) = \chi^E\ \mathbf{E}(\mathbf{r},t) \tag{2.11}$$

where χ^E is an *empirical* constant determined by the electrical properties of the medium. We therefore may rewrite the electric displacement field as

$$\mathbf{D}(\mathbf{r},t) = \left(1 + 4\pi\chi^E\right)\mathbf{E}(\mathbf{r},t) = \varepsilon'\mathbf{E}(\mathbf{r},t)\,, \tag{2.12}$$

where the real constant ε' is known as the electric permittivity. In free space (for the Gaussian system of units) $\chi^E = 0$ and hence $\varepsilon' = 1$. Thus, in this case the displacement current is linearly related to the electric field intensity. While this simple case is very widely applicable, there are other interesting cases where the relationship may be nonlinear, for example in long fibre optic lines. For a conducting medium, we write the electric current density as

$$\mathbf{J}(\mathbf{r},t) = \kappa\mathbf{E}(\mathbf{r},t)\,, \tag{2.13}$$

where the real number κ is the electrical conductivity of the medium. Finally, for a non-magnetic medium (most media of practical interest are non-magnetic), we have

$$\mathbf{M}(\mathbf{r},t) = \mathbf{0}. \tag{2.14}$$

2.3 Time-Harmonic Equations

It is customary to assume an harmonic time dependence in the field quantities, which is equivalent to expressing them as Fourier integrals in frequency space, i.e.,

$$\mathbf{f}(\mathbf{r},t) = \int_{-\infty}^{-\infty} \mathbf{F}(\mathbf{r},\omega)\,\mathrm{e}^{-i\omega t}d\omega \tag{2.15}$$

where $\mathbf{f}$ and $\mathbf{F}$ are a Fourier transform pair of one of the field quantities. The complex field vectors are convenient representations of the real field vectors. To recover the real space-time-dependent field vector, we simply use,

$$\mathbf{E}(\mathbf{r},t) = \mathrm{Real}\big\{\mathbf{E}(\mathbf{r})\,\mathrm{e}^{-i\omega t}\big\} = \frac{1}{2}\left[\mathbf{E}(\mathbf{r})\,\mathrm{e}^{-i\omega t} + \mathbf{E}^{*}(\mathbf{r})\,\mathrm{e}^{i\omega t}\right] \tag{2.16}$$

Note that we make no attempt through our notation to distinguish between the real field vectors and the complex field vectors in the frequency domain. While their meaning should be clear from the context, the complex vectors are expressed as a function of space only, and the real vectors are expressed as both a function of space and time.

With the time dependence $\exp(-i\omega t)$ suppressed throughout the remainder of our discussion, we obtain the time-harmonic Maxwell equations

$$\nabla \times \mathbf{E}(\mathbf{r}) - ik\mathbf{H}(\mathbf{r}) = \mathbf{0} \tag{2.17}$$

and

$$\nabla \times \mathbf{H}(\mathbf{r}) + i\varepsilon k\mathbf{E}(\mathbf{r}) = \mathbf{0}, \tag{2.18}$$

where $k = \omega/c$ is the free space wave number. We also abbreviate the dielectric constant

$$\varepsilon = \varepsilon' + i\frac{4\pi\kappa}{ck} \tag{2.19}$$

For conducting materials, it can be seen that the dielectric constant is in general a complex number, representing dissipative properties of the medium. In fact, energy considerations lead to $\mathrm{Im}(\varepsilon) > 0$ (see e.g. [6] and many others).

Continuity of the magnetic and

$$\nabla \cdot \mathbf{H}(\mathbf{r}) = 0 \tag{2.20}$$

and

$$\varepsilon'\nabla \cdot \mathbf{E}(\mathbf{r}) = 4\pi\rho(\mathbf{r})\,. \tag{2.21}$$

Finally, assuming linear non-magnetic media, the time-harmonic boundary conditions valid at the interface of a scattering object occupying $\mathcal{V}_1$ embedded in the larger region $\mathcal{V}_0$ are

$$\hat{\mathbf{n}}(\mathbf{r}) \cdot [\mathbf{H}_0(\mathbf{r}) - \mathbf{H}_1(\mathbf{r})] = 0 \qquad \hat{\mathbf{n}}(\mathbf{r}) \times [\mathbf{H}_0(\mathbf{r}) - \mathbf{H}_1(\mathbf{r})] = \frac{4\pi}{c}\mathbf{K}(\mathbf{r}) \tag{2.22}$$

and

$$\hat{\mathbf{n}}(\mathbf{r}) \cdot [\varepsilon_0 \mathbf{E}_0(\mathbf{r}) - \varepsilon_1 \mathbf{E}_1(\mathbf{r})] = 4\pi\sigma(\mathbf{r}) \qquad \hat{\mathbf{n}}(\mathbf{r}) \times [\mathbf{E}_0(\mathbf{r}) - \mathbf{E}_1(\mathbf{r})] = \mathbf{0}, \tag{2.23}$$

where ε_0 and ε_1 are the dielectric constants of the respective media. In this work, we always take one of the media to be vacuum, so $\varepsilon_0 = 1$. Recall that the unit normal vector is outward, i.e. it points from region $\mathcal{V}_1$ into $\mathcal{V}_0$. Also recall that the surface current $\mathbf{K}(\mathbf{r})$ and surface charge density $\sigma(\mathbf{r})$ are non-zero only for perfect conductor, which we will discuss shortly.

In the absence of a spatial charge distribution $\rho(\mathbf{r})$ in a medium continuity of the electric field intensity is $\nabla \cdot \mathbf{E}(\mathbf{r})$. In this case it is quite straightforward to show that Maxwell's equations may be combined to obtain vector wave equations for the electric and magnetic field intensities. To see this, we take the curl of equation (2.17) to get

$$\nabla \times \nabla \times \mathbf{E}(\mathbf{r}) - ik\nabla \times \mathbf{H}(\mathbf{r}) = \mathbf{0} \tag{2.24}$$

Combining this last equation with (2.18) then gives

$$\nabla \times \nabla \times \mathbf{E}(\mathbf{r}) - \varepsilon k^2 \mathbf{E}(\mathbf{r}) = \mathbf{0} \tag{2.25}$$

Finally using the well-known vector identity

$$\nabla \times \nabla \times \mathbf{E} = \nabla(\nabla \cdot \mathbf{E}) - \nabla^2 \mathbf{E}$$

we obtain a Helmholtz equation for the time harmonic electric field intensity:

$$\nabla^2 \mathbf{E}(\mathbf{r}) + \varepsilon k^2 \mathbf{E}(\mathbf{r}) = \mathbf{0} \tag{2.26}$$

The Helmholtz equation results of course from the second order linear wave equation when a harmonic time dependence is assumed.

One useful aspect of the equations (2.17), (2.18), (2.20), and (2.21) is known as duality. By duality we mean that if we set,

$$\mathbf{H} = -\varepsilon \mathbf{E}' \qquad \mathbf{E} = \mathbf{H}' \tag{2.27}$$

then the primed quantities will also satisfy the aforementioned set of equations. The principle of duality is useful since it allows us to obtain from the knowledge of the electric field vector, analogous results for the magnetic field vector. As a trivial application of duality we immediately infer from equation (2.28) the the magnetic field intensity also satisfies the Helmholtz equation:

$$\nabla^2 \mathbf{H}(\mathbf{r}) + \varepsilon k^2 \mathbf{H}(\mathbf{r}) = \mathbf{0}. \tag{2.28}$$

2.4 The Stratton-Chu Integral

The Stratton-Chu integral [3] is an exact relation which expresses the fields in a region of space in terms of the fields on a surface which encloses that region. Thus, if the surface fields are determined, then the fields at any point in space may be easily calculated. As we shall see, the Stratton-Chu integral is formally equivalent to other integral formulations such as Huygen's principle [3]. The Stratton-Chu integral is extremely useful for formulating scattering and radiation problems. Given its importance, we outline the mathematical derivation from Maxwell's equations in what follows.

As outlined above, is readily verified that the equations (2.17) and (2.18) may be decoupled with the aid of (2.20) through (2.21), so that both the electric and magnetic field intensities satisfy the homogeneous vector Helmholtz equation, i.e.,

$$\mathcal{L}\mathbf{E} = \mathbf{0} \tag{2.29}$$

and

$$\mathcal{L}\mathbf{H} = \mathbf{0}, \tag{2.30}$$

where we abbreviate the Helmholtz operator as

$$\mathcal{L} \equiv \nabla^2 + k^2. \tag{2.31}$$

Here $k^2 = \varepsilon k^2$ is the square of the material wavenumber. The Green's function is the solution of the equations for the field at $\mathbf{r}$ (observation point) due to a point source at $\mathbf{r}'$ (source point). Using the principle of linear superposition, the solution of the fields at an observation point $\mathbf{r}$ due to a general source function $f(\mathbf{r}')$ is the convolution of the Green's function with that source function[25]. The Green's function appropriate to the solution of equations (2.29) and (2.30) satisfies the inhomogeneous equation

$$\mathcal{L}\phi(\mathbf{r} - \mathbf{r}') = -4\pi\delta(\mathbf{r} - \mathbf{r}') \tag{2.32}$$

and the Sommerfeld radiation condition [1] [4]

$$\lim_{R\to\infty} R\left(\frac{\partial}{\partial R}\phi(R) - ik\phi(R)\right) = 0, \tag{2.33}$$

where $R = ||\mathbf{r} - \mathbf{r}'||$ is the Euclidean distance between the source and observation points. The radiation condition ensures that at large distances from the source, the field represents a divergent travelling wave, i.e., this ensures disturbances propagate away from sources. The Green's function which satisfies (2.32) and (2.33) is given by

$$\phi(\mathbf{r} - \mathbf{r}') = \frac{\mathrm{e}^{ik||\mathbf{r}-\mathbf{r}'||}}{||\mathbf{r} - \mathbf{r}'||}, \tag{2.34}$$

which is known as the free space space Green's function.

Suppose $\mathbf{a}$ is some constant vector. Taking the dot product of equation (2.29) with $\mathbf{a}\phi$, then taking the dot product of equation (2.32) multiplied by $\mathbf{a}$ with $\mathbf{E}$ and subtracting these two yields

$$(\mathcal{L}\mathbf{E}) \cdot \mathbf{a}\phi - \mathbf{E} \cdot \mathbf{a}\,(\mathcal{L}\phi) = 4\pi\mathbf{E} \cdot \mathbf{a}\,\delta(\mathbf{r} - \mathbf{r}')\,. \tag{2.35}$$

From the definition of the operator (2.31), it is readily seen that equation (2.35) simplifies to

$$\left(\nabla^2\mathbf{E}\right) \cdot \mathbf{a}\phi - \mathbf{E} \cdot \mathbf{a}\left(\nabla^2\phi\right) = 4\pi\mathbf{E} \cdot \mathbf{a}\,\delta(\mathbf{r} - \mathbf{r}')\,. \tag{2.36}$$

Since the vector $\mathbf{a}$ is arbitrary, it may be removed from both sides of the equation. We thus obtain

$$\left(\nabla^2\mathbf{E}\right)\phi - \mathbf{E}\left(\nabla^2\phi\right) = 4\pi\mathbf{E}\,\delta(\mathbf{r} - \mathbf{r}')\,. \tag{2.37}$$

Taking the integral of equation (2.37) over some arbitrary volume, $\mathcal{V}$, gives

$$\int_{\mathcal{V}} \mathbf{E}\,\delta(\mathbf{r} - \mathbf{r}')\,d\mathbf{r} = \frac{1}{4\pi}\int_{\mathcal{V}} \left(\nabla^2\mathbf{E}\right)\phi - \mathbf{E}\left(\nabla^2\phi\right)\,d\mathbf{r}. \tag{2.38}$$

The integrals that arise in (2.38) and all others that follow in this section are understood to be principal value integrals. The volume integral on the right-hand side of equation (2.38) may be converted to a surface integral using Green's theorem. If the surface of $\mathcal{V}$ is representable as some analytic function of the coordinates, $\mathbf{r}$, then equation (2.38) yields

$$\int_{\mathcal{V}} \mathbf{E}\,\delta(\mathbf{r}-\mathbf{r}')\,d\mathbf{r} = \frac{1}{4\pi}\int_{\mathcal{S}} (\hat{\mathbf{n}}\cdot\nabla\mathbf{E})\,\phi - \mathbf{E}\,(\hat{\mathbf{n}}\cdot\nabla\phi)\,dS, \tag{2.39}$$

where $\hat{\mathbf{n}}$ is an outward unit normal to the surface $\mathcal{S}$ of the volume $\mathcal{V}$. Equation (2.39) is the mathematical expression of Huygen's principle [5]. In what follows, without further assumptions, we derive from Huygen's principle to the Stratton-Chu integral, thus establishing their formal equivalence. Following [2], we find it convenient to rewrite the integral (2.39) as

$$\int_{\mathcal{V}} \mathbf{E}\,\delta(\mathbf{r}-\mathbf{r}')\,d\mathbf{r} = \frac{1}{4\pi}\int_{\mathcal{S}} \hat{\mathbf{n}}\cdot\nabla\,(\phi\mathbf{E}) - 2\mathbf{E}\,(\hat{\mathbf{n}}\cdot\nabla\phi)\,dS \tag{2.40}$$

Again using Green's theorem, we may convert the integral of the first term on the right-hand side to a volume integral. We thus obtain,

$$\int_{\mathcal{S}} \hat{\mathbf{n}}\cdot\nabla\,(\phi\mathbf{E})\,dS = \int_{\mathcal{V}} \nabla^2\,(\phi\mathbf{E})\,d\mathbf{r} \tag{2.41}$$

Using the identity

$$\nabla^2\,(\phi\mathbf{E}) = \nabla\,[\nabla\cdot(\phi\mathbf{E})] - \nabla\times\nabla\times(\phi\mathbf{E})$$

and converting the right-hand side of (2.41) back to a surface integral yields the result

$$\int_{\mathcal{S}} \hat{\mathbf{n}}\cdot\nabla\,(\phi\mathbf{E})\,dS = \int_{\mathcal{S}} \{\hat{\mathbf{n}}\,[\nabla\cdot(\phi\mathbf{E})] - \hat{\mathbf{n}}\times[\nabla\times(\phi\mathbf{E})]\}\,dS \tag{2.42}$$

Basic vector identities combined with Maxwell's equation (2.17), and continuity (2.21) give

$$\begin{aligned} \nabla\times(\phi\mathbf{E}) &= ik\phi\mathbf{H} + \nabla\phi\times\mathbf{E} \\ \nabla\cdot(\phi\mathbf{E}) &= \mathbf{E}\cdot\nabla\phi \end{aligned} \quad . \tag{2.43}$$

Combining equations (2.40), (2.42) and (2.43) and using the identity

$$\hat{\mathbf{n}}\times(\nabla\phi\times\mathbf{E}) = (\hat{\mathbf{n}}\cdot\mathbf{E})\,\nabla\phi - (\hat{\mathbf{n}}\cdot\nabla\phi)\,\mathbf{E}$$

results in the equation

$$\int_{\mathcal{V}} \mathbf{E}\,\delta(\mathbf{r}-\mathbf{r}')\,d\mathbf{r} = -\frac{1}{4\pi}\int_{\mathcal{S}} ik\,(\hat{\mathbf{n}}\times\mathbf{H})\,\phi + (\hat{\mathbf{n}}\cdot\mathbf{E})\,\nabla\phi + (\hat{\mathbf{n}}\cdot\nabla\phi)\,\mathbf{E} - (\mathbf{E}\cdot\nabla\phi)\,\hat{\mathbf{n}}dS. \tag{2.44}$$

Finally, using the identity

$$(\hat{\mathbf{n}}\times\mathbf{E})\times\nabla\phi = (\hat{\mathbf{n}}\cdot\nabla\phi)\,\mathbf{E} - (\mathbf{E}\cdot\nabla\phi)\,\hat{\mathbf{n}}$$

in equation (2.44) gives the famous Stratton-Chu equation [3]

$$\int_{\mathcal{V}} \mathbf{E}\,\delta(\mathbf{r}-\mathbf{r}')\,d\mathbf{r} = -\frac{1}{4\pi}\int_{\mathcal{S}} ik\,(\hat{\mathbf{n}}\times\mathbf{H})\,\phi + (\hat{\mathbf{n}}\times\mathbf{E})\times\nabla\phi + (\hat{\mathbf{n}}\cdot\mathbf{E})\,\nabla\phi dS \tag{2.45}$$

The integral on the left-hand side of equation (2.45) vanishes when the point $\mathbf{r}'$ lies outside of the volume whose elements are located at the points $\mathbf{r}$. We note that the only quantities which appear in the Stratton-Chu integral are those given by the boundary conditions (2.22) and (2.23). It is possible to derive the same result as equation (2.45) using the Vector Green's theorem and dyadic Green's functions [1], [7], [25]. In the present work, however, we need only a vector approach to properly characterize the scattering from dielectrics and perfect conductors.

When applying the Stratton-Chu equation in this thesis, we interchange the source and observation points ($\mathbf{r}$ and $\mathbf{r}'$ respectively), without change in the form of the integral (2.45). In what follows, we interchange the labels for the coordinates, so that the primed coordinate is understood to be the source point. The vector functions in the integrand of the Stratton-Chu equation are then understood to be functions of the source coordinates, $\mathbf{r}'$. Thus, the Stratton-Chu integral integrates field quantities over all source points on the surface to produce a field quantity at the observation point.

We now discuss application of Stratton-Chu integral to unbounded regions so that we can properly treat radiation problems in free space. A large spherical volume $\mathcal{V}_0$ (a vacuum) completely contains two bodies $\mathcal{V}_1$ and $\mathcal{V}_s$ but is otherwise devoid of sources. The volume $\mathcal{V}_1$ with surface $\mathcal{S}$ will be understood to be a scattering body while the volume $\mathcal{V}_s$ with surface $\mathcal{S}_s$ will be understood to be a source body. The large

spherical region $\mathcal{V}_0$ has surface $\mathcal{S}_0$. Applying the Stratton-Chu integral to the region $\mathcal{V}_0$ this gives

$$\begin{aligned}\int_{\mathcal{V}_0} \mathbf{E}(\mathbf{r}')\ \delta(\mathbf{r}-\mathbf{r}')\, d\mathbf{r}' &= -\frac{1}{4\pi}\int_{\mathcal{S}_0} ik\,(\hat{\mathbf{n}}\times\mathbf{H})\,\phi + (\hat{\mathbf{n}}\times\mathbf{E})\times\nabla'\phi + (\hat{\mathbf{n}}\cdot\mathbf{E})\,\nabla'\phi dS' \\ &+ \frac{1}{4\pi}\int_{\mathcal{S}_1} ik\,(\hat{\mathbf{n}}\times\mathbf{H})\,\phi + (\hat{\mathbf{n}}\times\mathbf{E})\times\nabla'\phi + (\hat{\mathbf{n}}\cdot\mathbf{E})\,\nabla'\phi dS' \\ &+ \frac{1}{4\pi}\int_{\mathcal{S}_s} ik\,(\hat{\mathbf{n}}\times\mathbf{H})\,\phi + (\hat{\mathbf{n}}\times\mathbf{E})\times\nabla'\phi + (\hat{\mathbf{n}}\cdot\mathbf{E})\,\nabla'\phi dS' \end{aligned} \tag{2.46}$$

In all cases described in equation (2.46), the unit normal points outward from the volume $\mathcal{V}_0$ (i.e. it points into $\mathcal{V}_1$ and $\mathcal{V}_s$). We now allow the radius of the spherical region $\mathcal{V}_0$ to become infinitely large. The integral over the surface $\mathcal{S}_0$ in (2.46) must then vanish as a result of Sommerfeld's radiation condition [4]. Next, we reverse the signs of the normal vectors to $\mathcal{V}_1$ and $\mathcal{V}_s$ in (2.46) so they are understood to be pointing into the vacuum region $\mathcal{V}_0$. Finally, the integral over the surface $\mathcal{S}_s$ of the source region $\mathcal{V}_s$ may be taken as the incident field; i.e.,

$$\mathbf{E}_{inc}(\mathbf{r}) = -\frac{1}{4\pi}\int_{\mathcal{S}_s} ik\,(\hat{\mathbf{n}}\times\mathbf{H})\,\phi + (\hat{\mathbf{n}}\times\mathbf{E})\times\nabla'\phi + (\hat{\mathbf{n}}\cdot\mathbf{E})\,\nabla'\phi dS'. \tag{2.47}$$

Typically, the incident field is prescribed as some function of the coordinates $\mathbf{r}$. Equation (2.46) thus gives the important surface integral relation for the fields in $\mathcal{V}_0$

$$\begin{aligned}\mathbf{E}_{inc}(\mathbf{r}) &- \frac{1}{4\pi}\int_{\mathcal{S}} \{ik\phi(\mathbf{r},\mathbf{r}')\,[\hat{\mathbf{n}}(\mathbf{r}')\times\mathbf{H}(\mathbf{r}')] + [\hat{\mathbf{n}}(\mathbf{r}')\times\mathbf{E}(\mathbf{r}')]\times\nabla'\phi(\mathbf{r},\mathbf{r}') \\ &+ [\hat{\mathbf{n}}(\mathbf{r}')\cdot\mathbf{E}(\mathbf{r}')]\,\nabla'\phi(\mathbf{r},\mathbf{r}')\}\, dS' = \begin{cases}\mathbf{E}(\mathbf{r}) & \mathbf{r}\in\mathcal{V}_0 \\ \mathbf{0} & \text{otherwise}\end{cases}\end{aligned} \tag{2.48}$$

Equation (2.48) represents the desired formulation of the electromagnetic field problem. One can see that if the observation point $\mathbf{r}$ lies in the vacuum region $\mathcal{V}_0$ then the total field $\mathbf{E}$ is the sum of the incident field $\mathbf{E}_{inc}$ and the scattered field, which is represented by the integral. If $\mathbf{r}$ lies inside the volume $\mathcal{V}_1$ then $\mathbf{E}_{inc}$ is exactly canceled out by the integral, and hence such a description is also known as the Ewald-Oseen extinction theorem [6].

Using duality, we may derive the analogous results corresponding to the magnetic fields. In the vacuum

region $\mathcal{V}_0$, we find for the magnetic field

$$\begin{aligned}\mathbf{H}_{inc}(\mathbf{r}) \quad &+ \quad \frac{1}{4\pi}\int_{\mathcal{S}} \{ik\phi(\mathbf{r},\mathbf{r}')\left[\hat{\mathbf{n}}(\mathbf{r}')\times\mathbf{E}(\mathbf{r}')\right] - \left[\hat{\mathbf{n}}(\mathbf{r}')\times\mathbf{H}(\mathbf{r}')\right]\times\nabla'\phi(\mathbf{r},\mathbf{r}') \\ &- \quad \left[\hat{\mathbf{n}}(\mathbf{r}')\cdot\mathbf{H}(\mathbf{r}')\right]\nabla'\phi(\mathbf{r},\mathbf{r}')\}\, dS' = \begin{cases} \mathbf{H}(\mathbf{r}) & \mathbf{r}\in\mathcal{V}_0 \\ \mathbf{0} & \text{otherwise} \end{cases}\end{aligned} \tag{2.49}$$

In this thesis, we assume that the form of the incident field is a plane wave. In this case, the source region, $\mathcal{V}_s$ must theoretically be allowed to recede to infinity. These and other details are given by Pattanayak [6].

2.5 Perfect Conductors and the Electric Field Integral Equation

Perfect conductors are a useful idealization of physical problems since the mathematics involved is greatly simplified over what we have seen in previous sections. They are generally considered accurate models for electromagnetic interactions with many metals. Electric and magnetic fields do not penetrate perfectly conducting bodies, so these interior fields are set to zero where they appear in previous sections. Thus, from equations (2.6) and (2.7) on the exterior surface of a perfect conductor lying in vacuum region we have boundary conditions

$$\hat{\mathbf{n}}\times\mathbf{E} = 0 \quad \text{and} \quad \hat{\mathbf{n}}\cdot\mathbf{H} = 0. \tag{2.50}$$

On the surface of a perfect conductor lying in a vaccum we also have

$$\hat{\mathbf{n}}\times\mathbf{H} = \frac{4\pi}{c}\mathbf{K} \tag{2.51}$$

and

$$\hat{\mathbf{n}}\cdot\mathbf{E} = 4\pi\sigma \tag{2.52}$$

Here $\mathbf{K}$ and σ are the time harmonic surface current and surface charge density, respectively; these quantities do not vanish in general on the surface of a perfect conductor. Conservation of charge for the surface quantities results directly from equation (2.5) by replacing ρ and $\mathbf{J}$ with the surface quantities σ and $\mathbf{K}$, respectively, and understanding the time dependence as harmonic:

$$-i\omega\sigma + \nabla_s\cdot\mathbf{K} = 0 \tag{2.53}$$

where $\nabla_s \cdot \mathbf{K}$ is the surface divergence of the surface current density. Combining equations (2.52) and (2.53) we have on the surface of a perfect conductor

$$\hat{\mathbf{n}} \cdot \mathbf{E} = \frac{1}{ik} \nabla_s \cdot \mathbf{J}_s, \tag{2.54}$$

where we have defined a new (scaled) surface current density

$$\mathbf{J}_s = \frac{4\pi}{c} \mathbf{K}. \tag{2.55}$$

The Stratton-Chu equation (2.48) now gives the following equation for the electric field in a vacuum region outside of a perfect conductor:

$$\mathbf{E}(\mathbf{r}) = \mathbf{E}_{inc}(\mathbf{r}) - \frac{i}{4\pi k} \int_{\mathcal{S}} k^2 \mathbf{J}_s(\mathbf{r}') \, \phi(\mathbf{r}, \mathbf{r}') - \nabla'_s \cdot \mathbf{J}_s(\mathbf{r}') \, \nabla' \phi(\mathbf{r}, \mathbf{r}') \, dS(\mathbf{r}') \tag{2.56}$$

Equation (2.56) is known as the Electric Field Integral Equation (EFIE) and is an important tool for calculating the fields scattered by a perfectly conducting body. Equation (2.55) states the the total field in the vacuum $\mathbf{E}$ is the sum of the incident field $\mathbf{E}_{inc}$ and the scattered field, represented by the integral. This equation also gives a clear mathematical picture for the fundamental mechanism of scatting, namely, an field incident upon a body excites surface currents on that body; those surface currents then produce an electric field which radiates away from the body.

Allowing $\mathbf{r}$ to approach the surface in equation (2.56) allows us to obtain a surface integral equation for the unknown surface currents by enforcing the boundary condition $\hat{\mathbf{n}} \times \mathbf{E} = 0$ [14]:

$$\hat{\mathbf{n}}(\mathbf{r}) \times \mathbf{E}_{inc}(\mathbf{r}) = \frac{i}{4\pi k} \hat{\mathbf{n}}(\mathbf{r}) \times \int_{\mathcal{S}} k^2 \mathbf{J}_s(\mathbf{r}') \phi(\mathbf{r}, \mathbf{r}') + \nabla'_s \cdot \mathbf{J}_s(\mathbf{r}') \nabla \phi(\mathbf{r}, \mathbf{r}') \, dS(\mathbf{r}') \tag{2.57}$$

Note that in obtaining equation (2.56) we have also used the identity $\nabla' \phi = -\nabla \phi$ which follows directly from the definition of the free space Green's function in equation (2.34). Equation (2.57) is the basis of our methods for computing the currents excited on thin wire antennas.

We may also produce integral equations for the magnetic field. Applying boundary conditions appropriate for a perfect conductor we find from equation (2.49) the Magnetic Field Integral Equation (MFIE) valid for $\mathbf{r}$ in the vacuum region outside the perfect conductor:

$$\mathbf{H}(\mathbf{r}) = \mathbf{H}_{inc}(\mathbf{r}) - \frac{1}{4\pi} \int_{\mathcal{S}} \mathbf{J}_s(\mathbf{r}') \times \nabla' \phi(\mathbf{r}, \mathbf{r}') \, dS(\mathbf{r}') \tag{2.58}$$

Allowing $\mathbf{r}$ to approach the surface in equation (2.58) allows us to obtain a surface integral equation for the unknown surface currents by enforcing the boundary condition $\hat{\mathbf{n}} \times \mathbf{H} = \mathbf{J}_s$ [14]:

$$\hat{\mathbf{n}}(\mathbf{r}) \times \mathbf{H}_{inc}(\mathbf{r}) = \frac{1}{2}\mathbf{J}_s(\mathbf{r}) + \frac{1}{4\pi}\hat{\mathbf{n}}(\mathbf{r}) \times \int_{\mathcal{S}} \mathbf{J}_s(\mathbf{r}') \times \nabla' \phi(\mathbf{r}, \mathbf{r}')\, dS(\mathbf{r}') \tag{2.59}$$

Equation (2.59) is a second kind integral equation for the unknown surface current density $\mathbf{J}_s$. Note that the factor of $1/2$ that appears in front of the unknown current density on the right-hand side of (2.59) is the result of a jump discontinuity in the integral operator at the surface [21]. Typically second kind equations produce superior numerical schemes due the the diagonal dominance of the discretized integral operator. However, schemes based on the MFIE are known to experience substantial numerical difficulties when applied to thin wire structures [14]; we thus base our numerical schemes on the EFIE above.

3 Thin Wire Equations

In this chapter we will specialize the EFIE (2.57) to general thin (possibly curved) wires. We will subsequently derive the famous straight wire equations of Pocklington[8] and Hallén [16]. Finally, based on the principles in the previous two sections, we will derive straight wire equations for arrays, which is the main subject of this thesis.

3.1 General Thin Wire Equations

The EFIE (2.56) is specialized to thin curvilinear wires of circular cross-section. The EFIE is universally used in this application due to well-known numerical problems that arise when the MFIE (2.59) is used for this purpose [14]. Further details in the development of the general thin wire equations may be found in [14] and [15].

We assume that the wire is a circular perfectly conducting tube of radius a whose centerline lies on the parametric curve $\mathbf{f}(s)$, $s \in [-1, 1]$, with unit tangent vector $\hat{\mathbf{t}}(s) = \mathbf{f}'(s)/||\mathbf{f}'(s)||$. In this description it is also useful to define the binormal and normal vectors as

$$\hat{\mathbf{b}}(s) = \frac{\mathbf{f}'(s) \times \mathbf{f}''(s)}{||\mathbf{f}'(s) \times \mathbf{f}''(s)||} \quad \text{and} \quad \hat{\mathbf{n}}(s) = \hat{\mathbf{b}}(s) \times \hat{\mathbf{t}}(s) \tag{3.1}$$

so that the orthonormal set $\{\hat{\mathbf{n}}, \hat{\mathbf{b}}, \hat{\mathbf{t}}\}$ form a right-handed coordinate system with origin $\mathbf{r} = \mathbf{f}(s)$. Despite the obvious conflict in notation, the curve normal vector $\hat{\mathbf{n}}(s)$ should not be confused with the outward surface normal vector $\hat{\mathbf{n}}(\mathbf{r})$. Thus, any point on the surface of the wire (excluding the end-caps) is given by the position vector

$$\mathbf{r}(s, \theta) = \mathbf{f}(s) + a\hat{\mathbf{n}}(s)\cos\theta + a\hat{\mathbf{b}}(s)\sin\theta$$

for $s \in [-1, 1]$ and $\theta = [-\pi, \pi]$.

The thin wire assumption requires that the wire radius a be sufficiently small with respect to the wavelength λ of the incident radiation so that the current does not vary in the azymuthal direction of the wire's cross section. More precisely, the thin wire assumption restricts $a/\lambda \ll 1$ or equivalently, since the wave number is defined as $k = \omega/c = 2\pi/\lambda$, the thin wire assumption restricts $ka \ll 1$. In this context, it makes sense to define the current density J as

$$\mathbf{J}(\mathbf{r}) = \frac{J(s)}{2\pi a}\hat{\mathbf{t}}(s) \quad \text{with} \quad J(s) = \int_0^{2\pi} \hat{\mathbf{t}}(s) \cdot \mathbf{J}(\mathbf{r}) d\theta. \tag{3.2}$$

The EFIE (2.57) is reduced to a one dimensional integral over the length of the wire, resulting in the Pocklington integro-differential equation [14][15]

$$\begin{aligned} -4\pi i k \hat{\mathbf{t}}(s) \cdot \mathbf{E}_{inc}(\mathbf{r}(s,\theta)) = \frac{\partial}{\partial s} \int_{-1}^{1} \frac{\partial}{\partial \sigma} J(\sigma) \Phi(s, \sigma; \theta) ||\mathbf{f}'(\sigma)|| \, d\sigma \\ + k^2 \int_{-1}^{1} \hat{\mathbf{t}}(s) \cdot \hat{\mathbf{t}}(\sigma) J(\sigma) \Phi(s, \sigma; \theta) ||\mathbf{f}'(\sigma)|| \, d\sigma. \end{aligned} \tag{3.3}$$

We denote the kernel of the integral equation as

$$\Phi(s, \sigma; \theta) = \frac{1}{2\pi} \int_{-\pi}^{\pi} \phi(\mathbf{r}(s,\theta) - \mathbf{r}(\sigma, \psi)) \, d\psi = \frac{1}{2\pi} \int_{-\pi}^{\pi} \frac{\mathrm{e}^{ik||\mathbf{r}(s,\theta) - \mathbf{r}(\sigma,\psi)||}}{||\mathbf{r}(s,\theta) - \mathbf{r}(\sigma,\psi)||} \, d\psi \tag{3.4}$$

The kernel (3.4) is generally difficult to evaluate numerically. Since both $\mathbf{r}(s,\theta)$ and $\mathbf{r}(\sigma,\psi)$ lie on the surface, the integrand is singular where these points coincide. In general the function $\Phi(s, \sigma; \theta)$ itself has a logarithmic singularity at $s = s'$[11]; we present details applicable to straight wires in the following sections.

Solutions of the integral equation (3.3) must satisfy the endpoint conditions

$$J(-1) = J(1) = 0. \tag{3.5}$$

We note that the inclusion of the angle θ in (3.3) is somewhat arbitrary. Given that the current is assumed invariant around the circumference of the wire, this angle may be fixed to some constant used throughout and subsequently dropped from the notation (which we do below). The angle ψ does need to be retained in our expressions to properly evaluate the kernel in the form (3.4).

3.2 Pocklington and Hallén Equations For a Straight Wire

In what follows, we show how the classic thin straight wire equations of Pocklington [8] and Hallén [16] may be produced from the more general formulation (3.3). We are specifically interested in producing a simplified version of the integro-differential equation (3.3) corresponding to a straight thin wire of radius a lying on the **z**-axis. In this case, some differential operators which arise in (3.3) may be factored out of the integrals owing to special symmetry properties of the kernel applicable to straight wires, thus resulting in a significant reduction in the complexity of the problem.

The surface vector describing the straight wire lying on the axis is

$$\mathbf{r}(z,\theta) = z\hat{\mathbf{z}} + a\hat{\mathbf{x}}\cos\theta + a\hat{\mathbf{y}}\sin\theta, \tag{3.6}$$

where $z \in [-1,1]$ and $\theta = [-\pi,\pi]$. Following the more general thin wire theory, in the case of a thin straight wire, we assume that the current acts in the $\hat{\mathbf{z}}$ direction, and that it is independent of the azimuthal angle. The surface current density may then be written in terms of the current as

$$\mathbf{J}(\mathbf{r}) = \frac{J(z)}{2\pi a}\hat{\mathbf{z}}. \tag{3.7}$$

The general thin wire equation (3.3) thus becomes

$$-4\pi ik\hat{\mathbf{z}}\cdot\mathbf{E}_{inc}(\mathbf{r}(z,\theta)) = \frac{\partial}{\partial z}\int_{-1}^{1}\frac{\partial}{\partial z'}J(z')\Phi(z,z';\theta)\,dz' + k^2\int_{-1}^{1}J(z')\Phi(z,z';\theta)\,dz'. \tag{3.8}$$

Solutions to equation (3.8) must also be subject to endpoint conditions (3.5). We now examine the first integral on the right-hand side of (3.8) carefully. Bringing the z-derivative inside the integral and integrating by parts it is not difficult to see that the following sequence holds:

$$\int_{-1}^{1}\frac{\partial}{\partial z'}J(z')\frac{\partial}{\partial z}\Phi(z,z';\theta)\,dz = -\int_{-1}^{1}J(z')\frac{\partial^2}{\partial z\partial z'}\Phi(z,z';\theta)\,dz' = \frac{\partial^2}{\partial z^2}\int_{-1}^{1}J(z')\Phi(z,z';\theta)\,dz' \tag{3.9}$$

Note that in arriving at (3.9) we have used the fact that current vanishes at the wire endpoints, i.e., $J(\pm 1) = 0$. We have also used an important symmetry property of the straight wire kernel

$$\frac{\partial}{\partial z}\Phi(z,z';\theta) = -\frac{\partial}{\partial z'}\Phi(z,z';\theta). \tag{3.10}$$

We will establish the property (3.10) soon in what follows, but we note that this property only holds for straight wires and not general curved wires. It is now not difficult to see that equation (3.8) further reduces to

$$-4\pi ik\hat{\mathbf{z}}\cdot\mathbf{E}_{inc}(\mathbf{r}(z,\theta))=\left(\frac{\partial^2}{\partial z^2}+k^2\right)\int_{-1}^{1}J(z')\Phi(z,z';\theta)\,dz'. \tag{3.11}$$

Equation (3.11) is the famed Pocklington equation for thin wire antennas first presented in [8] and forms the basis of much of the twentieth century analysis of the problem [9].

For straight wires there is also a significant reduction in complexity of the kernel. In cylindrical coordinates, we have

$$||\mathbf{r}(z,\theta)-\mathbf{r}(z',\psi)||^2=(z-z')^2+2a^2-2a^2\cos(\theta-\psi) \tag{3.12}$$

It is readily seen that with minimal effort, we may rewrite the straight wire kernel as,

$$\Phi(z,z';\theta)=\Phi_{sw}(z,z')=\frac{1}{\pi}\int_0^{\pi}\frac{\mathrm{e}^{ik\sqrt{(z-z')^2+4a^2\sin^2\xi}}}{\sqrt{(z-z')^2+4a^2\sin^2\xi}}\,d\xi \tag{3.13}$$

It is interesting to note that in arriving at the form of the kernel (3.13) the dependence of the kernel on the observation angle θ – although arbitrary under the straight wire assumptions – was entirely integrated out. This is a feature specific to straight wires and does not in general occur for curved wires; we thus suppress the dependence on the observation in our notation of the straight wire kernel $\Phi_{sw}(z,z')$. Further, inspection of (3.13) shows that the symmetry property is (3.10) is easily established.

Letting

$$\rho=\frac{z-z'}{2a} \tag{3.14}$$

the kernel (3.13) may be expressed as [10][11]

$$\Phi_{sw}(z,z')=\frac{1}{2\pi a}\int_0^{\pi}\frac{\exp[2ika\sqrt{\rho^2+\sin^2\xi}]}{\sqrt{\rho^2+\sin^2\xi}}d\xi. \tag{3.15}$$

As established in [11], these functions have a decomposition

$$\Phi_{sw}(z,z')=F_1(\rho)\ln|\rho|+F_2(\rho), \tag{3.16}$$

where $F_1(\rho)$ and $F_2(\rho)$ are analytic functions. An efficient method for evaluating the functions $F_1(\rho)$ and $F_2(\rho)$ is also presented in [11] and a Fortran code has been made available for the current study.

An alternative (and, in exact arithmetic, equivalent) formulation for the straight wire problem may be obtained as follows. If we let $e(z) = \mathbf{z} \cdot \mathbf{E}_{inc}(\mathbf{r}(z,\theta))$ and denote the potential

$$A(z) = \int_{-1}^{1} J(z')\Phi_{sw}(z,z')\,dz', \tag{3.17}$$

then the Pocklington equation (3.11) simply reads

$$\left(\frac{\partial^2}{\partial z^2} + k^2\right) A(z) = -4\pi i k e(z). \tag{3.18}$$

This last expression is simply an ordinary differential equation for the potential $A(z)$ which is easily solved to obtain

$$A(z) = \int_{-1}^{1} J(z')\Phi_{sw}(z,z')\,dz' = \alpha_1 \cos kz + \alpha_2 \sin kz - 4\pi i \int_{-1}^{z} e(t)\sin[k(z-t)]dt, \tag{3.19}$$

where α_1 and α_2 are constants which are chosen so that the current distribution satisfies the end-point conditions $J(\pm 1) = 0$. The expression (3.19) is known as the Hallén formulation of the straight wire problem [16].

The constants α_1 and α_2 in equation (3.19) may be explicitly computed using a straightforward method proposed by Jones [17]. To briefly summarize the method, suppose $J_c(z)$, $J_s(z)$ and $J_e(z)$ are solutions of

$$\int_{-1}^{1} J_c(z')\Phi_{sw}(z,z')\,dz' = \cos kz, \tag{3.20}$$

$$\int_{-1}^{1} J_s(z')\Phi_{sw}(z,z')\,dz' = \sin kz \tag{3.21}$$

and

$$\int_{-1}^{1} J_e(z')\Phi_{sw}(z,z')\,dz' = -4\pi i \int_{-1}^{z} e(t)\sin[k(z-t)]dt, \tag{3.22}$$

respectively. Then the solution to the Hallén problem (3.19) is

$$J(z) = \alpha_1 J_c(z) + \alpha_1 J_s(z) + J_e(z). \tag{3.23}$$

Enforcing the vanishing of the current at each endpoint $J(\pm 1) = 0$ thus produces from (3.23) two linear equations for the two unknowns α_1 and α_2.

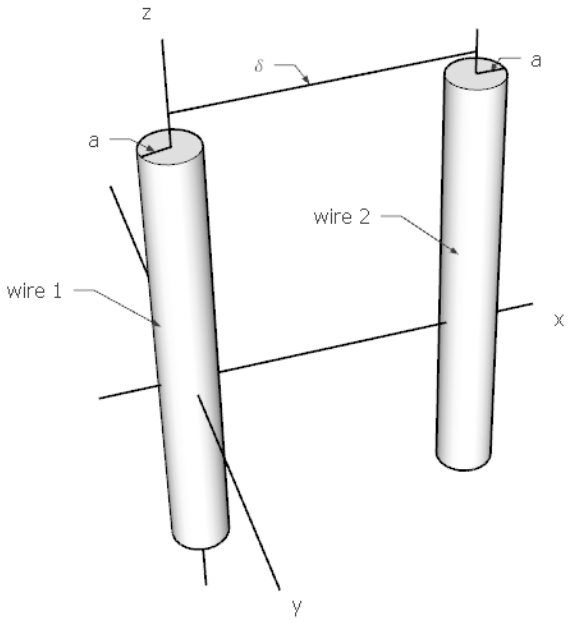

Figure 3.1: Wire 1 lies along the z-axis.Wire 2 lies on x-axis. Two wires are separated by distance δ. Both wires have radius a.

The Hallén formulation is generally beneficial for numerical implementations of the straight wire problem as it avoids numerical differentiations of the potential $A(z)$ which are present in the Pocklington formulation (3.18). While the Hallén is indeed important in practical calculations related to single straight wires, we did experience difficulties in adapting this formulation to arrays of straight wires, as discussed in the following section.

3.3 Thin Wire Arrays

We are now interested in solving a simplified version of the integro-differential equation (3.3) applicable to arrays of straight wires. While there are many common elements to the theory of a single straight wire discussed in the previous section, new issues also arise, as we will see in the following analysis.

We will specifically consider the case of two thin wires of radius a lying parallel to the **z**-axis and separated by a distance $\delta > 2a$. The surface vectors describing wire 1 and wire 2 are

$$\begin{aligned} \mathbf{r}_1(s,\theta) &= s\mathbf{z} + a\mathbf{x}\cos\theta + a\mathbf{y}\sin\theta \\ \mathbf{r}_2(s,\theta) &= s\mathbf{z} + \delta\mathbf{x} + a\mathbf{x}\cos\theta + a\mathbf{y}\sin\theta \end{aligned} \tag{3.24}$$

respectively, where $s \in [-1,1]$ and $\theta = [-\pi, \pi]$. The integrals that arise in equation (3.3) must now be taken over all conducting elements (i.e. wires) in the array. We let $J_1(s)$ be the current density on wire 1 and $J_2(s)$ the current density on wire 2. Under the thin wire approximation, the total tangential electric fields on wire 1 are thus given by

$$-4\pi ik\hat{\mathbf{z}} \cdot \mathbf{E}_{inc}(\mathbf{r}_1(s,\theta)) = \sum_{j=1}^{2} \left\{ \frac{\partial}{\partial s} \int_{-1}^{1} \frac{\partial}{\partial s'} J_j(s') \Phi_{1,j}(s,s';\theta)\, ds' + k^2 \int_{-1}^{1} J_j(s') \Phi_{1,j}(s,s';\theta)\, ds' \right\}. \quad (3.25)$$

Similarly, the total tangential electric fields on wire 2 are thus given by

$$-4\pi ik\hat{\mathbf{z}} \cdot \mathbf{E}_{inc}(\mathbf{r}_2(s,\theta)) = \sum_{j=1}^{2} \left\{ \frac{\partial}{\partial s} \int_{-1}^{1} \frac{\partial}{\partial s'} J_j(s') \Phi_{2,j}(s,s';\theta)\, ds' + k^2 \int_{-1}^{1} J_j(s') \Phi_{2,j}(s,s';\theta)\, ds' \right\}. \quad (3.26)$$

We denote the kernels that arise in the integro-differential equations (3.25) and (3.26) as

$$\Phi_{i,j}(s,s';\theta) = \frac{1}{2\pi} \int_{-\pi}^{\pi} \phi(\mathbf{r}_i(s,\theta) - \mathbf{r}_j(s',\psi))\, d\psi = \frac{1}{2\pi} \int_{-\pi}^{\pi} \frac{\mathrm{e}^{ik||\mathbf{r}_i(s,\theta) - \mathbf{r}_j(s',\psi)||}}{||\mathbf{r}_i(s,\theta) - \mathbf{r}_j(s',\psi)||}\, d\psi. \quad (3.27)$$

One should properly interpret the terms corresponding to $j = 1$ on the right-hand side of equation (3.25) as the contribution to the electric field on wire 1 produced by the current on that wire; the terms corresponding to $j = 2$ in that equation should be understood to be the contribution to the electric field on wire 1 produced by the current on wire 2. A similar statement can be made regarding the physical significance of the terms arising in equation (3.26). The unknowns of the problem, i.e. the currents J_1 and J_2, will be found by solving the coupled system on integro-differential equations (3.25) and (3.26) subject to the conditions that these currents vanish at the wire ends, i.e.,

$$J_j(-1) = J_j(1) = 0 \qquad j = 1, 2. \quad (3.28)$$

We now analyze the kernels of the wire array equations equations (3.25) and (3.26). It is readily seen that the kernels associated with the self-terms (ie the terms which produce the fields on the same wires as where the current is defined) act in precisely the same way as the single straight wire. Indeed, we have

$$\Phi_{i,i}(z,z';\theta) = \Phi_{sw}(z,z') = \frac{1}{\pi} \int_0^{\pi} \frac{\mathrm{e}^{ik\sqrt{(z-z')^2 + 4a^2 \sin^2 \xi}}}{\sqrt{(z-z')^2 + 4a^2 \sin^2 \xi}}\, d\xi \quad (3.29)$$

for $i = 1, 2$. Therefore, based on previous work on the straight wire problem [11] we have a means of decomposing the kernel (3.29) in the form (3.16) and efficiently computing the resulting component functions. Further, we are free to use the symmetry property (3.10).

To analyze the kernels associated with the interaction terms (ie the terms which produce the fields on a wire from the current excited of a different wire) we have to proceed carefully. If we define

$$b^2 = a^2 - 2a\delta\cos\theta + \delta^2 \quad \text{and} \quad \tan\gamma = \frac{a\sin\theta}{a\cos\theta - \delta}, \tag{3.30}$$

then it is possible to establish the following sequence:

$$\begin{aligned} ||\mathbf{r}_1(s,\theta) - \mathbf{r}_2(s',\theta')||^2 &= [b^2 + a^2 + (s-s')^2] + \cos\theta'[2a\delta - 2a^2\cos\theta] + \sin\theta'[-2a^2\sin\theta] \\ &= [b^2 + a^2 + (s-s')^2] + 2ab\cos(\theta' - \gamma) \\ &= [(a-b)^2 + (s-s')^2] + 4ab\sin^2\left(\frac{\theta' - \gamma + \pi}{2}\right). \end{aligned} \tag{3.31}$$

Next, if we define

$$\rho^2 = \frac{(s-s')^2 + (b-a)^2}{4ab} \tag{3.32}$$

then we have

$$||\mathbf{r}_1(s,\theta) - \mathbf{r}_2(s',\theta')||^2 = 4ab\left[\rho^2 + \sin^2\left(\frac{\theta' - \gamma + \pi}{2}\right)\right]. \tag{3.33}$$

These results produce the desired form of the kernel for the interaction terms, namely,

$$\Phi_{1,2}(s,s',\theta) = \Phi_{2,1}(s,s',\theta) = \frac{1}{2\pi\sqrt{ab}}\int_0^\pi \frac{\exp[2ik\sqrt{ab}\sqrt{\rho^2 + \sin^2\psi}]}{\sqrt{\rho^2 + \sin^2\psi}}d\psi. \tag{3.34}$$

Note that in contrast to the usual straight wire kernel (3.29), the dependence of the observation angle θ does not integrate out in equation (3.34), and indeed remains present in the parameter b via equation (3.30). Clearly the kernels (3.34) have the same essential form as the straight wire kernel (3.15) and therefore have a decomposition of the form (3.16). In particular we represent

$$\Phi_{i,j}(s,s',\theta) = F_1^{(i,j)}(\rho)\ln|\rho| + F_2^{(i,j)}(\rho). \tag{3.35}$$

Indeed the same routines described in [11] for computing the functions $F_1(\rho)$ and $F_2(\rho)$ that determine Φ_{sw} via equation (3.16) can be easily adapted for the component functions $F_1^{(i,j)}$ and $F_2^{(i,j)}$ in order to compute $\Phi_{i,j}$ including the case of interactions between adjacent wires. The primary difference is that for the case of interactions between wires, we will have a small but non-vanishing logarithmic term (a near-singularity) when $s = s'$. This can be seen as a result of the definition of the parameter ρ in (3.32); i.e. ρ does not vanish

for wire spacing $\delta > 0$ for any values of $s - s'$. Another very important fact to note about the kernel for the interaction term is that it must obey the symmetry relation

$$\frac{\partial}{\partial s}\Phi_{i,j}(s,s',\theta) = -\frac{\partial}{\partial s'}\Phi_{i,j}(s,s',\theta) \tag{3.36}$$

for $i \neq j$.

As a result of the symmetry relations (3.10) and (3.36) we may factor the differential operators which appear in the integro-differential equations (3.25) and (3.26) in a virtually identical manner as was done in the case of a single straight wire, thus resulting in a significant reduction in the complexity of the problem. Proceeding as outlined in the case of a single straight wire we obtain the following simplified equations:

$$\begin{aligned}\left(\frac{\partial^2}{\partial s^2} + k^2\right)\left[\int_{-1}^{1} \Phi_{1,1}(s,\sigma)J_1(\sigma)\,d\sigma + \int_{-1}^{1} \Phi_{1,2}(s,\sigma)J_2(\sigma)\,d\sigma\right] \\ = -4\pi i k \mathbf{z}\cdot\mathbf{E}_{inc}(\mathbf{r}_1(s,\theta)),\end{aligned} \tag{3.37}$$

$$\begin{aligned}\left(\frac{\partial^2}{\partial s^2} + k^2\right)\left[\int_{-1}^{1} \Phi_{2,1}(s,\sigma)J_1(\sigma)\,d\sigma + \int_{-1}^{1} \Phi_{2,2}(s,\sigma)J_2(\sigma)\,d\sigma\right] \\ = -4\pi i k \mathbf{z}\cdot\mathbf{E}_{inc}(\mathbf{r}_2(s,\theta)).\end{aligned} \tag{3.38}$$

The factored equations (3.37) and (3.38) are solved subject to current endpoint conditions (3.28). It is convenient in what follows to simplify the presentation of the array equations. Suppressing the dependence on the observation angle θ, we abbreviate the source functions as

$$e_1(s) = -4\pi i \mathbf{z}\cdot\mathbf{E}_{inc}(\mathbf{r}_1(s,\theta)), \qquad e_2(s) = -4\pi i \mathbf{z}\cdot\mathbf{E}_{inc}(\mathbf{r}_2(s,\theta)) \tag{3.39}$$

and abbreviate the potentials as

$$A_{i,j}(s) = \int_{-1}^{1} \Phi_{i,j}(s,s',\theta)J_j(s')\,ds'. \tag{3.40}$$

The integro-differential equations (3.37) and (3.38) are then written more concisely as

$$\left(\frac{\partial^2}{\partial s^2} + k^2\right)[A_{1,1}(s) + A_{1,2}(s)] = e_1(s) \tag{3.41}$$

$$\left(\frac{\partial^2}{\partial s^2} + k^2\right)[A_{2,1}(s) + A_{2,2}(s)] = e_2(s) \tag{3.42}$$

Proceeding as in the case of a single straight wire we can produce an an analogous set of equations akin to the Hallén formulation [11][16] of the problem. Indeed, the Helmholtz operator in (3.41) and (3.42) can be inverted yielding the following system of equations:

$$A_{1,1}(s) + A_{1,2}(s) = \alpha_1 \cos ks + \alpha_2 \sin ks + \frac{1}{k}\int_{-1}^{s} e_1(\sigma)\sin[k(s-\sigma)]d\sigma, \tag{3.43}$$

$$A_{2,1}(s) + A_{2,2}(s) = \beta_1 \cos ks + \beta_2 \sin ks + \frac{1}{k}\int_{-1}^{s} e_2(\sigma)\sin[k(s-\sigma)]d\sigma. \tag{3.44}$$

The constants α_1, α_2, β_1, β_2 which arise in equations (3.43) and (3.44) must chosen so that the endpoint conditions (3.28) are satisfied on each wire. Unfortunately, we did not find any simple way of extending the method of Jones [17] – outlined above for the case of a single straight wire – to the problem of finding the constants α_1, α_2, β_1, β_2 in the case of wire arrays. Our numerical method, outlined in the following section, is therefore strictly based on the Pocklington-type formulation given by equations (3.41) and (3.42).

3.4 Numerical Implementation

We now establish our numerical scheme for solving the Pocklington formulation of the wire array problem embodied by the coupled system of equations (3.41) and (3.42). It is well-known that the solutions $J_i(s)$ with the end-point conditions (3.28) tend to zero like $\sqrt{1-s^2}$ as $s \to \pm 1$ [10, 11, 17]. Indeed, it is established in the afore-mentioned works that an appropriate representation of the unknown current distributions is

$$J_i(s) = \frac{I_i(s)}{\sqrt{1-s^2}}\,, \quad s \in [-1,1], \tag{3.45}$$

where the functions $I_i(s)$ for $i = 1, 2$ are known as the reduced currents. Since the singular weight function $(1-s^2)^{-1/2}$ in the integrands on the left-hand side of equations (3.43) and (3.44) can be eliminated by means of the Chebyshev change of variables $s = \cos\theta$ [18, eqn. (1.1)], the set of Chebyshev polynomials $T_n(s)$ is a natural choice of basis functions to represent $I_i(s)$ for $s \in [-1, 1]$. We thus use the discretization

$$I_i(s) \approx \sum_{n=0}^{N-1}{}' b_n^{(i)} T_n(s), \tag{3.46}$$

where the prime indicates that the coefficient associated with $T_0(x)$ is to be halved. The coefficients $b_n^{(i)}$ are therefore related to the reduced current via the Chebyshev transform

$$b_n^{(i)} = \frac{2}{\pi} \int_{-1}^{1} \frac{T_n(s) I_i(s)}{\sqrt{1-s^2}} ds. \tag{3.47}$$

Indeed, equations (3.46) and (3.47) constitute the Chebyshev transform pair of the function $I_i(s)$. As is well-known, with the change of variables $s = \cos\theta$ we have $T_n(\cos\theta) = \cos(n\theta)$ and the Chebyshev transform in (3.47) thus becomes a cosine transform in the θ-variable. It follows that such quantities (where necessary) may be produced in $\mathcal{O}(N \log N)$ operations by means of a fast cosine transform [20]. With the reduced current expanded in this way, the Chebyshev coefficients $b_n^{(i)}$ become the unknowns of the problem. The use of such an expansion is highly advantageous: for the case of an incident plane wave, for example, the solution $I \in C^\infty[-1,1]$, and the Chebyshev series (3.46) thus converges faster than $\mathcal{O}(N^{-m})$ for any positive integer m—i.e. it achieves super-algebraic convergence [11].

With this expansion for the unknown reduced current, the Pocklington formulation of the problem embodied by the coupled system of equations (3.41) and (3.42) becomes

$$\sum_{n=0}^{N-1}{}' b_n^{(1)} C_n^{(1,1)}(s) + \sum_{n=0}^{N-1}{}' b_n^{(2)} C_n^{(1,2)}(s) = e_1(s) \tag{3.48}$$

$$\sum_{n=0}^{N-1}{}' b_n^{(1)} C_n^{(2,1)}(s) + \sum_{n=0}^{N-1}{}' b_n^{(2)} C_n^{(2,2)}(s) = e_2(s) \tag{3.49}$$

In equations (3.48) and (3.49) we denote quantities

$$C_n^{(i,j)}(s) = \left(\frac{\partial^2}{\partial s^2} + k^2 \right) A_n^{(i,j)}(s) \tag{3.50}$$

and

$$A_n^{(i,j)}(s) = \int_{-1}^{1} \Phi_{i,j}(s,\sigma) \frac{T_n(\sigma)}{\sqrt{1-\sigma^2}} \, d\sigma. \tag{3.51}$$

Equations (3.48) and (3.49) form the basis for a collocation method which we apply to the problem. Specifically, we obtain a linear system by testing these equations at the collocation points

$$s_i = \cos\alpha_i, \qquad \alpha_i = (i-1)\frac{\pi}{N-1}, \qquad i = 1, 2, \ldots, N. \tag{3.52}$$

These collocation points are specifically associated with the nodes of a DCT-I cosine/Chebyshev transform [20] which we exploit below.

To properly enforce boundary conditions and obtain a well-conditioned system, we find it is better to solve a transformed version of our last system of equations, namely

$$\sum_{n=0}^{N-1}{}' b_n^{(1)} D_{n,m}^{(1,1)} + \sum_{n=0}^{N-1}{}' b_n^{(2)} D_{n,m}^{(1,2)} = E_m^{(1)} \quad m = 0, \ldots, N-1, \tag{3.53}$$

$$\sum_{n=0}^{N-1}{}' b_n^{(1)} D_{n,m}^{(2,1)} + \sum_{n=0}^{N-1}{}' b_n^{(2)} D_{n,m}^{(2,2)} = E_m^{(2)} \quad m = 0, \ldots, N-1. \tag{3.54}$$

We denote for $m = 0, 1, \ldots, N-1$

$$D_{n,m}^{(i,j)} = \frac{2}{\pi} \int_{-1}^{1} C_n^{(i,j)}(\sigma) \frac{T_m(\sigma)}{\sqrt{1-\sigma^2}}\, d\sigma, \tag{3.55}$$

$$E_m^{(i)} = \frac{2}{\pi} \int_{-1}^{1} e_i(s) \frac{T_m(\sigma)}{\sqrt{1-\sigma^2}}\, d\sigma. \tag{3.56}$$

We specifically note that the quantities on the left-hand side of (3.55) and (3.56) represent Chebyshev transforms of the quantities $C_n^{(i,j)}(\sigma)$ and $e_i(s)$, respectively. In this way, the column vectors of the original discrete linear system (3.48) and (3.49) – each which represents a function sampled on the Chebyshev grid (3.52) – are transformed to obtain column vectors of the linear system (3.53) and (3.54). As is well-known, with the substitution $\sigma = \cos\theta$ in (3.55) and (3.56) these quantities become cosine transforms. In this work, we use the DCT-I cosine transform. Specifically, if $f_i = f(s_i)$ is a function sampled on the grid in equation (3.52) then the Chebyshev transform of this function (obtained by the DCT-I) is

$$a_i = \frac{1}{N-1} \left[f_1 + (-1)^i f_N + 2 \sum_{j=2}^{N-1} f_j \cos(i\alpha_j) \right] \qquad i = 0, 1, \ldots, N-1, \tag{3.57}$$

where a_i are the Chebyshev coefficients of the function $f(s)$. The function then can be reconstructed on the grid using the inverse transform

$$f_i = \sum_{j=0}^{N-1}{}' a_j \cos(j\alpha_i) = \sum_{j=0}^{N-1}{}' a_j T_j(s_i) \qquad i = 1, 2, \ldots, N. \tag{3.58}$$

Now, we don't actually evaluate the transforms using (3.57) (3.58); instead we use fast DCT-I algorithms [20][30].

The evaluation of the integrals (3.51) is one of the more challenging aspect of this work and is treated in detail in the following chapter. For now, assuming we know these integrals to a sufficient accuracy, we produce the matrix entries $C_n^{(i,j)}(s)$ of the original linear system (3.48) and (3.49) as follows. We assume a Chebyshev series representation

$$A_n^{(i,j)}(s) = \int_{-1}^{1} \Phi_{i,j}(s,\sigma) \frac{T_n(\sigma)}{\sqrt{1-\sigma^2}}\, d\sigma \approx {\sum_{m=0}^{N-1}}' a_{n,m}^{(i,j)} T_m(s); \tag{3.59}$$

that is

$$a_{n,m}^{(i,j)} = \frac{2}{\pi} \int_{-1}^{1} A_n^{(i,j)}(\sigma) \frac{T_m(\sigma)}{\sqrt{1-\sigma^2}}\, d\sigma. \tag{3.60}$$

In short, once the integrals $A_n^{(i,j)}(s)$ are computed for each s on the Chebyshev grid (3.52) (by means outlined in the following chapter) we may obtain their Chebyshev series coefficients by means of a straightforward Chebyshev (DCT-I) transform. Using identities related to the derivatives of the Chebyshev polynomials [18] [19] we can then show that the columns of the transformed system (3.53) and (3.54) are given by

$$D_{n,m}^{(i,j)} = k^2 a_{n,m}^{(i,j)} + 4 \sum_{\ell=1}^{\left[\frac{N-m}{2}\right]} \ell\,(\ell+m)(2\ell+m) a_{n,2\ell+m}^{(i,j)}. \tag{3.61}$$

Our method thus hinges on the accurate calculation of the functions $A_n^{(i,j)}(s)$ and their subsequent Chebyshev transforms.

We see that in deriving our transformed system of equations (3.53) and (3.54) we needed to twice differentiate coefficients of the original linear system (3.48) and (3.49). In differentiating (either numerically or symbolically via equation (3.61)) a finite data set representing the function $A_n^{(i,j)}(s)$ we are losing a certain amount of information about that function, specifically the linear terms in a polynomial representation. This loss of information actually makes our system of equations (3.53) and (3.54) singular, and therefore not invertible. Fortunately, this problem is easily rectified, and gives us a natural place to introduce the boundary conditions for the wire current. To enforce the vanishing of the current on the end of the wires we require

$${\sum_{n=0}^{N-1}}' b_n^{(i)} = 0 \quad \text{and} \quad {\sum_{n=0}^{N-1}}' (-1)^n b_n^{(i)} = 0. \tag{3.62}$$

for $i = 1, 2$. These conditions simply arise from evaluating a the Chebyshev series for the current on wire ends $s = \pm 1$ using $T_n(1) = 1$ and $T_n(-1) = (-1)^n$. The last two rows of the matrix corresponding to

$m = N-2$ and $m = N-1$ in each of the two systems of equations (3.53) and (3.54) are thus set to zero, and those matrix entries previously associated with the quantities $D_{n,N-1}^{(i,i)}$ and $D_{n,N-2}^{(i,i)}$ are replaced with these new conditions. Note that the matrix entries previously associated with the quantities $D_{n,N-1}^{(i,j)}$ and $D_{n,N-2}^{(i,j)}$ for $j \neq i$ remain zero. The result is a well-conditioned linear system of equations.

4 Numerical Integration

In what follows we are concerned with the evaluation of the integrals in equation (3.51). To evaluate the functions $A_n^{(i,j)}(s)$ on a Chebyshev grid in s and to eliminate the end-point singularities we introduce the substitutions $s = \cos\alpha$ and $\sigma = \cos\theta$, which reduce the corresponding integrals to

$$\begin{aligned} A_n^{(i,j)}(\cos\alpha) &= \int_0^\pi \Phi_{i,j}(\cos\alpha, \cos\theta)\cos n\theta d\theta \\ &= \int_0^\pi \left[F_1^{(i,j)}(\rho)\ln|\rho| + F_2^{(i,j)}(\rho)\right]\cos n\theta d\theta, \end{aligned} \tag{4.1}$$

for $\alpha \in [0, \pi]$. Note that in the second equation (4.1) we have from equations (3.14) and (3.32) the quantity ρ in terms of the angular variables

$$\rho = \left[\frac{(\cos\alpha - \cos\theta)^2}{4a^2}\right]^{1/2} \tag{4.2}$$

and

$$\rho = \left[\frac{(\cos\alpha - \cos\theta)^2 + (b-a)^2}{4ab}\right]^{1/2}. \tag{4.3}$$

Specifically, the definition (4.2) corresponds to cases when the source and observation points lie on the same wire (i.e. $i = j$), while the definition (4.3) corresponds to cases when the source and observation points lie on different wires (i.e. $i \neq j$). The quantity b which appears in (4.3) is defined in equation (3.30), and is related to the spacing between wires in the array δ. Formally, in the limit $\delta \to 0$ we have $b \to a$ (with a the wire radius and b defined in equation 3.30) and both definitions of ρ above produce the same result.

In the form (4.1) we see that the functions $A_n^{(i,j)}$ can be determined as the cosine transform of $\Phi_{i,j}$ sampled on the cosine grid $\sigma = \cos\theta$. Under normal circumstances (i.e. for smooth integrands), for each value of α, one would proceed by taking a uniform sampling of $\Phi_{i,j}$ in θ and transforming this data using a fast cosine transform to obtain the desired integrals. In the present case, however, we have two separate

issues that prevent such a direct approach, and they must be addressed in order to evaluate the required set of integrals efficiently. Firstly, from equation (4.1) we see that the integrand contains a logarithmic singularity (or near-singularity for closely spaced wires) when $\alpha = \theta$, so specialized quadratures are required to evaluate these integrals efficiently. Second, independent of this logarithmic singularity, the component functions $F_1^{(i,j)}$ and $F_2^{(i,j)}$ possess sharp features in a neighborhood of $\sigma = s$ or equivalently $\theta = \alpha$; these functions would thus require a very fine grid in θ to properly resolve, even in the absence of a logarithmic singularity; see reference [11] for further details. In order to avoid very large samplings of these functions $F_1^{(i,j)}$ and $F_2^{(i,j)}$ (and hence large data sets to transform), we apply a local integration scheme using a fine grid in a neighborhood of $\alpha = \theta$. Our local integration scheme specifically accounts for a logarithmic singularity when it is present. Outside this domain, integration on a much coarser grid is sufficient to achieve the desired accuracy.

Significant savings in evaluating the set of integrals (one for each value of α, or equivalently s) can be obtained by exploiting simple symmetry relations. It is easy to verify from equations (3.29) and (3.34) that $\Phi_{i,j}(-s, -\sigma) = \Phi_{i,j}(s, \sigma)$. Hence it follows, using the standard identity $T_n(-s) = (-1)^n T_n(s)$ and a simple change of variables in the integral that

$$A_n^{(i,j)}(-s) = (-1)^n A_n^{(i,j)}(s) \tag{4.4}$$

Thus, although the values of $A_n^{(i,j)}(s)$ in the full interval $s \in [-1, 1]$ are required by our method, actual integrations to produce these functions numerically need only be performed for $s \in [0, 1]$ and this symmetry relation is used to produce the remaining required values of the integrals.

In this chapter we outline the specific domain decomposition used in computing the integrals. In setting up this localized numerical integration, a numerical quadrature rule is required to deal with subsequent integrals that appear. We derive new closed form results for the quadratures through careful mathematical analysis.

4.1 Domain Decomposition and Localized Integration

For each Chebyshev mode n we partition the integration domain $[0, \pi]$ of the integral in equation (4.1) into two regions, the fine- and coarse-discretization domains. To define the fine-discretization region which lies in a neighborhood of $\theta = \alpha$, in most cases it is sufficient to restrict the angular coordinate in equation (4.1) to the domain $\theta \in [\theta_1, \theta_2]$, with $\theta_1 = \cos^{-1}(z+\Delta)$ and $\theta_2 = \cos^{-1}(z-\Delta)$, where $\Delta > 0$ is a splitting parameter. One notable exception occurs when $z + \Delta > 1$; this special case is treated by setting $\theta_1 = 0$. The analogous case, when $z - \Delta < 1$ does not occur in our method, since values of (4.1) for $s \in [-1, 0)$, or equivalently $\alpha \in (\pi/2, \pi]$ are obtained by the symmetry relation (4.4). Setting $\varepsilon_1 = \alpha - \theta_1$ and $\varepsilon_2 = \theta_2 - \alpha$, the domain of integration is thus partitioned as

$$[0, \pi] \equiv [0, \alpha - \varepsilon_1] \cup [\alpha - \varepsilon_1, \alpha] \cup [\alpha, \alpha + \varepsilon_2] \cup [\alpha + \varepsilon_2, \pi]\,. \tag{4.5}$$

Owing to the symmetry relation (4.4), we have the restriction $\alpha \in [0, \pi/2]$. In the fine-discretization region $\theta \in [\alpha - \varepsilon_1, \alpha + \varepsilon_2]$ we develop a special integration method which treats the logarithmic singularity or near-logarithmic singularity of $\Phi_{i,j}$. Outside of this region, different methods are applied on a coarse grid.

4.1.1 Integration in the fine-discretization region

We first describe the method of computation of contributions to $A_n^{(i,j)}(\cos\alpha)$ with α fixed for the left-hand interval (left of the singularity) $\theta \in [\alpha - \varepsilon_1, \alpha]$. To do this, we map $x(\theta) \in [-1, 1]$ to $\theta \in [\alpha - \varepsilon_1, \alpha]$ with the change of variables

$$\theta = \varepsilon_1(x - 1)/2 + \alpha. \tag{4.6}$$

In the case when both source and observation points lie on the same wire (i.e. $i = j$) the integrand contains a logarithmic singularity, which we treat to high order using the method developed below. By addition and subtraction of powers of $(x - 1)$ it is trivial to establish the following identities:

$$\ln|\cos\alpha - \cos\theta| = \ln\left|\frac{\cos\alpha - \cos\theta}{x - 1}\right| + \ln|x - 1| \qquad \alpha \neq 0; \tag{4.7}$$

$$\ln|1 - \cos\theta| = \ln\left|\frac{1 - \cos\theta}{(x - 1)^2}\right| + 2\ln|x - 1| \qquad \alpha = 0. \tag{4.8}$$

The Taylor expansion

$$\cos\alpha - \cos\theta = \frac{\varepsilon_1}{2}\,(x-1)\sin\alpha + \frac{\varepsilon_1^2}{8}\,(x-1)^2\cos\alpha + \mathcal{O}\big(\varepsilon_1^3(x-1)^3\big) \tag{4.9}$$

then shows that the first logarithmic term on the right-hand side of each of equations (4.7) and (4.8) is regular, and can therefore be approximated well using standard numerical integration techniques. Suppressing the dependence on α, the kernel function in (4.1) may be written as

$$\Phi_{i,i}(\cos\alpha, \cos\theta) = G_1^{(i,i)}(x)\ln|x-1| + G_2^{(i,i)}(x). \tag{4.10}$$

When $\alpha \neq 0$ we have

$$G_1^{(i,i)}(x) = F_1^{(i,i)}\left(\frac{\cos\alpha - \cos\theta}{2a}\right), \quad \theta = \theta(x), \tag{4.11}$$

and

$$G_2^{(i,i)}(x) = F_1^{(i,i)}\left(\frac{\cos\alpha - \cos\theta}{2a}\right)\ln\left|\frac{\cos\alpha - \cos\theta}{2a(x-1)}\right| + F_2^{(i,i)}\left(\frac{\cos\alpha - \cos\theta}{2a}\right), \quad \theta = \theta(x). \tag{4.12}$$

On the other hand, when $\alpha = 0$ we have

$$G_1^{(i,i)}(x) = 2F_1^{(i,i)}\left(\frac{1-\cos\theta}{2a}\right), \quad \theta = \theta(x), \tag{4.13}$$

and

$$G_2^{(i,i)}(x) = F_1^{(i,i)}\left(\frac{1-\cos\theta}{2a}\right)\ln\left|\frac{1-\cos\theta}{2a(x-1)^2}\right| + F_2^{(i,i)}\left(\frac{1-\cos\theta}{2a}\right), \quad \theta = \theta(x). \tag{4.14}$$

In either case $\alpha = 0$ or $\alpha \neq 0$ for each n, we introduce the approximations

$$G_1^{(i,i)}(x)\cos n\theta \approx {\sum_{m=0}^{M_2-1}}' e_m^{(n)} T_m(x), \quad \theta = \theta(x), \tag{4.15}$$

and

$$G_2^{(i,i)}(x)\cos n\theta \approx {\sum_{m=0}^{M_2-1}}' f_m^{(n)} T_m(x), \quad \theta = \theta(x). \tag{4.16}$$

The quantity M_2 is the number of the fast cosine transform used to compute the Chebyshev series coefficients $e_m^{(n)}$ and $f_m^{(n)}$ for each n in this fine scale region. We thus see that the contribution to the integral $A_n^{(i,i)}$ from the left-hand interval $\theta \in [\alpha - \varepsilon_1, \alpha]$ given by

$$\int_{\alpha-\varepsilon_1}^{\alpha} \Phi_{i,i}(\cos\alpha, \cos\theta)\cos n\theta d\theta \approx \frac{\varepsilon_1}{2}{\sum_{m=0}^{M_2-1}}' \left(w_m e_m^{(n)} + u_m f_m^{(n)}\right). \tag{4.17}$$

Here we denote the integration weights as

$$u_m = \int_{-1}^{1} T_m(x)dx = \begin{cases} 2/(1-m^2) & m \text{ even} \\ 0 & m \text{ odd} \end{cases} \tag{4.18}$$

and

$$w_m = \int_{-1}^{1} T_m(t)\ln(1-t)\,dt. \tag{4.19}$$

While producing the weights u_m is straightforward using the formula (4.18), producing the weights w_m (4.18) is quite a bit more complicated, and is one of the main subjects of this chapter.

In the case when both source and observation points lie on different wires (i.e. $i \neq j$) the integrand contains a near-logarithmic singularity, which we treat according to the methods we now outline. If fact, we will outline two separate methods of integration; the first method treats the near singularity explicitly, while the second essentially treats it as a smooth function.

Denoting

$$C = \frac{2(b-a)}{\varepsilon_1} \tag{4.20}$$

from equations (4.3) and (4.6) we may establish the following Taylor series expansion:

$$\frac{1}{4ab}\frac{(\cos\alpha - \cos\theta)^2 + (b-a)^2}{(x-1)+C^2} = \frac{1}{4ab}\left(\frac{\varepsilon_1}{2}\right)^2 - \frac{\varepsilon_1^2}{16abC^2}(x-1) + \mathcal{O}(x-1)^2. \tag{4.21}$$

Simultaneously dividing and multiplying the argument of the logarithm in the integrand of equation (4.1) by $(x-1)+C^2$ and suppressing the dependence on α then produces the following decomposition for the kernel function:

$$\Phi_{i,j}(\cos\alpha, \cos\theta) = H_1^{(i,j)}(x)\ln|x-1+C^2| + H_2^{(i,j)}(x). \tag{4.22}$$

In equation (4.22) we denote the kernel functions as

$$H_1^{(i,j)}(x) = \frac{1}{2}F_1^{(i,j)}(\rho)\,, \quad \rho = \rho(x), \tag{4.23}$$

and

$$H_2^{(i,j)}(x) = \frac{1}{2}F_1^{(i,j)}(\rho)\ln\left|\frac{1}{4ab}\frac{(\cos\alpha - \cos\theta)^2 + (b-a)^2}{(x-1)+C^2}\right| + F_2^{(i,j)}(\rho)\,, \quad \rho = \rho(x), \quad \theta = \theta(x). \tag{4.24}$$

In view of the Taylor series (4.21), since $F_1^{(i,j)}$ and $F_2^{(i,j)}$ are regular, $H_1^{(i,j)}$ and $H_2^{(i,j)}$ are also regular. In particular, we see that the argument of the logarithm in (4.24) is a smooth function that does not vanish in the interval of integration. The near-singular behaviour of the kernel function in (4.22) is strictly due to the logarithmic term which we've isolated in that expression. Given the regularity of the functions $H_1^{(i,j)}$ and $H_2^{(i,j)}$, it is appropriate to introduce the following Chebyshev series expansions:

$$H_1^{(i,j)}(x)\cos n\theta \approx {\sum_{m=0}^{M_3-1}}' g_m^{(n)} T_m(x), \quad \theta = \theta(x), \tag{4.25}$$

and

$$H_2^{(i,j)}(x)\cos n\theta \approx {\sum_{m=0}^{M_3-1}}' h_m^{(n)} T_m(x), \quad \theta = \theta(x). \tag{4.26}$$

The quantity M_3 is the length of the fast cosine transform used to compute the Chebyshev series coefficients $g_m^{(n)}$ and $h_m^{(n)}$ for each n in this fine scale region. We thus see that the contribution to the integral $A_n^{(i,j)}$ from the left-hand interval $\theta \in [\alpha - \varepsilon_1, \alpha]$ is given by

$$\int_{\alpha-\varepsilon_1}^{\alpha} \Phi_{i,j}(\cos\alpha, \cos\theta)\cos n\theta d\theta \approx \frac{\varepsilon_1}{2} {\sum_{m=0}^{M_3-1}}' \left(v_m g_m^{(n)} + u_m h_m^{(n)} \right). \tag{4.27}$$

The integrations weights u_m are given by equation (4.18) above, while the integration weights v_m are given by

$$v_m = \int_{-1}^{1} T_m(t) \ln\left(1 - t + C^2\right) dt. \tag{4.28}$$

Quadrature methods such as this which explicitly account for nearly-logarithmic singularities are not well-documented in the literature and pose their own unique challenges. In this chapter we will develop explicit formulas for the integrals in equation (4.19). Deriving explicit formulas is one of the important contributions of this thesis

At this point we note that the case of nearly singular functions may be treated more simply (albeit less accurately) simply by ignoring the singularity and treating the integrand as a smooth function. Specifically, for each integer n we assume a Chebyshev expansion of the form

$$\Phi_{i,j}(\cos\alpha, \cos\theta)\cos n\theta \approx {\sum_{m=0}^{M_3-1}}' d_m^{(n)} T_m(x), \quad \theta = \theta(x). \tag{4.29}$$

Again, M_3 is the length of the fast cosine transform used to compute the Chebyshev series coefficients $d_m^{(n)}$ for each n in this fine scale region. We thus see that the contribution to the integral $A_n^{(i,j)}$ from the left-hand interval $\theta \in [\alpha - \varepsilon_1, \alpha]$ is given by

$$\int_{\alpha-\varepsilon_1}^{\alpha} \Phi_{i,j}(\cos\alpha, \cos\theta) \cos n\theta d\theta \approx \frac{\varepsilon_1}{2} {\sum_{m=0}^{M_3-1}}' u_m d_m^{(n)}. \tag{4.30}$$

This approach can be used when two wires are spaced closely together, but its simplicity comes at the cost of lower accuracy than the method explicitly accounting for the nearly-singular logarithm above. However, as the wire spacing in the array increases, this method becomes much more attractive.

We briefly discuss here the method of computation of contributions to $A_n^{(i,j)}(\cos\alpha)$ with α fixed for the right-hand interval (right of the singularity) $\theta \in [\alpha, \alpha + \varepsilon_2]$. To do this, we map $x \in [-1, 1]$ to $\theta \in [\alpha, \alpha + \varepsilon_2]$ with the change of variables

$$\theta = \varepsilon_2(x + 1)/2 + \alpha. \tag{4.31}$$

The isolation of the logarithmic or near-logarithmic singularities proceeds in a virtually identical manner as was outlined about for the fine-discretization interval immediately left of the singularity. The quadrature weights that arise are also closely related to the left-hand case. Specifically, the weights corresponding to the right-hand interval may be obtained from those corresponding to the left-hand interval using the relations

$$\int_{-1}^{1} T_m(t) \ln(1 + t)\, dt = (-1)^m w_m \tag{4.32}$$

and

$$\int_{-1}^{1} T_m(t) \ln\left(1 + t + C^2\right) dt = (-1)^m v_m. \tag{4.33}$$

The standard Clenshaw-Curtis integration weights u_m which are given in equation (4.18) remain unchanged.

4.1.2 Integration in the coarse-discretization region

We now discuss the numerical integration in the coarse-discretization regions $\theta \in [0, \alpha - \varepsilon_1]$ and $\theta \in [\alpha + \varepsilon_2, \pi]$. In these regions, which lie away from the $\theta = \alpha$ singularity, the kernel $\Phi_{i,j}$ is smooth in both cases where sources and observation points lie on the same wire (i.e. $i = j$) and when they lie on different wires (i.e.

$i \neq j$). To do this in a general case, we map $x \in [-1, 1]$ to $\theta \in [\theta_1, \theta_2]$ for $\theta_2 > \theta_1$ with the change of variables

$$\theta = \frac{\theta_2 - \theta_1}{2} x + \frac{\theta_2 + \theta_1}{2}. \tag{4.34}$$

For each integer n we assume a Chebyshev expansion of the form

$$\Phi_{i,j}(\cos\alpha, \cos\theta) \cos n\theta \approx {\sum_{m=0}^{M_1-1}}' c_m^{(n)} T_m(x), \quad \theta = \theta(x). \tag{4.35}$$

Here M_1 is the number of the fast cosine transform terms used to compute the Chebyshev series coefficients $c_m^{(n)}$ for each n in this course scale region. We see that the contribution to the integral $A_n^{(i,j)}$ from the interval $\theta \in [\theta_1, \theta_2]$ is given by

$$\int_{\theta_1}^{\theta_2} \Phi_{i,j}(\cos\alpha, \cos\theta) \cos n\theta d\theta \approx \frac{\theta_2 - \theta_1}{2} {\sum_{m=0}^{M_1-1}}' u_m c_m^{(n)}. \tag{4.36}$$

This method is a standard Clenshaw-Curtis integration rule [20].

4.2 Quadrature Formulas

In the previous sections outlining our method of integration, it became obvious that we required the evaluation of the integrals

$$w_n(y) = \int_{-1}^{1} \ln|y - x|\, T_n(x) dx \tag{4.37}$$

for the cases $y \in [-1, 1]$ and $|y| > 1$. The first such case corresponds to integrations when both source and observation points lie on the same wire, while the second case corresponds to integrations when source and observation points lie on different wires, but these points may become close to one another. Note that our notation is such that $w_n(1) = w_n$ with w_n defined in equation (4.19). In the following, we use the identity [18, eqn. 2.43] which gives

$$T_0(x) = \frac{d}{dx} T_1(x), \quad T_1(x) = \frac{1}{4} \frac{d}{dx} T_2(x), \quad T_n(x) = \frac{1}{2} \frac{d}{dx} \left[\frac{T_{n+1}(x)}{n+1} - \frac{T_{n-1}(x)}{n-1} \right] \quad n > 1. \tag{4.38}$$

The expression (4.37) can thus be integrated by parts, giving

$$w_0(y) = \left[\ln|y - x|\, T_1(x) \right]_{x=-1}^{x=1} + \int_{-1}^{1} \frac{T_1(x)}{y - x} dx, \tag{4.39}$$

$$w_1(y) = \frac{1}{4}\left[\ln|y-x|\, T_2(x)\right]_{x=-1}^{x=1} + \frac{1}{4}\int_{-1}^{1} \frac{T_2(x)}{y-x} dx, \tag{4.40}$$

and

$$w_n(y) = \frac{1}{2}\left[\ln|y-x|\left(\frac{T_{n+1}(x)}{n+1} - \frac{T_{n-1}(x)}{n-1}\right)\right]_{x=-1}^{x=1} + \frac{1}{2}\int_{-1}^{1} \frac{1}{y-x}\left(\frac{T_{n+1}(x)}{n+1} - \frac{T_{n-1}(x)}{n-1}\right) dx, \tag{4.41}$$

for $n > 1$. The integral on the right-hand side of (4.39), (4.40) and (4.41) should be understood to be a Cauchy principal value integral when $y \in [-1, 1]$. Using the standard identities [18] $T_n(1) = 1$ and $T_n(-1) = (-1)^n$, these equations may be re-written as

$$w_0(y) = \ln|y-1| + \ln|y+1| + I_1(y), \tag{4.42}$$

$$w_1(y) = \frac{1}{4}\left[\ln|y-1| - \ln|y+1|\right] + \frac{1}{4} I_2(y), \tag{4.43}$$

and

$$w_n(y) = \frac{1}{1-n^2}\left[\ln|y-1| + (-1)^n \ln|y+1|\right] + \frac{I_{n+1}(y)}{2(n+1)} - \frac{I_{n-1}(y)}{2(n-1)}, \quad n > 1, \tag{4.44}$$

where

$$I_n(y) = \int_{-1}^{1} \frac{T_n(x)}{y-x}\, dx. \tag{4.45}$$

Again, the integral in (4.45) should be understood as a Cauchy principal value integral when $|y| < 1$. While this principal value integral is not formally defined when $y = \pm 1$, as we establish below, finite results do exist for the quantities $w_n(y)$ in equations (4.42), (4.43) and (4.44) at $y = \pm 1$. Indeed to establish these results, limits have to be taken carefully as there is a cancelation of logarithmic singularities.

Experimenting in the Maple symbolic algebra system for with many explicit Chebyshev polynomials expanded as a function of x, evaluating the integrals in (4.45), and appropriately collecting terms allowed us to deduce the following important relationships:

$$⨍_{-1}^{1} \frac{T_n(x)}{y-x} dx = T_n(y) \ln\left(\frac{1+y}{1-y}\right) - 4 \sum_{k=1}^{[(n+1)/2]}{}' \frac{T_{n-2k+1}(y)}{2k-1}, \quad |y| < 1, \tag{4.46}$$

$$\int_{-1}^{1} \frac{T_n(x)}{y-x}\, dx = T_n(y) \ln\left(\frac{y+1}{y-1}\right) - 4 \sum_{k=1}^{[(n+1)/2]}{}' \frac{T_{n-2k+1}(y)}{2k-1}, \quad |y| > 1. \tag{4.47}$$

Here the prime indicates that the coefficient associated with $T_0(x)$ is to be halved, if it appears. The notation $[u]$ signifies the greatest integer not exceeding u. Note that the integral in (4.46) actually represents the Cauchy principal value. Formally speaking the identity (4.46) represents the Hilbert transform of $T_n(x)$. In the sections below we will rigorously prove the statements (4.46) and (4.47) are true. Indeed, equations (4.46) and (4.47) provide the basis for an efficient algorithm to generate the integrals in equations (4.42), (4.43) and (4.44), thus enabling the efficient calculation of the functions $A_n^{(i,j)}(s)$ required for our collocation method for the coupled thin wire problem.

4.2.1 A Proof of Some Simpler Integral Identities

In order to establish a formal proof of the identities (4.46) and (4.47) we first consider proving the related (but simpler) identities

$$\fint_{-1}^{1} \frac{x^n}{y-x} dx = y^n \ln\left(\frac{1+y}{1-y}\right) - 2Q_n(y), \quad |y| < 1, \tag{4.48}$$

and

$$\int_{-1}^{1} \frac{x^n}{y-x} dx = y^n \ln\left(\frac{y+1}{y-1}\right) - 2Q_n(y), \quad |y| > 1, \tag{4.49}$$

where we denote the polynomials

$$Q_n(y) = \sum_{m=0}^{\lfloor (n-1)/2 \rfloor} \frac{y^{n-2m-1}}{2m+1}. \tag{4.50}$$

The identities (4.48) and (4.49) were deduced by simple experiments in the Maple language. Formally speaking the identity (4.48) represents the Hilbert transform of x^n; surprisingly we were unable to find these results in standard literature. To prove these results we first establish the validity of (4.49) and use this result to subsequently establish the validity of (4.48).

To prove (4.49) is true, we note that Eurler's integral representation of the Gaussian hypergeometric function [27] gives

$$\int_0^1 \frac{x^n}{y-x}\, dx = \frac{1}{(n+1)y}\, {}_2F_1\left(1, n+1; n+2; \frac{1}{y}\right) = -\frac{1}{n} + \Psi\left(\frac{1}{y}, 1, n\right), \tag{4.51}$$

where

$$\Psi(z, s, a) = \sum_{k=0}^{\infty} \frac{z^k}{(a+k)^s} \tag{4.52}$$

is the Lerch transcendent [23]. Using the identity (4.51) it is straightforward to now show that

$$\int_{-1}^{1} \frac{x^n}{y-x}\,dx = -\frac{1}{n}\left[1-(-1)^n\right] + \Psi\left(\frac{1}{y},1,n\right) - (-1)^n\Psi\left(-\frac{1}{y},1,n\right). \tag{4.53}$$

Now, the Lerch transcendent has the properties [23]

$$\Psi(z,s,a) = z^m\Psi(z,s,a+m) + \sum_{k=0}^{m-1}\frac{z^k}{(a+k)^s} \tag{4.54}$$

and

$$\Psi(z,1,1) = -\frac{1}{z}\ln(1-z). \tag{4.55}$$

These last two equations then combine with equation (4.53) to lead directly to the result (4.49).

Next, to establish the validity of the identity (4.48) we will write the principal value integral as the standard limit

$$⨍_{-1}^{1} \frac{x^n}{y-x}dx = \lim_{\epsilon\to 0}\Big(\int_{-1}^{y-\epsilon}\frac{x^n dx}{y-x} + \int_{y+\epsilon}^{1}\frac{x^n dx}{y-x}\Big). \tag{4.56}$$

We note that each one of the integrals that appears in (4.56) can be evaluated by means of (4.49) since ϵ is taken as a positive real quantity, and hence the integrand is nonsingular on the interval of integration. Once these integrals are evaluated, the limit appearing in (4.56) is applied to establish our result.

In the first integral on the right hand side of equation (4.56) we make the change of variables $x = Az + B$ with

$$A = \frac{y-\epsilon+1}{2} \qquad \text{and} \qquad B = \frac{y-\epsilon-1}{2}. \tag{4.57}$$

The integral then becomes

$$\int_{-1}^{y-\epsilon}\frac{x^n dx}{y-x} = \int_{-1}^{1}\frac{A(Az+B)^n}{y-Az-B}dz = \int_{-1}^{1}\frac{(Az+B)^n}{\frac{y-B}{A}-z}dz. \tag{4.58}$$

Using the binomial theorem

$$(Az+B)^n = \sum_{k=0}^{n}\binom{n}{k}(Az)^k B^{n-k}, \tag{4.59}$$

the last integral in (4.58) can then be written as

$$\int_{-1}^{1}\frac{(Az+B)^n}{\frac{y-B}{A}-z}dz = \sum_{k=0}^{n}\binom{n}{k}A^k B^{n-k}\int_{-1}^{1}\frac{z^k dz}{\left(\frac{y-B}{A}\right)-z}. \tag{4.60}$$

From equation (4.57) it is easy to show that

$$\frac{y-B}{A} = \frac{y+1+\epsilon}{y+1-\epsilon}. \tag{4.61}$$

Since ϵ is taken as a positive real quantity, it is therefore clear that

$$\Big|\frac{y-B}{A}\Big| > 1,$$

and hence the identity (4.49) can indeed be used to evaluate the integral on the right-hand side of equation (4.60). We thus obtain

$$\begin{aligned}\int_{-1}^{y-\epsilon} \frac{x^n dx}{y-x} &= \sum_{k=0}^{n} \binom{n}{k} A^k B^{n-k} \Big(\Big(\frac{y-B}{A}\Big)^k \ln\Big(\frac{\frac{y-B}{A}+1}{\frac{y-B}{A}-1}\Big) - 2Q_k\Big(\frac{y-B}{A}\Big)\Big) \\ &= \ln\Big(\frac{y-B+A}{y-B-A}\Big) \sum_{k=0}^{n} \binom{n}{k} B^{n-k}(y-B)^k \\ &\quad -2\sum_{k=0}^{n} \binom{n}{k} A^k B^{n-k} Q_k\Big(\frac{y-B}{A}\Big).\end{aligned} \tag{4.62}$$

Using the binomial theorem again we have

$$((y-B)+B)^n = \sum_{k=0}^{n} \binom{n}{k} B^{n-k}(y-B)^k = y^n. \tag{4.63}$$

Thus the integral in (4.62) simplifies to

$$\int_{-1}^{y-\epsilon} \frac{x^n dx}{y-x} = \ln\Big(\frac{y-B+A}{y-B-A}\Big) y^n - 2\sum_{k=0}^{n} \binom{n}{k} A^k B^{n-k} Q_k\Big(\frac{y-B}{A}\Big). \tag{4.64}$$

A nearly identical procedure can be applied to treat the second integral on the right hand side of equation (4.56). We make the change of variables $x = Cz + D$ with

$$C = \frac{1-y-\epsilon}{2} \qquad \text{and} \qquad D = \frac{1+y+\epsilon}{2}. \tag{4.65}$$

We note that using the definition (4.65) we have

$$\frac{y-D}{C} = -\frac{1-y+\epsilon}{1-y-\epsilon}. \tag{4.66}$$

Hence it is clear that

$$\Big|\frac{y-D}{C}\Big| > 1,$$

and we thus conclude again that we can use the identity (4.49) to evaluate the integral that results from using our change of variables in the second integral in equation (4.56). We thus obtain the result

$$\int_{y+\epsilon}^{1} \frac{x^n dx}{y-x} = \ln\Big(\frac{y-D+C}{y-D-C}\Big) y^n - 2\sum_{k=0}^{n} \binom{n}{k} C^k D^{n-k} Q_k\Big(\frac{y-D}{C}\Big). \tag{4.67}$$

Combining the equations (4.64) and (4.67) then produces the result

$$\begin{aligned}\int_{-1}^{y-\epsilon} \frac{x^n dx}{y-x} + \int_{y+\epsilon}^{1} \frac{x^n dx}{y-x} &= y^n\Big(\ln\Big(\frac{y-B+A}{y-B-A}\Big) + \ln\Big(\frac{y-D+C}{y-D-C}\Big)\Big) \\ &\quad - 2\sum_{k=0}^{n} \binom{n}{k}\Big(A^k B^{n-k} Q_k\Big(\frac{y-B}{A}\Big) + C^k D^{n-k} Q_k\Big(\frac{y-D}{C}\Big)\Big).\end{aligned} \tag{4.68}$$

From definitions (4.57) and (4.65) it is straightforward to see that the arguments of the logarithms in (4.68) can be written as

$$\frac{y-B+A}{y-B-A} = \frac{1+y}{\epsilon} \qquad \text{and} \qquad \frac{y-D+C}{y-D-C} = \frac{\epsilon}{1-y}. \tag{4.69}$$

The important thing to see from (4.69) is that term $\ln\epsilon$ cancels identically from each of the logarithms. Next, we apply the limit $\epsilon \to 0$ in the following expressions to get (in that limit) the following results:

$$A = D = \frac{y+1}{2}; \quad B = -C = \frac{y-1}{2}; \tag{4.70}$$

$$A + B = y; \quad A - B = 1; \quad C + D = 1; \quad C - D = -y. \tag{4.71}$$

We also obtain in the limit $\epsilon \to 0$ the results

$$\frac{y-B}{A} = 1 \qquad \text{and} \qquad \frac{y-D}{C} = -1. \tag{4.72}$$

Thus, applying the limit $\epsilon \to 0$ in equation (4.68) produces the following expression for our principal value integral in (4.56):

$$⨍_{-1}^{1} \frac{x^n}{y-x} dx = y^n \ln\Big(\frac{1+y}{1-y}\Big) - 2\sum_{k=0}^{n} \binom{n}{k}\Big(A^k B^{n-k} Q_k(1) + (-1)^k B^k A^{n-k} Q_k(-1)\Big) \tag{4.73}$$

From the definition of the polynomials $Q_n(y)$ in (4.50) it is clear that

$$Q_k(1) = \sum_{m=0}^{\lfloor \frac{k-1}{2} \rfloor} \frac{1}{2m+1} \tag{4.74}$$

and

$$(-1)^k Q_k(-1) = (-1)^k \sum_{m=0}^{\lfloor \frac{k-1}{2} \rfloor} \frac{(-1)^{k-2m-1}}{2m+1} = -Q_k(1) \tag{4.75}$$

From equation (4.73) we thus obtain the expression

$$\fint_{-1}^{1} \frac{x^n}{y-x} dx = y^n \ln\Big(\frac{1+y}{1-y}\Big) - 2\sum_{k=0}^{n} \binom{n}{k} \Big(A^k B^{n-k} - B^k A^{n-k}\Big) Q_k(1). \tag{4.76}$$

It now remains to show that

$$Q_n(y) = \sum_{k=0}^{n} \binom{n}{k} (A^k B^{n-k} - B^k A^{n-k}) Q_k(1) \tag{4.77}$$

with $A = (y+1)/2$ and $B = (y-1)/2$ so that equation (4.76) formally proves that our identity (4.48) is true. The fact that the polynomial expansion (4.77) is true is indeed tricky to prove, but we do so in the following sections.

4.2.2 A Proof of a Polynomial Identity

In order to establish a formal proof of the polynomial expansion (4.77), we will require the following simple polynomial identity to hold:

$$\sum_{m=0}^{\lfloor \frac{n}{2} \rfloor} \frac{1}{2m+1} \binom{n}{2m} (B^{2m+1} A^{n-2m} - A^{2m+1} B^{n-2m}) = \begin{cases} \frac{-1}{n+1} & n \text{ even} \\ 0 & n \text{ odd} \end{cases} \tag{4.78}$$

with $A = (y+1)/2$ and $B = (y-1)/2$. In order to prove this result, we rewrite the left-hand side of (4.78) as

$$\begin{aligned} &\sum_{m=0}^{\lfloor \frac{n}{2} \rfloor} \frac{1}{2m+1} \binom{n}{2m} (B^{2m+1} A^{n-2m} - A^{2m+1} B^{n-2m}) \\ =&A^{n+1} \sum_{m=0}^{\lfloor \frac{n}{2} \rfloor} \frac{1}{2m+1} \binom{n}{2m} \frac{B^{2m+1}}{A^{2m+1}} + B^{n+1} \sum_{m=0}^{\lfloor \frac{n}{2} \rfloor} \frac{1}{2m+1} \binom{n}{2m} \frac{A^{2m+1}}{B^{2m+1}}. \end{aligned} \tag{4.79}$$

Next, let

$$x_1 = \frac{B}{A} \qquad \text{and} \qquad x_2 = \frac{A}{B}, \tag{4.80}$$

and define the quantity

$$S_i = \sum_{m=0}^{\lfloor \frac{n}{2} \rfloor} \binom{n}{2m} \frac{{x_i}^{2m+1}}{2m+1} \qquad i = 1, 2. \tag{4.81}$$

It is straightforward to see from (4.81) that

$$\frac{dS_i}{dx_i} = \sum_{m=0}^{\lfloor \frac{n}{2} \rfloor} \binom{n}{2m} {x_i}^{2m} \quad , \quad i = 1, 2. \tag{4.82}$$

Since there is no constant term x_i^0 in the expression (4.81), taking derivative with respect to x_i in (4.82) does not produce a loss of information (i.e., we can reverse this process by taking an antiderivative, and the associated constant of integration must vanish). With reference to equation (4.79), the left-hand side of (4.78) becomes

$$\sum_{m=0}^{\lfloor \frac{n}{2} \rfloor} \frac{1}{2m+1} \binom{n}{2m} (B^{2m+1} A^{n-2m} - A^{2m+1} B^{n-2m}) = A^{n+1} S_1 - B^{n+1} S_2 \tag{4.83}$$

It turns out that the sums on the right-hand side of equation (4.83) can be evaluated in closed form. We will do this for cases when n is even and n is odd. For $n = 2N$, the binomial theorem gives

$$\frac{dS_i}{dx_i} = \sum_{m=0}^{N} \binom{2N}{2m} {x_i}^{2m} = \frac{1}{2}((x_i + 1)^{2N} + (x_i - 1)^{2N}) \tag{4.84}$$

Taking the antiderivative of each side of (4.84) and setting the constant of integration to zero (as discussed above) we obtain for $n = 2N$ the result

$$S_i = \frac{(x_i + 1)^{n+1} + (x_i - 1)^{n+1}}{2(n+1)}. \tag{4.85}$$

Similarly, for $n = 2N + 1$ we have

$$\frac{dS_i}{dx_i} = \sum_{m=0}^{N} \binom{2N+1}{2m} {x_i}^{2m} = \frac{1}{2}((x_i + 1)^{2N+1} - (1 - x_i)^{2N+1}). \tag{4.86}$$

Taking the antiderivative of each side of (4.86) and again setting the constant of integration to zero (as discussed above) we obtain for $n = 2N + 1$ the result

$$S_i = \frac{(x_i + 1)^{n+1} - (1 - x_i)^{n+1}}{2(n+1)}. \tag{4.87}$$

Both results (4.85) and (4.87) can be combined in a single expression for n even or odd using

$$S_i = \frac{(x_i + 1)^{n+1} + (-1)^n (x_i - 1)^{n+1}}{2(n+1)}. \tag{4.88}$$

Using the definitions for x_i in equation (4.80) and our result (4.88), the right-hand side of equation (4.83) becomes

$$\begin{aligned}
&A^{n+1}S_1 - B^{n+1}S_2 \\
=&A^{n+1}\frac{(x_1+1)^{n+1}+(-1)^n(x_1-1)^{n+1}}{2(n+1)} - B^{n+1}\frac{(x_2+1)^{n+1}+(-1)^n(x_2-1)^{n+1}}{2(n+1)} \\
=&A^{n+1}\frac{(\frac{B}{A}+1)^{n+1}+(-1)^n(\frac{B}{A}-1)^{n+1}}{2(n+1)} - B^{n+1}\frac{(\frac{A}{B}+1)^{n+1}+(-1)^n(\frac{A}{B}-1)^{n+1}}{2(n+1)} \\
=&\frac{(B+A)^{n+1}+(-1)^n(B-A)^{n+1}}{2(n+1)} - \frac{(A+B)^{n+1}+(-1)^n(A-B)^{n+1}}{2(n+1)} \\
=&\frac{(-1)^n(B-A)^{n+1}-(-1)^n(A-B)^{n+1}}{2(n+1)}
\end{aligned} \tag{4.89}$$

Finally, since $A - B = 1$ in equation (4.71), equation (4.89) then yields

$$A^{n+1}S_1 - B^{n+1}S_2 = \frac{(-1)^n(-1)^{n+1}-(-1)^n}{2(n+1)} = \frac{-1-(-1)^n}{2(n+1)}. \tag{4.90}$$

From equation (4.90) via equation (4.83), it is now clear that our polynomial identity (4.78) holds.

4.2.3 A Proof of Polynomial Expansion

We now proceed to prove that the polynomial expansion (4.77) is true by examining in detail of the right-hand side. Using the definition for $Q_k(1)$ in (4.74) and reversing the order of summation in the right-hand side of equation (4.78) gives

$$R_n(y) = \sum_{k=0}^{n}\sum_{m=0}^{\lfloor\frac{k-1}{2}\rfloor}\frac{\binom{n}{k}(A^kB^{n-k}-B^kA^{n-k})}{2m+1} = \sum_{m=0}^{\lfloor\frac{n-1}{2}\rfloor}\frac{1}{2m+1}\sum_{k=2m+1}^{n}\binom{n}{k}(A^kB^{n-k}-B^kA^{n-k}) \tag{4.91}$$

with $A = (y+1)/2$ and $B = (y-1)/2$. A trivial rearrangement of the inner sum on the right-hand side of equation (4.91) gives

$$\sum_{k=2m+1}^{n}\binom{n}{k}(A^kB^{n-k}-B^kA^{n-k}) = \sum_{k=0}^{n}\binom{n}{k}(A^kB^{n-k}-B^kA^{n-k}) - \sum_{k=0}^{2m}\binom{n}{k}(A^kB^{n-k}-B^kA^{n-k}). \tag{4.92}$$

The first sum on the right-hand side of (4.92) can be explicitly evaluated by means of the binomial theorem. Indeed, we have

$$\sum_{k=0}^{n}\binom{n}{k}(A^kB^{n-k}-B^kA^{n-k}) = (A+B)^n - (B+A)^n = 0. \tag{4.93}$$

Hence the right-hand side of equation (4.77) can be written as

$$R_n(y) = \sum_{m=0}^{\lfloor \frac{n-1}{2} \rfloor} \frac{1}{2m+1} \sum_{k=0}^{2m} \binom{n}{k} (B^k A^{n-k} - A^k B^{n-k}) \tag{4.94}$$

with $A = (y+1)/2$ and $B = (y-1)/2$. Our goal with thus be to show that $R_n(y) = Q_n(y)$ for all $n \geq 0$. While it may be tempting as a quick avenue for a proof, in general it should be noted that

$$\sum_{k=0}^{2m} \binom{n}{k} (B^k A^{n-k} - A^k B^{n-k}) \neq y^{n-2m-1} \qquad 2m \leq n.$$

In order to establish that $R_n(y) = Q_n(y)$ we note that the polynomials $Q_n(y)$ in equation (4.50) have recursion relations

$$Q_{2N+2}(y) = yQ_{2N+1}(y), \qquad N \geq 0, \tag{4.95}$$

and

$$Q_{2N+1}(y) = yQ_{2N}(y) + \frac{1}{2N+1}, \qquad N \geq 0, \tag{4.96}$$

with starting values $Q_0(y) = 0$ and $Q_1(y) = 1$. Our method of proof will be to show that both $R_n(y)$ and $Q_n(y)$ share the same recursion relations and same starting values. If that is true, then by the uniqueness of solutions of linear recurrence relations (or equivalently by the principle of mathematical induction) these quantities must be the same for all $n \geq 0$.

First we show that recursion relation (4.95) also holds for $R_n(y)$. Noting from equation (4.71) that $y = A + B$ we have

$$\begin{aligned} &yR_{2N+1}(y) = (A+B)R_{2N+1}(y) \\ &= \sum_{m=0}^{N} \frac{1}{2m+1} \left[\sum_{k=0}^{2m} \binom{2N+1}{k} (B^k A^{2N-k+2} - A^k B^{2N-k+2}) \right] \\ &+ \sum_{m=0}^{N} \frac{1}{2m+1} \left[\sum_{k=0}^{2m} \binom{2N+1}{k} (B^{k+1} A^{2N-k+1} - A^{k+1} B^{2N-k+1}) \right] \end{aligned} \tag{4.97}$$

Next, we note that the inner sum in the middle line of equation (4.97) can be written as

$$\begin{aligned} &\sum_{k=0}^{2m} \binom{2N+1}{k} (B^k A^{2N-k+2} - A^k B^{2N-k+2}) \\ &= A^{2N+2} - B^{2N+2} + \sum_{k=1}^{2m} \binom{2N+1}{k} (B^k A^{2N-k+2} - A^k B^{2N-k+2}) \end{aligned} \tag{4.98}$$

Applying Pascal's rule for binomial coefficients, we have

$$\binom{2N+1}{k} + \binom{2N+1}{k-1} = \binom{2N+2}{k}. \tag{4.99}$$

Hence the sum in equation (4.98) becomes

$$\begin{aligned}
&\sum_{k=0}^{2m} \binom{2N+1}{k} (B^k A^{2N-k+2} - A^k B^{2N-k+2}) \\
&= \sum_{k=0}^{2m} \binom{2N+2}{k} (B^k A^{2N-k+2} - A^k B^{2N-k+2}) \\
&- \sum_{k=1}^{2m} \binom{2N+1}{k-1} (B^k A^{2N-k+2} - A^k B^{2N-k+2})
\end{aligned} \tag{4.100}$$

Adding and subtracting the term corresponding to $k = 2m+1$ in the last sum in equation (4.100), we then get

$$\begin{aligned}
&\sum_{k=0}^{2m} \binom{2N+1}{k} (B^k A^{2N-k+2} - A^k B^{2N-k+2}) \\
&= \sum_{k=0}^{2m} \binom{2N+2}{k} (B^k A^{2N-k+2} - A^k B^{2N-k+2}) \\
&- \sum_{k=1}^{2m+1} \binom{2N+1}{k-1} (B^k A^{2N-k+2} - A^k B^{2N-k+2}) \\
&+ \binom{2N+1}{2m} (B^{2m+1} A^{2N-2m+1} - A^{2m+1} B^{2N-2m+1})
\end{aligned} \tag{4.101}$$

The simple relabeling of indices $k-1 \to k$ in the last sum in equation (4.101) gives

$$\begin{aligned}
&\sum_{k=0}^{2m} \binom{2N+1}{k} (B^k A^{2N-k+2} - A^k B^{2N-k+2}) \\
&= \sum_{k=0}^{2m} \binom{2N+2}{k} (B^k A^{2N-k+2} - A^k B^{2N-k+2}) \\
&- \sum_{k=0}^{2m} \binom{2N+1}{k} (B^{k+1} A^{2N-k+1} - A^{k+1} B^{2N-k+1}) \\
&+ \binom{2N+1}{2m} (B^{2m+1} A^{2N-2m+1} - A^{2m+1} B^{2N-2m+1})
\end{aligned} \tag{4.102}$$

Finally, substituting (4.102) into equation (4.97) we, obtain immediately (due to the cancelation of sums)

$$\begin{aligned}
y R_{2N+1}(y) &= \sum_{m=0}^{N} \frac{1}{2m+1} \left[\sum_{k=0}^{2m} \binom{2N+2}{k} (B^k A^{2N-k+2} - A^k B^{2N-k+2}) \right] \\
&+ \sum_{m=0}^{N} \frac{1}{2m+1} \binom{2N+1}{2m} (B^{2m+1} A^{2N-2m+1} - A^{2m+1} B^{2N-2m+1})
\end{aligned} \tag{4.103}$$

It is easy to verify from equation (4.94) that

$$R_{2N+2}(y) = \sum_{m=0}^{N} \frac{1}{2m+1} \left[\sum_{k=0}^{2m} \binom{2N+2}{k} (B^k A^{2N-k+2} - A^k B^{2N-k+2}) \right]. \tag{4.104}$$

Further, it may be seen that the second sum in equation (4.103) vanishes as a result of our polynomial identity (4.78). From equations (4.103)(4.104) and (4.78), we have

$$R_{2N+2}(y) = yR_{2N+1}(y), \qquad N \geq 0. \tag{4.105}$$

Now we show that recursion relation (4.96) also holds for $R_n(y)$. Noting from equation (4.71) that $y = A + B$ we have

$$\begin{aligned} & yR_{2N}(y) = (A+B)R_{2N}(y) \\ & = \sum_{m=0}^{N-1} \frac{1}{2m+1} \left[\sum_{k=0}^{2m} \binom{2N}{k} (B^k A^{2N-k+1} - A^k B^{2N-k+1}) \right] \\ & + \sum_{m=0}^{N-1} \frac{1}{2m+1} \left[\sum_{k=0}^{2m} \binom{2N}{k} (B^{k+1} A^{2N-k} - A^{k+1} B^{2N-k}) \right]. \end{aligned} \tag{4.106}$$

Next, we note that, when explicitly extracting the $k = 0$ term, the inner sum in equation (4.106) can be written as

$$\begin{aligned} & \sum_{k=0}^{2m} \binom{2N}{k} (B^k A^{2N-k+1} - A^k B^{2N-k+1}) \\ & = A^{2N+1} - B^{2N+1} + \sum_{k=1}^{2m} \binom{2N}{k} (B^k A^{2N-k+1} - A^k B^{2N-k+1}). \end{aligned} \tag{4.107}$$

Applying Pascal's rule for binomial coefficients we have

$$\binom{2N}{k} + \binom{2N}{k-1} = \binom{2N+1}{k}. \tag{4.108}$$

Hence the sum in equation (4.107) becomes

$$\begin{aligned} & \sum_{k=0}^{2m} \binom{2N}{k} (B^k A^{2N-k+1} - A^k B^{2N-k+1}) \\ & = \sum_{k=0}^{2m} \binom{2N+1}{k} (B^k A^{2N-k+1} - A^k B^{2N-k+1}) \\ & - \sum_{k=1}^{2m} \binom{2N}{k-1} (B^k A^{2N-k+1} - A^k B^{2N-k+1}). \end{aligned} \tag{4.109}$$

Adding and subtracting the term corresponding to $k = 2m + 1$ in the last sum in equation (4.109) we then get

$$\begin{aligned}
&\sum_{k=0}^{2m} \binom{2N}{k} (B^k A^{2N-k+1} - A^k B^{2N-k+1}) \\
&= \sum_{k=0}^{2m} \binom{2N+1}{k} (B^k A^{2N-k+1} - A^k B^{2N-k+1}) \\
&- \sum_{k=1}^{2m+1} \binom{2N}{k-1} (B^k A^{2N-k+1} - A^k B^{2N-k+1}) \\
&+ \binom{2N}{2m} (B^{2m+1} A^{2N-2m} - A^{2m+1} B^{2N-2m}).
\end{aligned} \tag{4.110}$$

A simple relabeling of indices $k - 1 \to k$ in the last sum in equation (4.110) then gives

$$\begin{aligned}
&\sum_{k=0}^{2m} \binom{2N}{k} (B^k A^{2N-k+1} - A^k B^{2N-k+1}) \\
&= \sum_{k=0}^{2m} \binom{2N+1}{k} (B^k A^{2N-k+1} - A^k B^{2N-k+1}) \\
&- \sum_{k=0}^{2m} \binom{2N}{k} (B^{k+1} A^{2N-k} - A^{k+1} B^{2N-k}) \\
&+ \binom{2N}{2m} (B^{2m+1} A^{2N-2m} - A^{2m+1} B^{2N-2m}).
\end{aligned} \tag{4.111}$$

Finally, placing the result (4.111) back into equation (4.106) we obtain immediately (due to the cancelation of sums)

$$\begin{aligned}
yR_{2N}(y) &= \sum_{m=0}^{N-1} \frac{1}{2m+1} \left[\sum_{k=0}^{2m} \binom{2N+1}{k} (B^k A^{2N-k+1} - A^k B^{2N-k+1}) \right] \\
&+ \sum_{m=0}^{N-1} \frac{1}{2m+1} \binom{2N}{2m} (B^{2m+1} A^{2N-2m} - A^{2m+1} B^{2N-2m}).
\end{aligned} \tag{4.112}$$

Adding and subtracting the term corresponding to $m = N$, it is readily seen that the second sum in equation (4.112) may be rewritten as

$$\begin{aligned}
&\sum_{m=0}^{N-1} \frac{1}{2m+1} \binom{2N}{2m} (B^{2m+1} A^{2N-2m} - A^{2m+1} B^{2N-2m}) \\
&= -\frac{B^{2N+1} - A^{2N+1}}{2N+1} + \sum_{m=0}^{N} \frac{1}{2m+1} \binom{2N}{2m} (B^{2m+1} A^{2N-2m} - A^{2m+1} B^{2N-2m}).
\end{aligned} \tag{4.113}$$

Using our polynomial identity (4.78) to reduce the sum on the right-hand side of (4.113) we obtain

$$\sum_{m=0}^{N-1} \frac{1}{2m+1} \binom{2N}{2m} (B^{2m+1} A^{2N-2m} - A^{2m+1} B^{2N-2m}) = \frac{A^{2N+1} - B^{2N+1}}{2N+1} - \frac{1}{2N+1}. \tag{4.114}$$

To finish the proof, we note that the first sum in equation (4.112) can be written as

$$\begin{aligned}
&\sum_{m=0}^{N-1} \frac{1}{2m+1} \left[\sum_{k=0}^{2m} \binom{2N+1}{k} (B^k A^{2N-k+1} - A^k B^{2N-k+1}) \right] \\
&= \sum_{m=0}^{N} \frac{1}{2m+1} \left[\sum_{k=0}^{2m} \binom{2N+1}{k} (B^k A^{2N-k+1} - A^k B^{2N-k+1}) \right] \\
&- \frac{1}{2N+1} \sum_{k=0}^{2N} \binom{2N+1}{k} (B^k A^{2N-k+1} - A^k B^{2N-k+1}).
\end{aligned} \tag{4.115}$$

From equation (4.94) it may be seen that the first sum on the right-hand side of equation (4.115) is the polynomial $R_{2N+1}(y)$; the second sum can then be reduced by means of the binomial theorem to obtain

$$\sum_{m=0}^{N-1} \frac{1}{2m+1} \left[\sum_{k=0}^{2m} \binom{2N+1}{k} (B^k A^{2N-k+1} - A^k B^{2N-k+1}) \right] = R_{2N+1}(y) - \frac{A^{2N+1} - B^{2N+1}}{2N+1}. \tag{4.116}$$

Finally, combining the results in equations (4.112), (4.114) and (4.116) we obtain our desired result, namely,

$$R_{2N+1}(y) = yR_{2N}(y) + \frac{1}{2N+1}, \qquad N \geq 0. \tag{4.117}$$

We have thus show through the analysis leading to equations (4.105) and (4.117) that the polynomial $R_n(y)$ defined in (4.94) share the same recurrence relations as the polynomials $Q_n(y)$ defined in (4.50). Further, since it is easy to check that $R_0(y) = 0$ and $R_1(y) = 1$, these polynomials also share the same starting values. Thus, by the uniqueness of solutions of linear recurrence relations (or equivalently by the principle of mathematical induction), $Q_n(y) = R_n(y)$ for all $n \geq 0$. This firmly establishes the polynomial expansion (4.77) is correct, and in turn, establishes that the identity (4.48) is also true for all $n \geq 0$.

4.2.4 A Proof of New Chebyshev Identities (4.46) and (4.47)

We now turn to the main task of establishing the Chebyshev identities (4.46) and (4.47) using the simpler polynomial identities (4.48) and (4.49) we have established as true in the preceeding sections. As is well-known [18, 19] for $n > 0$ the Chebyshev polynomials have the explicit expansion

$$T_n(x) = \sum_{k=0}^{[n/2]} c_k^{(n)} x^{n-2k}, \tag{4.118}$$

where an expression for the coefficients given by Rivlin [19] is

$$c_k^{(n)} = (-1)^k \sum_{j=k}^{[n/2]} \binom{n}{2j} \binom{j}{k}. \tag{4.119}$$

Simpler formulas given by Mason and Handscomb [18] are

$$c_k^{(n)} = \frac{(-1)^k}{2^{2k-n+1}} \left[2\binom{n-k}{k} - \binom{n-k-1}{k} \right], \quad 2k < n. \tag{4.120}$$

and

$$c_k^{(2k)} = (-1)^k, \quad k \geq 0. \tag{4.121}$$

These, in turn, may be simplified to get [18] $c_0^{(0)} = 1$ and

$$c_k^{(n)} = \frac{(-1)^k}{2^{2k-n+1}} \frac{n}{n-k} \binom{n-k}{k}, \quad n > 0. \tag{4.122}$$

In both cases $|y| > 1$ and $|y| < 1$, summing (4.48) and (4.49) correspond to the Chebyshev coefficients $c_k^{(n)}$ results in

$$\int_{-1}^{1} \frac{T_n(x)}{y-x} dx = \sum_{k=0}^{[n/2]} c_k^{(n)} \int_{-1}^{1} \frac{x^{n-2k}}{y-x} dx = T_n(y) \ln\left(\frac{1+y}{1-y}\right) - 2L_n(y), \quad |y| < 1, \tag{4.123}$$

and

$$\int_{-1}^{1} \frac{T_n(x)}{y-x}\, dx = \sum_{k=0}^{[n/2]} c_k^{(n)} \int_{-1}^{1} \frac{x^{n-2k}}{y-x} dx = T_n(y) \ln\left(\frac{y+1}{y-1}\right) - 2L_n(y), \quad |y| > 1. \tag{4.124}$$

where

$$L_n(y) = \sum_{k=0}^{[n/2]} c_k^{(n)} Q_{n-2k}(y). \tag{4.125}$$

We thus see from equations (4.123) and (4.124) that for identities (4.46) and (4.47) to hold we must necessarily have

$$L_n(y) = H_n(y), \tag{4.126}$$

where

$$H_n(y) = 2 \sum_{k=1}^{[(n+1)/2]}{}' \frac{T_{n-2k+1}(y)}{2k-1}. \tag{4.127}$$

Again, the prime indicates that the coefficient associated with $T_0(x)$ is to be halved, if it appears. We will establish that (4.126) is true separately for cases when n is even and odd by direct proof.

We first consider the case when $n = 2N$ is an even positive integer. Since $Q_0(y) = 0$, for $N \geq 0$ we have

$$L_{2N}(y) = \sum_{k=0}^{N} c_k^{(2N)} Q_{2N-2k}(y) = \sum_{k=0}^{N-1} c_k^{(2N)} \sum_{m=0}^{N-k-1} \frac{y^{2N-2k-2m-1}}{2m+1}. \tag{4.128}$$

The sum clearly vanishes for $N = 0$. Using a simple series rearrangement technique [27], this double sum may then be rewritten as

$$L_{2N}(y) = \sum_{k=0}^{N-1} \left(\sum_{m=0}^{k} \frac{c_{k-m}^{(2N)}}{2m+1} \right) y^{2N-2k-1}. \tag{4.129}$$

Similarly, for $n = 2N$ we have

$$H_{2N}(y) = 2\sum_{k=1}^{N} \frac{T_{2N-2k+1}(y)}{2k-1} = 2\sum_{k=1}^{N} \frac{1}{2k-1} \sum_{m=0}^{N-k} c_m^{(2N-2k+1)} y^{2N-2k-2m+1}. \tag{4.130}$$

With the substitution $\ell = k - 1$ the expression (4.130) may then be written as

$$H_{2N}(y) = 2\sum_{\ell=0}^{N-1} \frac{1}{2\ell+1} \sum_{m=0}^{N-\ell-1} c_m^{(2N-2\ell-1)} y^{2N-2\ell-2m-1}. \tag{4.131}$$

Again, using a simple series rearrangement technique [27], the double sum in (4.131) may then be rewritten as

$$H_{2N}(y) = \sum_{\ell=0}^{N-1} \left(\sum_{m=0}^{\ell} \frac{2c_m^{(2N-2\ell+2m-1)}}{2\ell-2m+1} \right) y^{2N-2\ell-1}. \tag{4.132}$$

From equations (4.129) and (4.132) we see that enforcing $L_{2N}(y) = H_{2N}(y)$ (i.e. equating like-powers of y) thus requires the following identity to hold:

$$\sum_{m=0}^{k} \frac{c_{k-m}^{(2N)}}{2m+1} = 2\sum_{m=0}^{\ell} \frac{c_m^{(2N-2\ell+2m-1)}}{2\ell-2m+1}. \tag{4.133}$$

Further, setting $k = \ell + m$ in the sum on the right hand side of (4.133) and setting $N \to N+1$ in both sums then gives the required identity

$$\sum_{m=0}^{k} \frac{c_{k-m}^{(2N+2)}}{2m+1} = 2\sum_{m=0}^{k} \frac{c_{k-m}^{(2N-2m+1)}}{2m+1}, \qquad 0 \le k \le N \qquad N \ge 0 \tag{4.134}$$

To the best of our knowledge, equation (4.134) represents a new identity for the Chebyshev coefficients. It is straightforward to see this is true using the expansion (4.119) for the coefficients and reversing the order of either sum in (4.133).

Proceeding in close analogy to the analysis above, we now consider the case when $n = 2N + 1$ is an odd positive integer. It is not difficult to see that we have the expansions

$$L_{2N+1}(y) = \sum_{k=0}^{N} c_k^{(2N+1)} Q_{2N-2k+1}(y) = \sum_{k=0}^{N} c_k^{(2N+1)} \sum_{m=0}^{N-k} \frac{y^{2N-2k-2m}}{2m+1}. \tag{4.135}$$

Using a simple series rearrangement technique [27], this double sum may then be rewritten as

$$L_{2N+1}(y) = \sum_{k=0}^{N} \left(\sum_{m=0}^{k} \frac{c_{k-m}^{(2N+1)}}{2m+1} \right) y^{2N-2k}. \tag{4.136}$$

Similarly, for $n = 2N+1$ a positive odd integer we have

$$\begin{aligned} H_{2N+1}(y) &= \frac{T_0(y)}{2N+1} + 2\sum_{k=1}^{N} \frac{T_{2N-2k+2}(y)}{2k-1} \\ &= \frac{1}{2N+1} + 2\sum_{k=1}^{N} \frac{1}{2k-1} \sum_{m=0}^{N-k+1} c_m^{(2N-2k+2)} y^{2N-2k-2m+2}. \end{aligned} \tag{4.137}$$

Next, making the replacement $k = \ell + 1$ equation (4.137) gives

$$H_{2N+1}(y) = \frac{1}{2N+1} + 2\sum_{\ell=0}^{N-1} \frac{1}{2\ell+1} \sum_{m=0}^{N-\ell} c_m^{(2N-2\ell)} y^{2N-2\ell-2m}. \tag{4.138}$$

Notice that the term corresponding to $\ell = N$ in the sum in (4.138) would be $2c_0^{(0)}/(2N+1) = 2/(2N+1)$. Adding and subtracting this term from the right-hand side of equation (4.138) thus results in

$$H_{2N+1}(y) = -\frac{1}{2N+1} + 2\sum_{\ell=0}^{N} \frac{1}{2\ell+1} \sum_{m=0}^{N-\ell} c_m^{(2N-2\ell)} y^{2N-2\ell-2m}. \tag{4.139}$$

The point of this last manipulation is to bring the sum in equation (4.139) into the correct form so that standard series rearrangement [27] can be applied. Doing so results in the expansion

$$H_{2N+1}(y) = -\frac{1}{2N+1} + 2\sum_{\ell=0}^{N} \left(\sum_{m=0}^{\ell} \frac{c_m^{(2N-2\ell+2m)}}{2\ell-2m+1} \right) y^{2N-2\ell}. \tag{4.140}$$

From equations (4.136) and (4.140) we see that enforcing $L_{2N+1}(y) = H_{2N+1}(y)$ (equating like-powers of y) thus requires the following identities to hold:

$$2\sum_{m=0}^{k} \frac{c_m^{(2N-2k+2m)}}{2k-2m+1} = \sum_{m=0}^{k} \frac{c_{k-m}^{(2N+1)}}{2m+1} \quad , \quad 0 \le k < N \quad , \quad N > 0 \tag{4.141}$$

and

$$-\frac{1}{2N+1} + 2\sum_{m=0}^{N} \frac{c_m^{(2m)}}{2N-2m+1} = \sum_{m=0}^{N} \frac{c_{N-m}^{(2N+1)}}{2m+1} \quad , \quad k = N \quad , \quad N \ge 0. \tag{4.142}$$

Finally, making the replacements $k - m \to m$ in the sum on the left-hand side of (4.141) and $N - m \to m$ in the sum on the left-hand side of (4.142)

$$2\sum_{m=0}^{k} \frac{c_{k-m}^{(2N-2m)}}{2m+1} = \sum_{m=0}^{k} \frac{c_{k-m}^{(2N+1)}}{2m+1} \quad , \quad 0 \le k < N \quad , \quad N > 0 \tag{4.143}$$

and

$$-\frac{1}{2N+1}+2\sum_{m=0}^{N}\frac{c_{N-m}^{(2N-2m)}}{2m+1}=\sum_{m=0}^{N}\frac{c_{N-m}^{(2N+1)}}{2m+1}\quad,\quad k=N\quad,\quad N\geq 0, \tag{4.144}$$

respectively. Again, to the best of our knowledge, equations (4.143) and (4.144) represent new identities for the Chebyshev coefficients. It is straightforward to see these are true using the expansion (4.119) for the coefficients and reversing the order of the sums in (4.141) and (4.142).

We have thus established the equivalence of the polynomial expansions embodied by equation (4.126), and hence the validity of the Chebyshev identities (4.46) and (4.47).

4.2.5 Important Resulting Quadrature Formulas

Now that we have proved our main identities, we produce from equations (4.42), (4.43) and (4.44) some expressions to use in practice. In our numerical implementation, we specifically require evaluations of these integrals when the singularities lie at the interval endpoints. Finite results do exist at $y=\pm 1$ but limits have to be taken carefully as there is a cancelation of logarithmic singularities. We note that $w_n(-y)=(-1)^n w_n(y)$ so we only need to consider details for $w_n(1)$. Since $T_n(1)=1$, we have

$$\begin{aligned} w_n(1) &= \ln 2\left[\frac{1+(-1)^n}{1-n^2}\right]-\frac{2}{n+1}\sum_{k=1}^{[(n+2)/2]}\frac{1}{(2k-1)(1+\delta_{2k,n+2})} \\ &+ \frac{2}{n-1}\sum_{k=1}^{[n/2]}\frac{1}{(2k-1)(1+\delta_{2k,n})}, \end{aligned} \tag{4.145}$$

where $\delta_{k,n}$ is the Kronecker delta symbol. In particular, separating the results into contributions from even and odd indices, we have

$$w_{2n}(1)=\frac{2\ln 2}{1-4n^2}-\frac{4}{1-4n^2}\sum_{k=1}^{n}\frac{1}{2k-1}-\frac{2(4n^2+1)}{(2n-1)^2(2n+1)^2} \tag{4.146}$$

and

$$w_{2n+1}(1)=\frac{1}{n(n+1)}\sum_{k=1}^{n}\frac{1}{2k-1}-\frac{1}{(2n+1)(n+1)}. \tag{4.147}$$

Each of these equations, in turn, may be written in terms of the digamma function. We have

$$w_{2n}(1)=-\frac{2}{1-4n^2}\left[\Psi\left(n+\frac{1}{2}\right)+\ln 2+\gamma\right]-\frac{2(4n^2+1)}{(2n-1)^2(2n+1)^2} \tag{4.148}$$

and

$$w_{2n+1}(1) = \frac{1}{2n(n+1)}\left[\Psi\left(n+\frac{1}{2}\right) + 2\ln 2 + \gamma\right] - \frac{1}{(2n+1)(n+1)}, \tag{4.149}$$

where $\gamma = 0.57721566\ldots$ is Euler's constant and $\Psi(z)$ is the digamma function. We note that the digamma function can be written as a finite sum for half integer arguments, and is easily evaluated recursively. While we do not derive explicit results here, we can easily obtain large-n estimates from equations (4.148) and (4.149) using the well-known asypmtotic expansion of the digamma function [29, eqn. 6.3.18]

$$\Psi(z) \sim \ln z - \frac{1}{2z} - \sum_{m=1}^{\infty} \frac{B_{2m}}{2mz^{2m}} \tag{4.150}$$

where B_{2m} are the Bernoulli numbers.

Equations (4.148) and (4.149) are the basis for our numerical quadrature method to treat the singular integrals that arise when source and observation points lie on the same wire. We note that these expressions are easily evaluated to full machine precision. These expressions are an improvement on what has been previously used in the literature. In particular, in reference [11] the same quantities were produced using the formulas $w_0 = 2\ln 2 - 2$, $w_1 = -1$, and for $n > 1$,

$$w_n(1) = \frac{[1+(-1)^n]}{1-n^2}\ln 2 - 2n\sum_{m=0}^{n} \frac{(-1)^{n+m}2^{2n-2m}}{(n-m+1)(2n-m)}\binom{2n-m}{m}\left[\gamma + \Psi(n-m+2)\right]. \tag{4.151}$$

The formula (4.151) is mathematically correct, but but a direct implementation in finite precision arithmetic is ill-conditioned (and leads to total loss of accuracy for moderate values of the index n) due to addition and subtraction of very large numbers resulting from the binomial term. The authors of [11] dealt with this problem by pre-computing tables of values using symbolic software, storing them to file to be read in for each execution of their code. That is a little problematic since the code is then limited to whatever values were stored in the data file. Our new formulas completely remove this difficulty.

In this chapter, we also produced quadrature formulas applicable for the case when the observation point lies slightly outside the domain of integration, specifically equation (4.28). These, in turn, would be produced from (4.42), (4.43) and (4.44) for $y = 1 + \varepsilon$. Unfortunately, in this case we ran into significant numerical difficulties that we were not able to resolve. For $|x| > 1$ we represent $x = \cosh\theta$ and we have the Chebyshev

identity $T_n(\cosh\theta) = \cosh(n\theta)$; these terms clearly grow very rapidly (exponentially so) with increasing values of n. This very large growth in the terms in the sum in (4.47) were somehow canceled out by a similar growth in the logarithmic term, resulting in a numerically small quantity. This naturally led to very large subtractive cancelations and we were unable to produce a large set of these integration weights (4.28) to high accuracy. While we still believe this difficulty can be resolved with careful study of the problem, our current implementation of the code uses a simple local refinement, embodied in equations (4.29) and (4.30).

5 Results and Discussion

In previous chapters of this thesis we have developed an algorithm for computing the electromagnetic response of an array of thin wires. In this chapter we examine in detail the performance of the numerical implementation of our algorithm for various excitation frequencies ω and array spacings δ. Recall that ω (an angular frequency) is related to the ordinary frequency f (measured in Hz) via the formula $\omega = 2\pi f$; the wavelength of the radiated field is then given by $\lambda = c/f$ and the wavenumber is given by $k = 2\pi/\lambda$. In presenting results, we will generally specify frequencies f in MHz. The position z will be taken in units of meters (m) and the length of the wire array elements will be fixed at 2m in length. The radius of the wire will be fixed at $a = 0.01m$.

To add substance to our results, we assume that the array is illuminated by incident field in the form of a plane wave, i.e.

$$\mathbf{E}_{inc}(\mathbf{r}) = \frac{1}{\zeta_0}\mathbf{a}\mathrm{e}^{i\mathbf{k}\cdot\mathbf{r}}. \tag{5.1}$$

Here we denote $\zeta_0 = 120\pi\ \Omega$ the impedance of free space. Defining incident wave number k as above, the incident wave vector is given by

$$\mathbf{k} = k(\cos\theta\cos\phi, \sin\theta\sin\phi, \sin\phi), \tag{5.2}$$

where θ is the azimuth angle and ϕ elevation angle. Further, defining the polarization angle ψ, the unit amplitude vector is defined as

$$\mathbf{a} = \cos\psi\mathbf{v} + \sin\psi\mathbf{h}; \tag{5.3}$$

the horizontal and vertical polarization vectors are

$$\mathbf{h} = \frac{\mathbf{k}\times\mathbf{z}}{||\mathbf{k}\times\mathbf{z}||} \quad \text{and} \quad \mathbf{v} = \frac{\mathbf{k}\times\mathbf{h}}{||\mathbf{k}\times\mathbf{h}||}, \tag{5.4}$$

respectively. In the results presented in this chapter we fix all of these angles as $\theta = \pi/4$, $\phi = \pi/6$ and $\psi = 0$.

In this section the estimated relative errors (as a function of wire position) are given by

$$\text{error}(z) = \frac{|J(z) - J^*(z)|}{\max|J^*(z)|} \tag{5.5}$$

where the reference data sets $J^*(z)$ are fully-resolved solutions obtained from very fine discretizations. In this work, we compute this error function on grids involving 1000 evaluation points per wire. The maximum relative error e_{max} reported in the data tables contained in this chapter is defined as

$$e_{max} = \max\{\text{error}(z)\}. \tag{5.6}$$

Some details concerning the accurate evaluation of the total current $J_i(z) = I_i(z)/\sqrt{1-z^2}$ from the reduced current $I_i(z)$ are important to understand. Clearly, a straightforward division does give rise to significant error increases—unbounded, in fact, as the evaluation points tend toward the end-points at $z = \pm 1$. To resolve this difficulty it is convenient to rewrite $J_i(z)$ in terms of a trigonometric series, and avoid the explicit division by the quantity $\sqrt{1-z^2}$. With the substitution $z = \cos\theta$ in equations (3.45) and (3.46) we see that we can write

$$J_i(\cos\theta) = \sum_{n=1}^{N} c_n^{(i)} \sin(n\theta) = \frac{1}{\sin\theta} \sum_{n=0}^{N-1}{}' b_n^{(i)} \cos(n\theta) \tag{5.7}$$

multiplying each side of equation (5.7) by $\sin\theta$ and applying orthogonality relations of the resulting trigonometric functions gives $c_1^{(i)} = b_0^{(i)}$, $c_2^{(i)} = 2b_1^{(i)}$ and

$$c_{n+1}^{(i)} = 2b_n^{(i)} + c_{n-1}^{(i)} \qquad 2 \le n \le N-1. \tag{5.8}$$

The coefficients $c_n^{(i)}$ for $n \ge 2$ are easily found by forward recursion using equation (5.8). Using the sine series representation for the current in (5.7) we may now evaluate these functions everywhere on a fine mesh in order to accurately estimate the relative errors as discussed above.

In what follows in this chapter we examine the convergence rates of our algorithms with increasing numbers of Chebyshev modes retained in the expansions for the unknown currents of the problem. We also present code execution times with parameters used in the numerical integration routines. We do this for

N	M_1	M_2	M_3	e_{max}	t_{exe} (s)
20	2^5	2^5	2^5	7.03×10^{-1}	0.07
40	2^5	2^5	2^5	1.34×10^{-4}	0.16
60	2^6	2^5	2^5	3.28×10^{-6}	0.38
80	2^6	2^5	2^5	3.53×10^{-7}	0.59
100	2^6	2^5	2^5	4.75×10^{-8}	0.82
120	2^6	2^5	2^5	4.12×10^{-9}	1.12
140	2^6	2^5	2^5	5.87×10^{-10}	1.51
160	2^6	2^6	2^6	1.71×10^{-11}	2.42
180	2^6	2^6	2^6	3.74×10^{-12}	3.06

Table 5.1: Code parameters, errors and execution times for $f = 1000$ MHz and $\delta = 5a$. Errors were computed from reference case $N = 600$, $M_1 = M_2 = M_3 = 2^9$. The splitting parameter for the integration domain decomposition was fixed at $\Delta = 10a$ in all runs.
.

three cases of frequency $f = 1000$ MHz, $f = 500$ MHz and $f = 100$ MHz, which we take as high, moderate and low frequency cases, respectively. For each case of frequency we also examine the effect of the array spacing δ on the solutions. We consider cases $\delta = 5a$, $\delta = 10a$, $\delta = 20a$ and $\delta = 100a$, where again, $a = 0.01m$ is the wire radius. All computations presented here were performed on an AMD Opteron 6366 HE 1.8GHz server. Solutions of all linear systems were obtained by means of the LU-based direct solvers provided in the LAPACK linear algebra package (www.netlib.org/lapack/).

5.1 High Frequency Results

We consider the electromagnetic response of the wire array at high frequency $f = 1000$ MHz and several wire spacings δ. Code performance data corresponding to high frequency and $\delta = 5a$ is presented in Table 5.1. We note the extremely rapid convergence in the solution (superalgebraic convergence) for increasing number of Cheyshev modes N retained in the problem. Execution times are also very small, with single precision accuracies achieved in less than one second with $N = 100$ Chebyshev modes. Accuracies nearing double precision are obtained in three second computing times using $N = 180$ Chebyshev modes. Plots of the current along each wire are shown in Figure 5.1. Both wires are extremely close together in this case, and there is substantial electromagnetic interaction between the two.

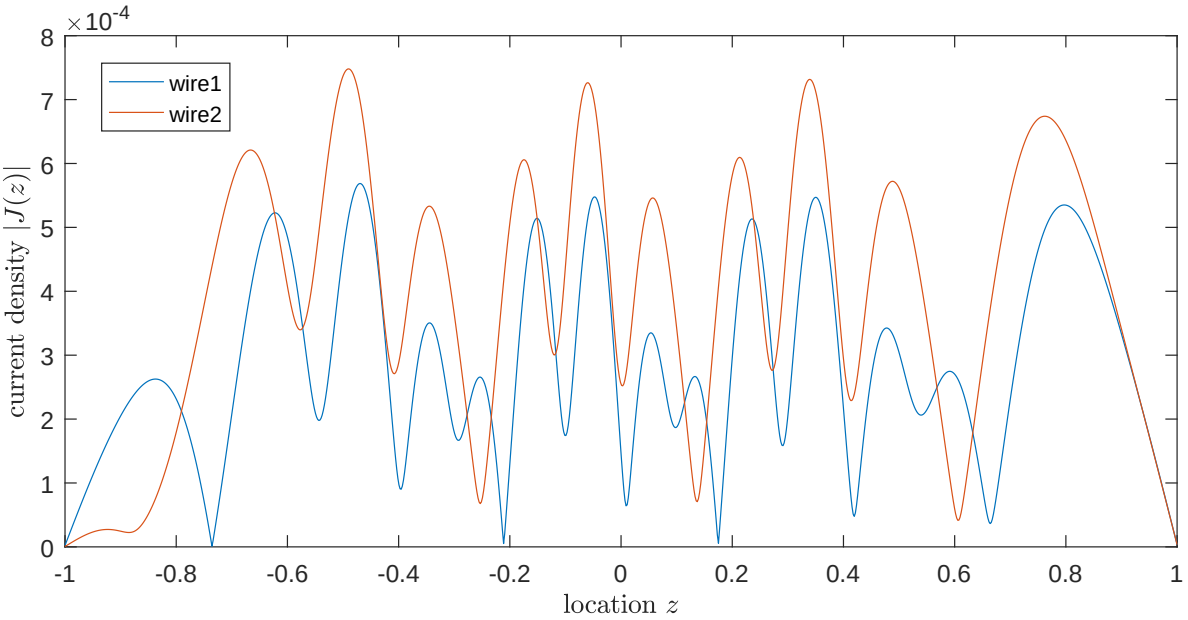

Figure 5.1: Profiles of the current density $J(z)$ for case $f = 1000$ MHz and $\delta = 5a$. The data was computed from the reference case $N = 600$, $M_1 = M_2 = M_3 = 2^9$.

Code performance data corresponding to high frequency and $\delta = 10a$ is presented in Table 5.2. Again, we note the superalgebraic convergence in the solution for increasing number of Cheyshev modes N retained in the problem. Execution times are also very small, with single precision accuracies achieved in less than one second with $N = 100$ Chebyshev modes. Accuracies nearing double precision are obtained using $N = 180$ Chebyshev modes in just over three seconds. Plots of the current along each wire are shown in Figure 5.2. Both wires are spaced further apart than in the previous case, but still substantial interaction between the two wires may be seen.

Code performance data corresponding to high frequency and $\delta = 20a$ is presented in Table 5.3. Again, we note the superalgebraic convergence in the solution for increasing number of Cheyshev modes N retained in the problem. Execution times are also very small, with single precision accuracies achieved in less than one second with $N = 100$ Chebyshev modes. Accuracies nearing double precision are obtained in just over three second computing times using $N = 180$ Chebyshev modes. Plots of the current along each wire are shown in Figure 5.3. Both wires are spaced further apart than in the previous case, and now the interaction

N	M_1	M_2	M_3	e_{max}	t_{exe} (s)
20	2^5	2^5	2^5	7.11×10^{-1}	0.07
40	2^5	2^5	2^5	1.88×10^{-4}	0.17
60	2^6	2^5	2^5	3.39×10^{-6}	0.39
80	2^6	2^5	2^5	3.06×10^{-7}	0.61
100	2^6	2^5	2^5	4.22×10^{-8}	0.87
120	2^6	2^5	2^5	3.68×10^{-9}	1.18
140	2^6	2^5	2^5	5.40×10^{-10}	1.53
160	2^6	2^6	2^6	1.48×10^{-11}	2.47
180	2^6	2^6	2^6	2.77×10^{-12}	3.10

Table 5.2: Code parameters, errors and execution times for $f = 1000$ MHz and $\delta = 10a$. Errors were computed from reference case $N = 600$, $M_1 = M_2 = M_3 = 2^9$. The splitting parameter for the integration domain decomposition was fixed at $\Delta = 10a$ in all runs.
.

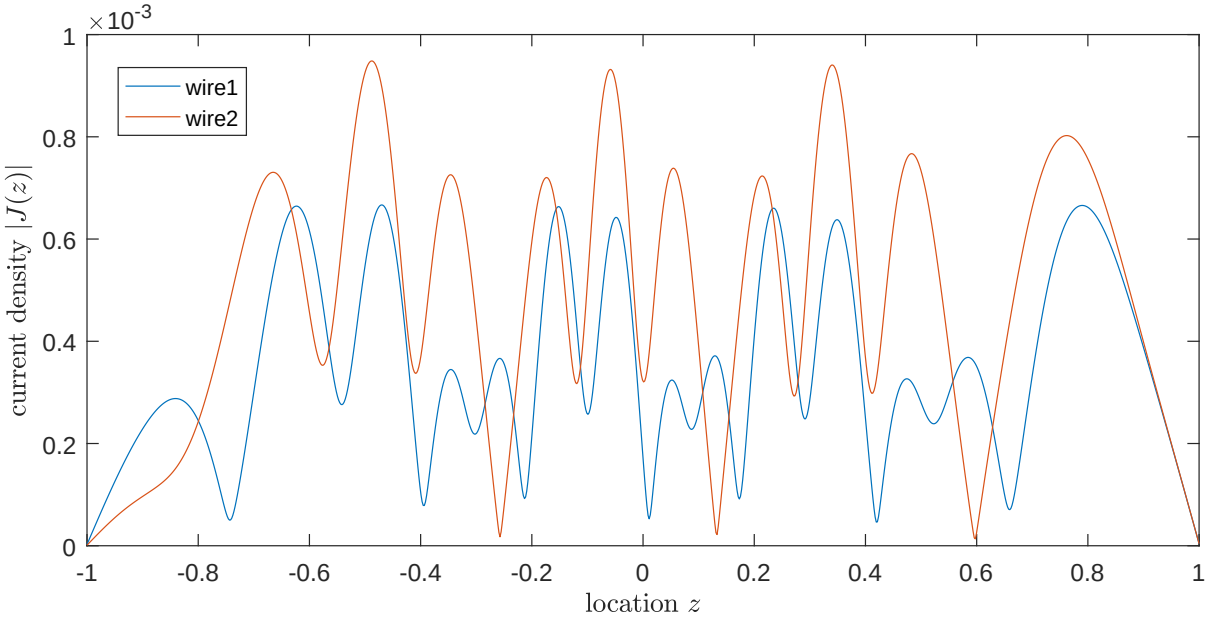

Figure 5.2: Profiles of the current density $J(z)$ for case $f = 1000$ MHz and $\delta = 10a$. The data was computed from the reference case $N = 600$, $M_1 = M_2 = M_3 = 2^9$.

N	M_1	M_2	M_3	e_{max}	t_{exe} (s)
20	2^5	2^5	2^5	7.42×10^{-1}	0.09
40	2^5	2^5	2^5	2.82×10^{-4}	0.18
60	2^6	2^5	2^5	4.41×10^{-6}	0.42
80	2^6	2^5	2^5	3.87×10^{-7}	0.65
100	2^6	2^5	2^5	5.37×10^{-8}	0.91
120	2^6	2^5	2^5	4.68×10^{-9}	1.27
140	2^6	2^5	2^5	6.70×10^{-10}	1.56
160	2^6	2^6	2^6	2.07×10^{-11}	2.61
180	2^6	2^6	2^6	8.31×10^{-12}	3.25

Table 5.3: Code parameters, errors and execution times for $f = 1000$ MHz and $\delta = 20a$. Errors were computed from reference case $N = 600$, $M_1 = M_2 = M_3 = 2^9$. The splitting parameter for the integration domain decomposition was fixed at $\Delta = 10a$ in all runs.
.

between the two wires is weaker than in previous cases.

Code performance data corresponding to high frequency and $\delta = 100a$ is presented in Table 5.4. Again, we note the superalgebraic convergence in the solution for increasing number of Cheyshev modes N retained in the problem. Execution times are also very small, with single precision accuracies achieved in less than one second with $N = 100$ Chebyshev modes. Accuracies nearing double precision are obtained in under four second computing times using $N = 180$ Chebyshev modes. Plots of the current along each wire are shown in Figure 5.4. Both wires are spaced further apart than in the previous case, and now it appears there is virtually no electromagnetic interaction between the wires; i.e, they behave as though there are no other wires in their vicinity, effectively producing the response of a single straight wire to the incident field.

5.2 Moderate Frequency Results

We consider the electromagnetic response of the wire array at moderate frequency $f = 500$ MHz and several wire spacings δ. Code performance data corresponding to high frequency and $\delta = 5a$ is presented in Table 5.5. We note the extremely rapid convergence in the solution (superalgebraic convergence) for increasing number of Cheyshev modes N retained in the problem. Execution times are also very small, with single precision accuracies achieved in one half second with $N = 100$ Chebyshev modes. Accuracies nearing double

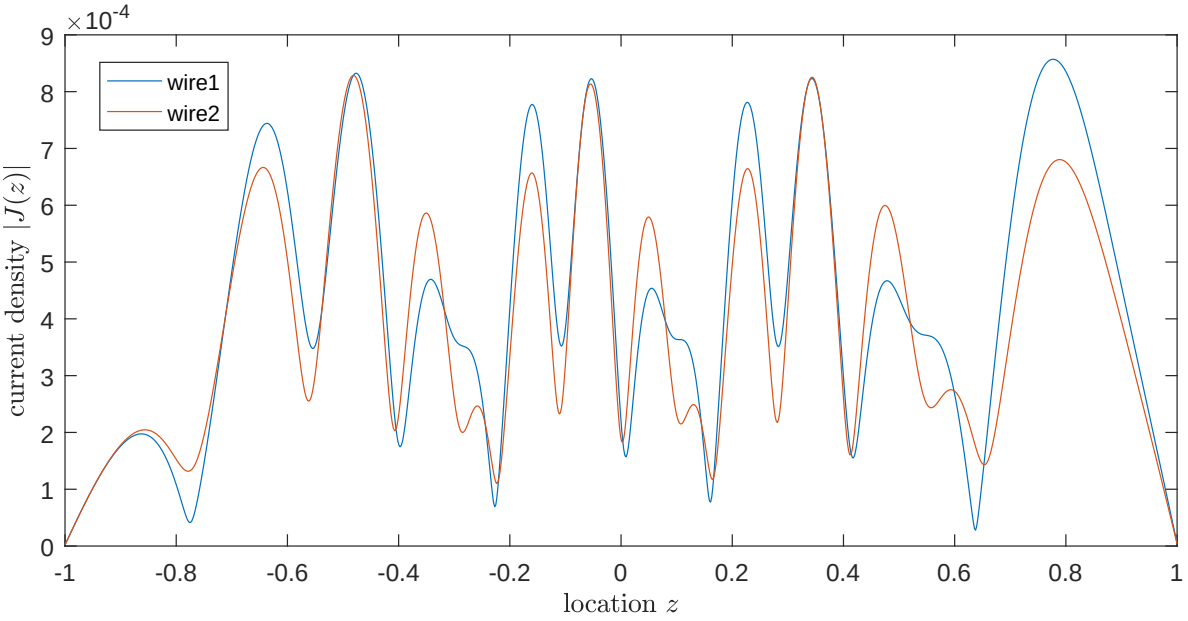

Figure 5.3: Profiles of the current density $J(z)$ for case $f = 1000$ MHz and $\delta = 20a$. The data was computed from the reference case $N = 600$, $M_1 = M_2 = M_3 = 2^9$.

N	M_1	M_2	M_3	e_{max}	t_{exe} (s)
20	2^5	2^5	2^5	6.54×10^{-1}	0.10
40	2^5	2^5	2^5	1.99×10^{-4}	0.24
60	2^6	2^5	2^5	3.90×10^{-6}	0.60
80	2^6	2^5	2^5	3.55×10^{-7}	0.83
100	2^6	2^5	2^5	4.89×10^{-8}	1.12
120	2^6	2^5	2^5	4.26×10^{-9}	1.47
140	2^6	2^5	2^5	6.06×10^{-10}	1.89
160	2^6	2^6	2^6	1.65×10^{-11}	3.19
180	2^6	2^6	2^6	1.92×10^{-11}	3.82

Table 5.4: Code parameters, errors and execution times for $f = 1000$ MHz and $\delta = 100a$. Errors were computed from reference case $N = 600$, $M_1 = M_2 = M_3 = 2^9$. The splitting parameter for the integration domain decomposition was fixed at $\Delta = 10a$ in all runs.

.

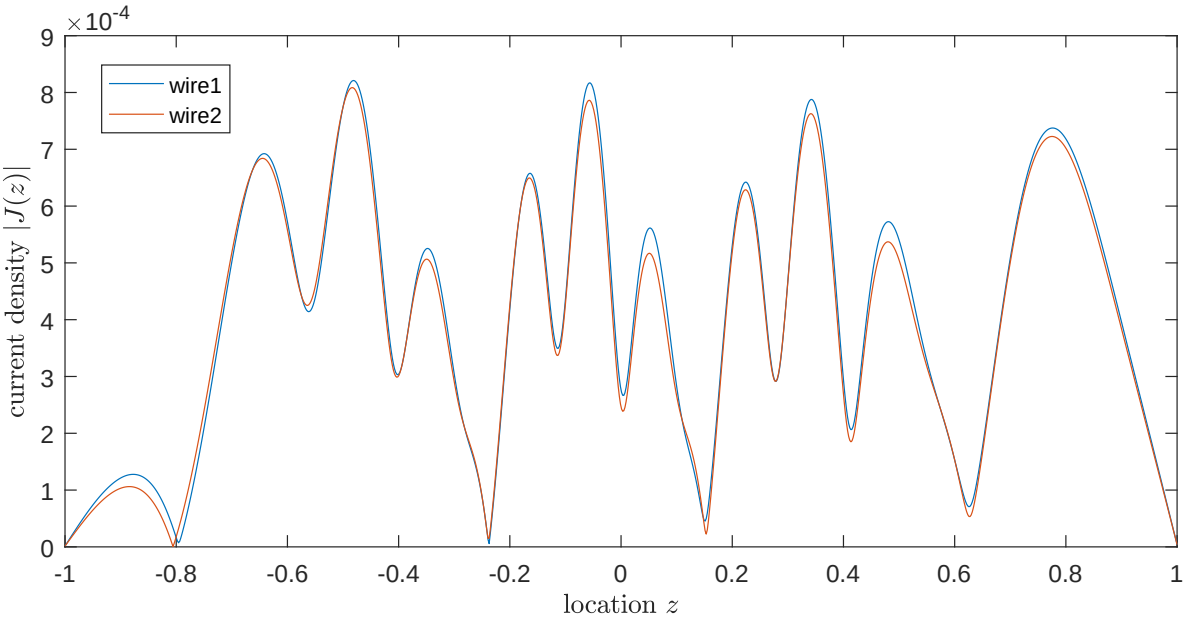

Figure 5.4: Profiles of the current density $J(z)$ for case $f = 1000$ MHz and $\delta = 100a$. The data was computed from the reference case $N = 600$, $M_1 = M_2 = M_3 = 2^9$.

precision are obtained in under three second computing times using $N = 180$ Chebyshev modes. Plots of the current along each wire are shown in Figure 5.5. Both wires are extremely close together in this case, and there is substantial electromagnetic interaction between the two.

Code performance data corresponding to moderate frequency and $\delta = 10a$ is presented in Table 5.6. Again, we note the superalgebraic convergence in the solution for increasing number of Cheyshev modes N retained in the problem. Execution times are also very small, with single precision accuracies achieved in just over a half second with $N = 100$ Chebyshev modes. Accuracies nearing double precision are obtained using $N = 180$ Chebyshev modes in under three seconds. Plots of the current along each wire are shown in Figure 5.6. Both wires are spaced further apart than in the previous case, but still substantial interaction between the two wires may be seen.

Code performance data corresponding to moderate frequency and $\delta = 20a$ is presented in Table 5.7. Again, we note the superalgebraic convergence in the solution for increasing number of Cheyshev modes N

N	M_1	M_2	M_3	e_{max}	t_{exe} (s)
20	2^4	2^4	2^4	6.21×10^{-3}	0.04
40	2^4	2^4	2^4	2.59×10^{-4}	0.08
60	2^5	2^4	2^4	2.52×10^{-6}	0.20
80	2^5	2^5	2^5	2.48×10^{-7}	0.38
100	2^5	2^5	2^5	3.20×10^{-8}	0.54
120	2^6	2^5	2^5	2.54×10^{-9}	1.10
140	2^6	2^5	2^5	2.12×10^{-10}	1.34
160	2^6	2^6	2^6	1.12×10^{-11}	2.20
180	2^6	2^6	2^6	3.29×10^{-12}	2.75

Table 5.5: Code parameters, errors and execution times for $f = 500$ MHz and $\delta = 5a$. Errors were computed from reference case $N = 400$, $M_1 = M_2 = M_3 = 2^8$. The splitting parameter for the integration domain decomposition was fixed at $\Delta = 10a$ in all runs.

.

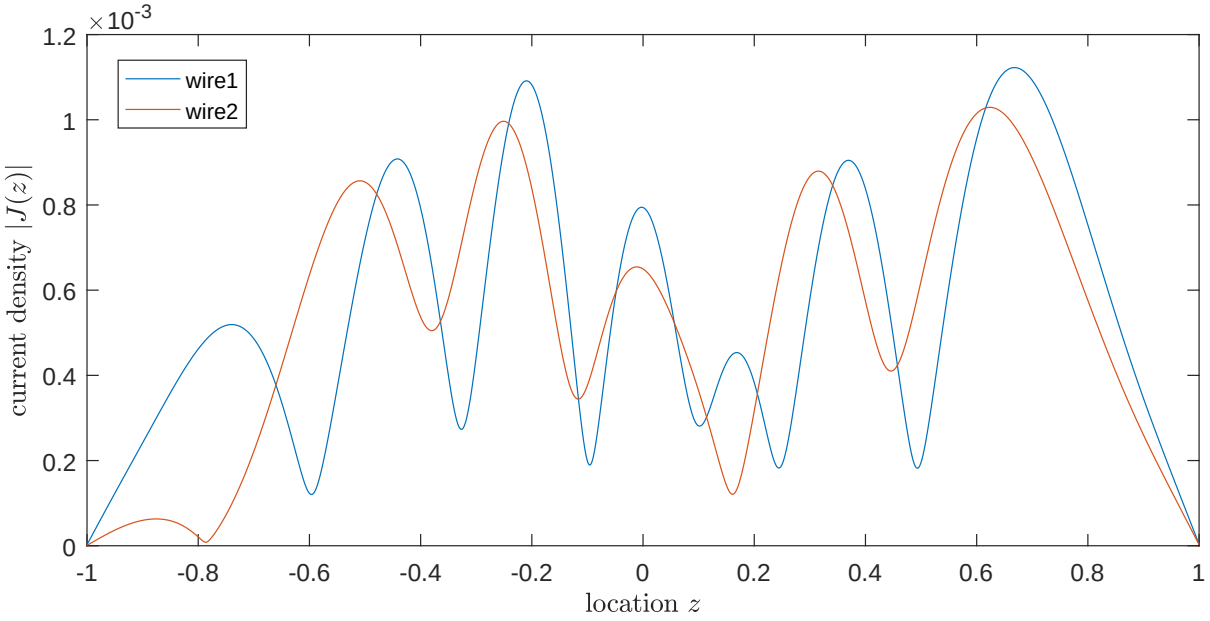

Figure 5.5: Profiles of the current density $J(z)$ for case $f = 500$ MHz and $\delta = 5a$. The data was computed from the reference case $N = 400$, $M_1 = M_2 = M_3 = 2^8$.

N	M_1	M_2	M_3	e_{max}	t_{exe} (s)
20	2^4	2^4	2^4	7.05×10^{-3}	0.04
40	2^4	2^4	2^4	2.73×10^{-4}	0.08
60	2^5	2^4	2^4	2.41×10^{-6}	0.20
80	2^5	2^5	2^5	2.35×10^{-7}	0.39
100	2^5	2^5	2^5	3.06×10^{-8}	0.55
120	2^6	2^5	2^5	2.45×10^{-9}	1.11
140	2^6	2^5	2^5	2.25×10^{-10}	1.37
160	2^6	2^6	2^6	1.03×10^{-11}	2.22
180	2^6	2^6	2^6	3.18×10^{-12}	2.77

Table 5.6: Code parameters, errors and execution times for $f = 500$ MHz and $\delta = 10a$. Errors were computed from reference case $N = 400$, $M_1 = M_2 = M_3 = 2^8$. The splitting parameter for the integration domain decomposition was fixed at $\Delta = 10a$ in all runs.

.

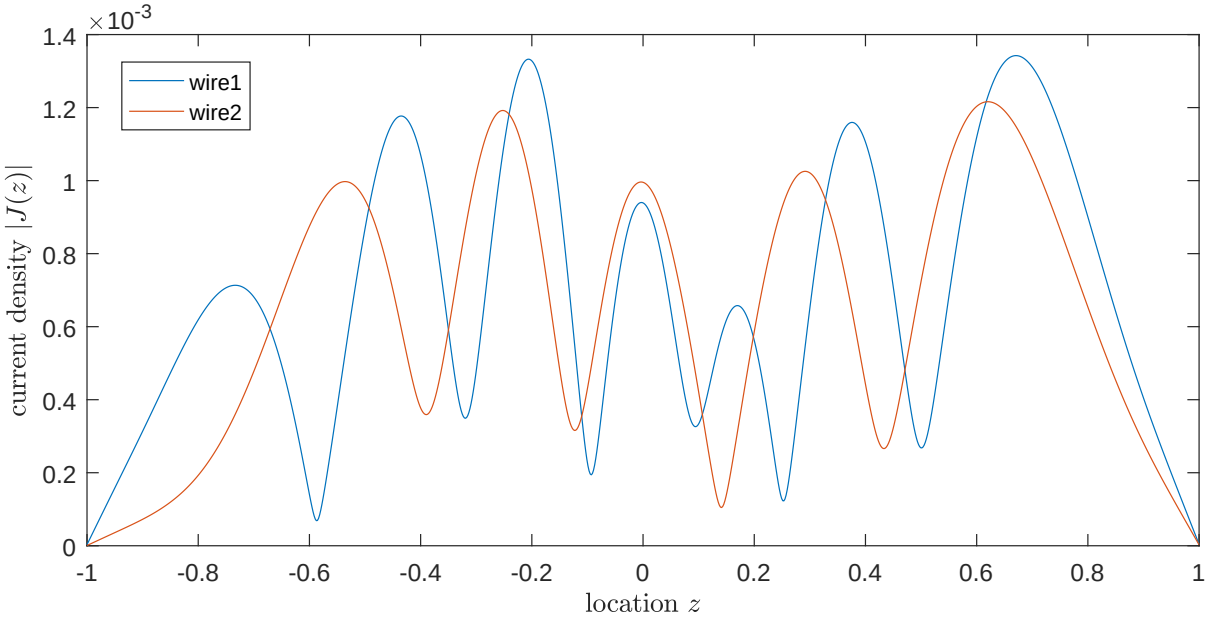

Figure 5.6: Profiles of the current density $J(z)$ for case $f = 500$ MHz and $\delta = 10a$. The data was computed from the reference case $N = 400$, $M_1 = M_2 = M_3 = 2^8$.

N	M_1	M_2	M_3	e_{max}	t_{exe} (s)
20	2^4	2^4	2^4	7.21×10^{-3}	0.04
40	2^4	2^4	2^4	2.43×10^{-4}	0.09
60	2^5	2^4	2^4	2.45×10^{-6}	0.21
80	2^5	2^5	2^5	2.10×10^{-7}	0.43
100	2^5	2^5	2^5	2.70×10^{-8}	0.60
120	2^6	2^5	2^5	2.24×10^{-9}	1.15
140	2^6	2^5	2^5	1.87×10^{-10}	1.45
160	2^6	2^6	2^6	8.89×10^{-12}	2.37
180	2^6	2^6	2^6	3.79×10^{-12}	2.94

Table 5.7: Code parameters, errors and execution times for $f = 500$ MHz and $\delta = 20a$. Errors were computed from reference case $N = 400$, $M_1 = M_2 = M_3 = 2^8$. The splitting parameter for the integration domain decomposition was fixed at $\Delta = 10a$ in all runs.
.

retained in the problem. Execution times are also very small, with single precision accuracies achieved in just over one second with $N = 100$ Chebyshev modes. Accuracies nearing double precision are obtained in under three second computing times using $N = 180$ Chebyshev modes. Plots of the current along each wire are shown in Figure 5.7. Both wires are spaced further apart than in the previous case, but there is still substantial interaction between the wires.

Code performance data corresponding to moderate frequency and $\delta = 100a$ is presented in Table 5.8. Again, we note the superalgebraic convergence in the solution for increasing number of Cheyshev modes N retained in the problem. Execution times are also very small, with single precision accuracies achieved in less than one second with $N = 100$ Chebyshev modes. Accuracies nearing double precision are obtained in under four second computing times using $N = 180$ Chebyshev modes. Plots of the current along each wire are shown in Figure 5.8. Both wires are spaced further apart than in the previous case, and now it appears there is virtually no electromagnetic interaction between the wires; i.e, they behave as though there are no other wires in their vicinity, effectively producing the response of a single straight wire to the incident field.

5.3 Low Frequency Results

We consider the electromagnetic response of the wire array at low frequency $f = 100$ MHz and several wire spacings δ. Code performance data corresponding to high frequency and $\delta = 5a$ is presented in Table 5.9.

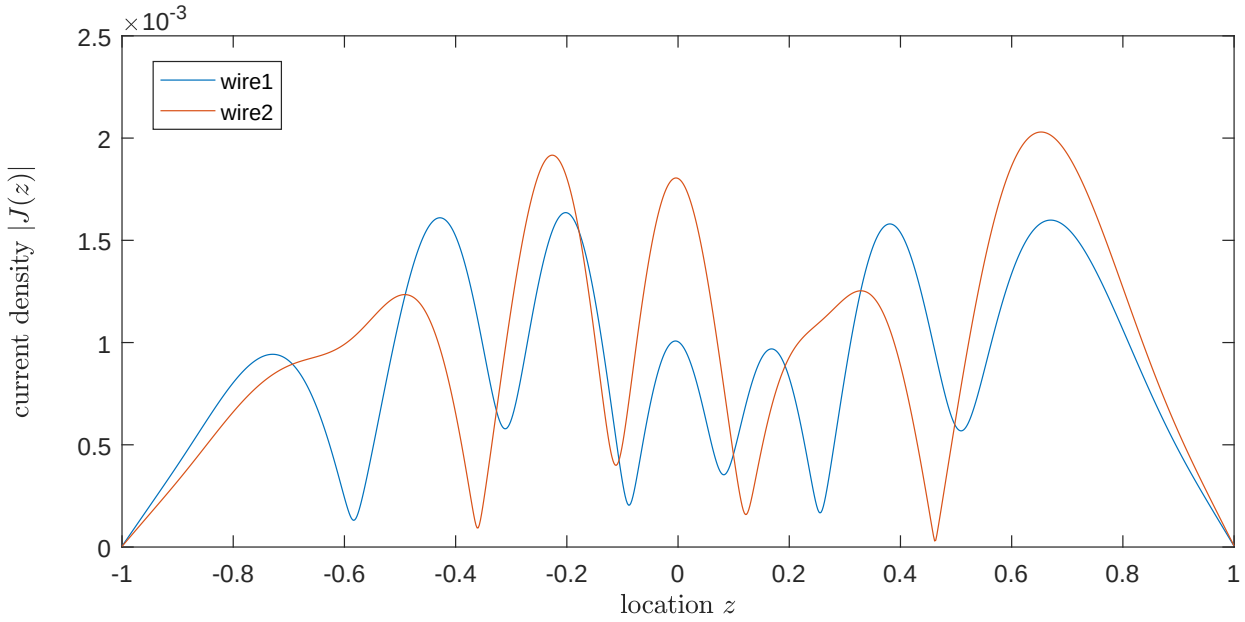

Figure 5.7: Profiles of the current density $J(z)$ for case $f = 500$ MHz and $\delta = 20a$. The data was computed from the reference case $N = 400$, $M_1 = M_2 = M_3 = 2^8$.

N	M_1	M_2	M_3	e_{max}	t_{exe} (s)
20	2^4	2^4	2^4	5.71×10^{-3}	0.05
40	2^4	2^4	2^4	2.17×10^{-4}	0.11
60	2^5	2^4	2^4	2.46×10^{-6}	0.27
80	2^5	2^5	2^5	1.97×10^{-7}	0.54
100	2^5	2^5	2^5	2.64×10^{-8}	0.73
120	2^6	2^5	2^5	2.09×10^{-9}	1.37
140	2^6	2^5	2^5	1.55×10^{-10}	1.72
160	2^6	2^6	2^6	8.89×10^{-12}	2.81
180	2^6	2^6	2^6	5.32×10^{-12}	3.39

Table 5.8: Code parameters, errors and execution times for $f = 500$ MHz and $\delta = 100a$. Errors were computed from reference case $N = 400$, $M_1 = M_2 = M_3 = 2^8$. The splitting parameter for the integration domain decomposition was fixed at $\Delta = 10a$ in all runs.

.

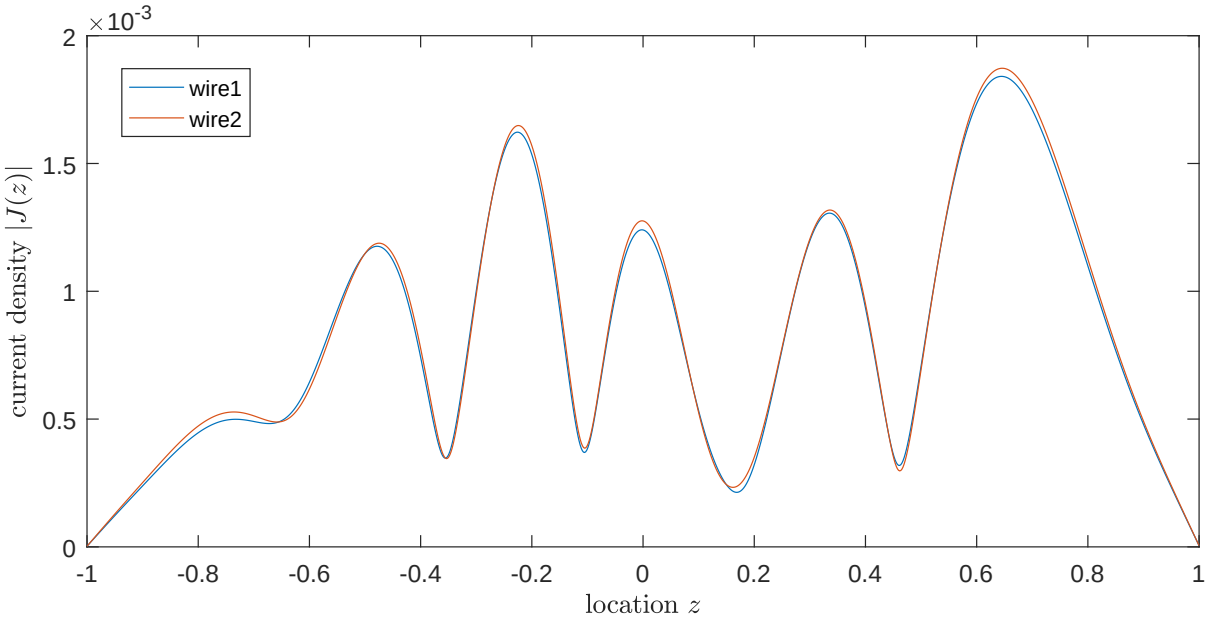

Figure 5.8: Profiles of the current density $J(z)$ for case $f = 500$ MHz and $\delta = 100a$. The data was computed from the reference case $N = 400$, $M_1 = M_2 = M_3 = 2^8$.

We note the extremely rapid convergence in the solution (superalgebraic convergence) for increasing number of Cheyshev modes N retained in the problem. Execution times are also very small, with single precision accuracies achieved in under one half second with $N = 80$ Chebyshev modes. Accuracies nearing double precision are obtained in under three second computing times using $N = 180$ Chebyshev modes. Plots of the current along each wire are shown in Figure 5.9. Both wires are extremely close together in this case, and there is substantial electromagnetic interaction between the two.

Code performance data corresponding to moderate frequency and $\delta = 10a$ is presented in Table 5.10. Again, we note the superalgebraic convergence in the solution for increasing number of Cheyshev modes N retained in the problem. Execution times are also very small, with single precision accuracies achieved in under a half second with $N = 80$ Chebyshev modes. Accuracies nearing double precision are obtained using $N = 180$ Chebyshev modes in under three seconds. Plots of the current along each wire are shown in Figure 5.10. Both wires are spaced further apart than in the previous case, but still substantial interaction between

N	M_1	M_2	M_3	e_{max}	t_{exe} (s)
20	2^4	2^3	2^3	1.68×10^{-3}	0.02
40	2^4	2^4	2^4	3.70×10^{-5}	0.08
60	2^4	2^4	2^4	3.40×10^{-6}	0.13
80	2^5	2^5	2^5	7.11×10^{-8}	0.38
100	2^5	2^5	2^5	9.36×10^{-9}	0.52
120	2^5	2^5	2^5	6.69×10^{-10}	0.72
140	2^6	2^5	2^5	4.11×10^{-11}	1.31
160	2^6	2^6	2^6	3.82×10^{-12}	2.19
180	2^6	2^6	2^6	1.15×10^{-12}	2.63

Table 5.9: Code parameters, errors and execution times for $f = 100$ MHz and $\delta = 5a$. Errors were computed from reference case $N = 400$, $M_1 = M_2 = M_3 = 2^8$. The splitting parameter for the integration domain decomposition was fixed at $\Delta = 10a$ in all runs.

.

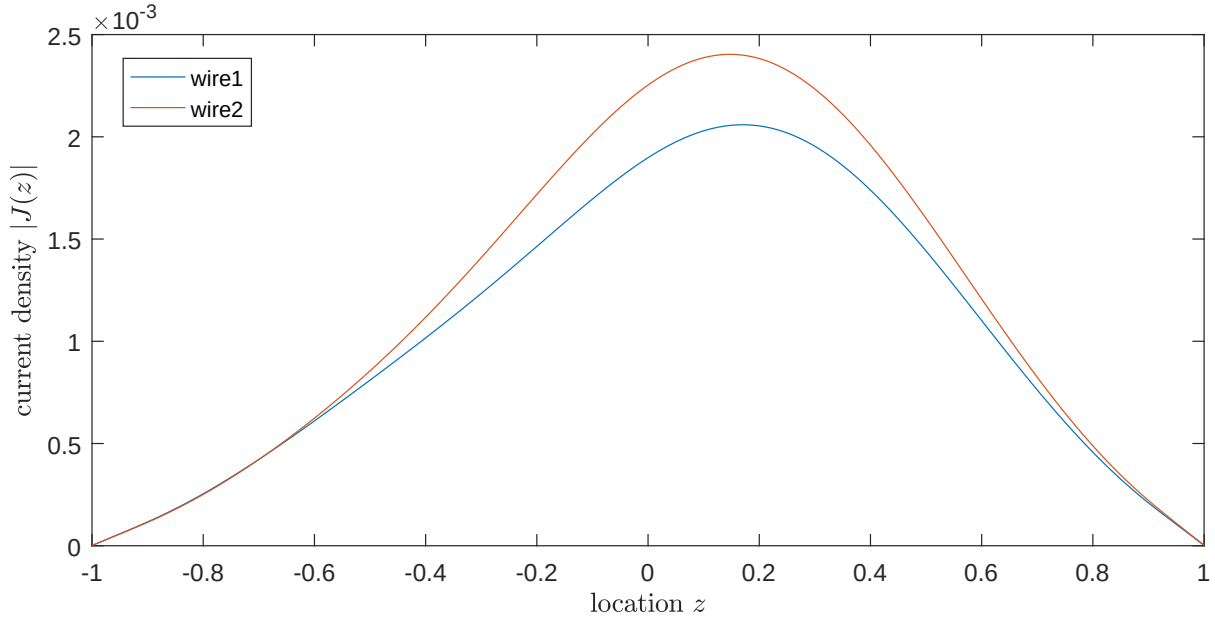

Figure 5.9: Profiles of the current density $J(z)$ for case $f = 100$ MHz and $\delta = 5a$. The data was computed from the reference case $N = 400$, $M_1 = M_2 = M_3 = 2^8$.

N	M_1	M_2	M_3	e_{max}	t_{exe} (s)
20	2^4	2^3	2^3	1.89×10^{-3}	0.02
40	2^4	2^4	2^4	4.17×10^{-5}	0.08
60	2^4	2^4	2^4	3.11×10^{-6}	0.13
80	2^5	2^5	2^5	6.61×10^{-8}	0.38
100	2^5	2^5	2^5	8.86×10^{-9}	0.52
120	2^5	2^5	2^5	5.94×10^{-10}	0.72
140	2^6	2^5	2^5	4.09×10^{-11}	1.31
160	2^6	2^6	2^6	3.88×10^{-12}	2.26
180	2^6	2^6	2^6	1.09×10^{-12}	2.67

Table 5.10: Code parameters, errors and execution times for $f = 100$ MHz and $\delta = 10a$. Errors were computed from reference case $N = 400$, $M_1 = M_2 = M_3 = 2^8$. The splitting parameter for the integration domain decomposition was fixed at $\Delta = 10a$ in all runs.
.

N	M_1	M_2	M_3	e_{max}	t_{exe} (s)
20	2^4	2^3	2^3	1.80×10^{-3}	0.03
40	2^4	2^4	2^4	3.92×10^{-5}	0.09
60	2^4	2^4	2^4	3.65×10^{-6}	0.16
80	2^5	2^5	2^5	6.14×10^{-8}	0.45
100	2^5	2^5	2^5	8.27×10^{-9}	0.56
120	2^5	2^5	2^5	5.59×10^{-10}	0.76
140	2^6	2^5	2^5	3.94×10^{-11}	1.38
160	2^6	2^6	2^6	3.52×10^{-12}	2.29
180	2^6	2^6	2^6	1.31×10^{-12}	2.77

Table 5.11: Code parameters, errors and execution times for $f = 100$ MHz and $\delta = 20a$. Errors were computed from reference case $N = 400$, $M_1 = M_2 = M_3 = 2^8$. The splitting parameter for the integration domain decomposition was fixed at $\Delta = 10a$ in all runs.
.

the two wires may be seen.

Code performance data corresponding to moderate frequency and $\delta = 20a$ is presented in Table 5.11. Again, we note the superalgebraic convergence in the solution for increasing number of Cheyshev modes N retained in the problem. Execution times are also very small, with single precision accuracies achieved in under one half second with $N = 80$ Chebyshev modes. Accuracies nearing double precision are obtained in under three second computing times using $N = 180$ Chebyshev modes. Plots of the current along each wire are shown in Figure 5.11. Both wires are spaced further apart than in the previous case, but there is still substantial interaction between the wires.

Code performance data corresponding to moderate frequency and $\delta = 100a$ is presented in Table 5.12.

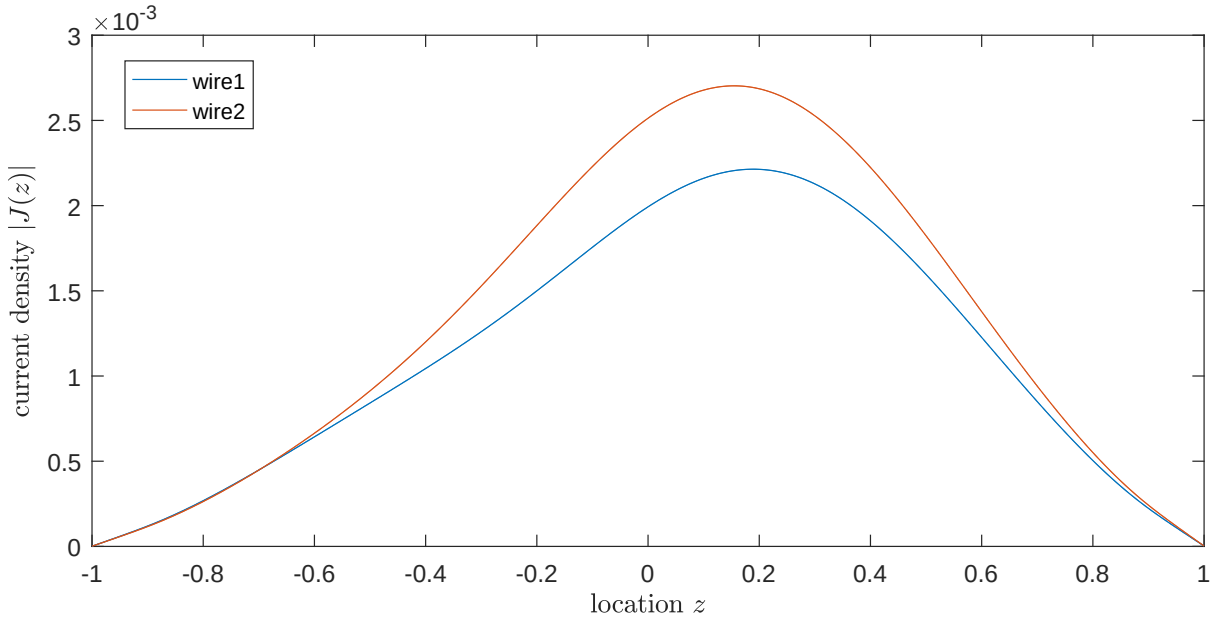

Figure 5.10: Profiles of the current density $J(z)$ for case $f = 100$ MHz and $\delta = 10a$. The data was computed from the reference case $N = 400$, $M_1 = M_2 = M_3 = 2^8$.

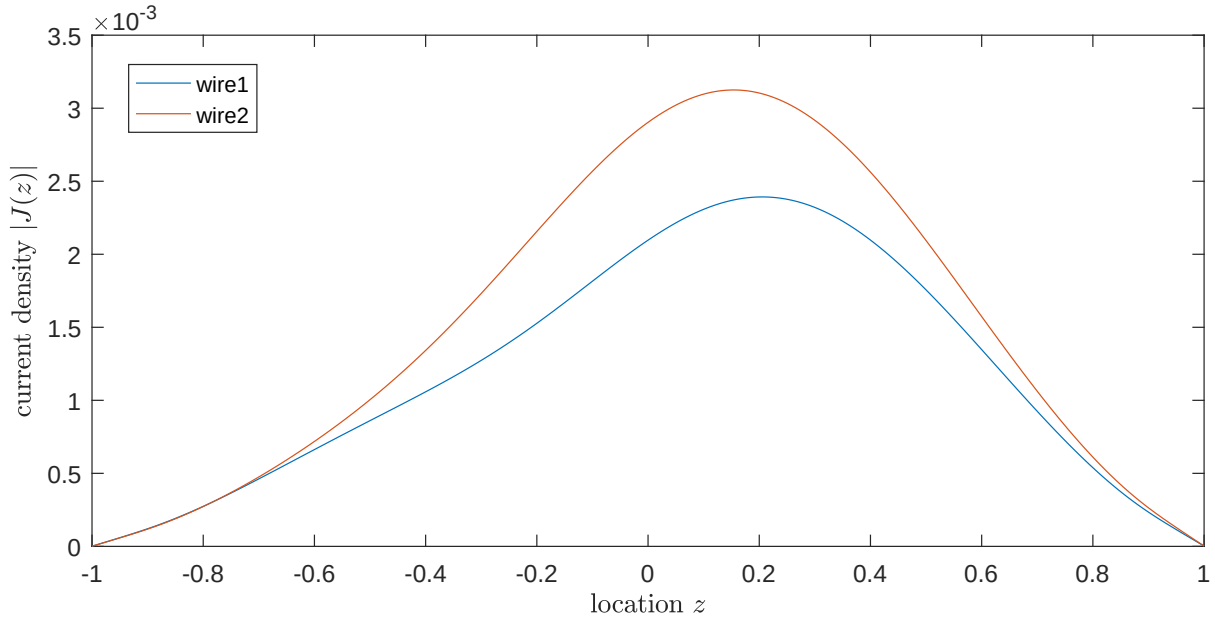

Figure 5.11: Profiles of the current density $J(z)$ for case $f = 100$ MHz and $\delta = 20a$. The data was computed from the reference case $N = 400$, $M_1 = M_2 = M_3 = 2^8$.

N	M_1	M_2	M_3	e_{max}	t_{exe} (s)
20	2^4	2^3	2^3	1.46×10^{-3}	0.04
40	2^4	2^4	2^4	3.18×10^{-5}	0.11
60	2^4	2^4	2^4	4.01×10^{-6}	0.18
80	2^5	2^5	2^5	5.01×10^{-8}	0.51
100	2^5	2^5	2^5	6.72×10^{-9}	0.70
120	2^5	2^5	2^5	4.65×10^{-10}	0.93
140	2^6	2^5	2^5	3.24×10^{-11}	1.65
160	2^6	2^6	2^6	2.84×10^{-12}	2.72
180	2^6	2^6	2^6	1.72×10^{-12}	3.28

Table 5.12: Code parameters, errors and execution times for $f = 100$ MHz and $\delta = 100a$. Errors were computed from reference case $N = 400$, $M_1 = M_2 = M_3 = 2^8$. The splitting parameter for the integration domain decomposition was fixed at $\Delta = 10a$ in all runs.
.

Again, we note the superalgebraic convergence in the solution for increasing number of Cheyshev modes N retained in the problem. Execution times are also very small, with single precision accuracies achieved in one half second with $N = 80$ Chebyshev modes. Accuracies nearing double precision are obtained in under four second computing times using $N = 180$ Chebyshev modes. Plots of the current along each wire are shown in Figure 5.12. Both wires are spaced further apart than in the previous case, but there is still substantial interaction between the wires.

5.4 Discussion

In addition to the very fast (super-algebraic) convergence of the solution in the number of Chebyshev modes N and resulting fast computing times of our algorithm, we have seen some interesting features in the data presented that we would like to discuss. Clearly the current profiles are much simpler at lower frequencies than higher frequencies. In particular, one would expect that many fewer Chebyshev modes are needed to represent the current to high accuracy at lower frequencies. This statement is true to some extent: we see that from all data tables presented solutions at lower frequencies initially converge faster than solutions at higher frequencies (i.e. higher accuracy is obtained with fewer Chebyshev modes). However, we also see that solutions at all frequencies appear to need approximately $N = 180$ Chebyshev modes to resolve about 12 digits in the solution. This means that there are two distinct phases of convergence for these problems: one

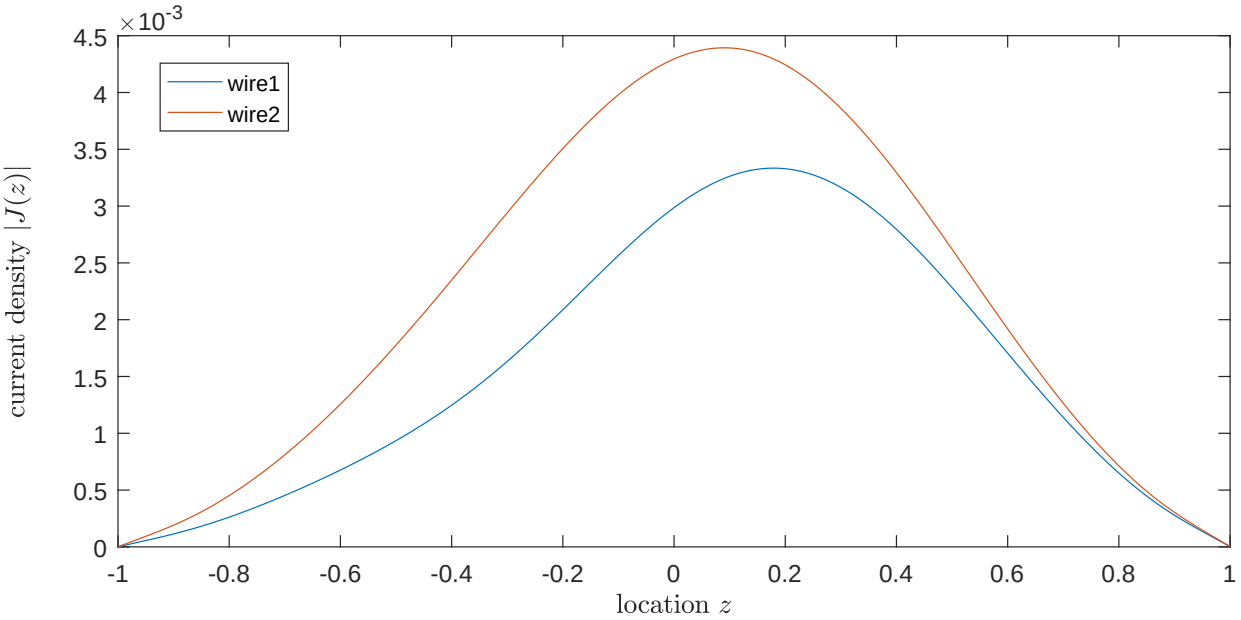

Figure 5.12: Profiles of the current density $J(z)$ for case $f = 100$ MHz and $\delta = 100a$. The data was computed from the reference case $N = 400$, $M_1 = M_2 = M_3 = 2^8$.

initial phase that is governed by the frequency, and a second phase where the convergence in the solution appears to be independent of the frequency. The dependence of the convergence of the solution on the array spacing δ was very weak.

To clearly illustrate our point above, we present three figures showing the decay in the Chebyshev coefficients for the array spacing $\delta = 5a$ and frequencies $f = 1000$ MHz, $f = 500$ MHz and $f = 100$ MHz; these are shown in Figure 5.13, Figure 5.14 and Figure 5.15, respectively. In these figures, it does appear that there are two distinct sets of values of the Chebyshev modes for either the real part or the imaginary of the solution; in fact, what one sees is that the even and odd contributions to the real or imaginary parts may behave differently. What is clear from each one of these figures is that there is indeed an initial phase of convergence which is faster for lower frequency. There is also a secondary phase of convergence common to all frequency cases where the convergence in the solution slows down (but is still super-algebraic) and eventually leads to machine precision accuracies at the same pace for all cases of frequency. A similar phenomenon related to a single wire was reported in [11]. The cause of the slow convergence was speculated to be the

result of a small-weight singularity in the thin-wire solutions located near the origin on the imaginary axis (associated with a corresponding singularity the kernel itself has at $(z - z') = 2ai$).

To discuss this point further, we have produced plots of the error in the solution as a function of the position along the wire in Figure 5.16. In this figure we show the error corresponding to $f = 1000$ MHz and $\delta = 5a$ as an illustrative example; similar results are seen for all other physical cases examined in this work. The figure indicates that as the number of Chebyshev modes is refined from $N = 40$ to $N = 100$ to $N = 180$, the maximum errors in the solution concentrate near the endpoints of the wire.

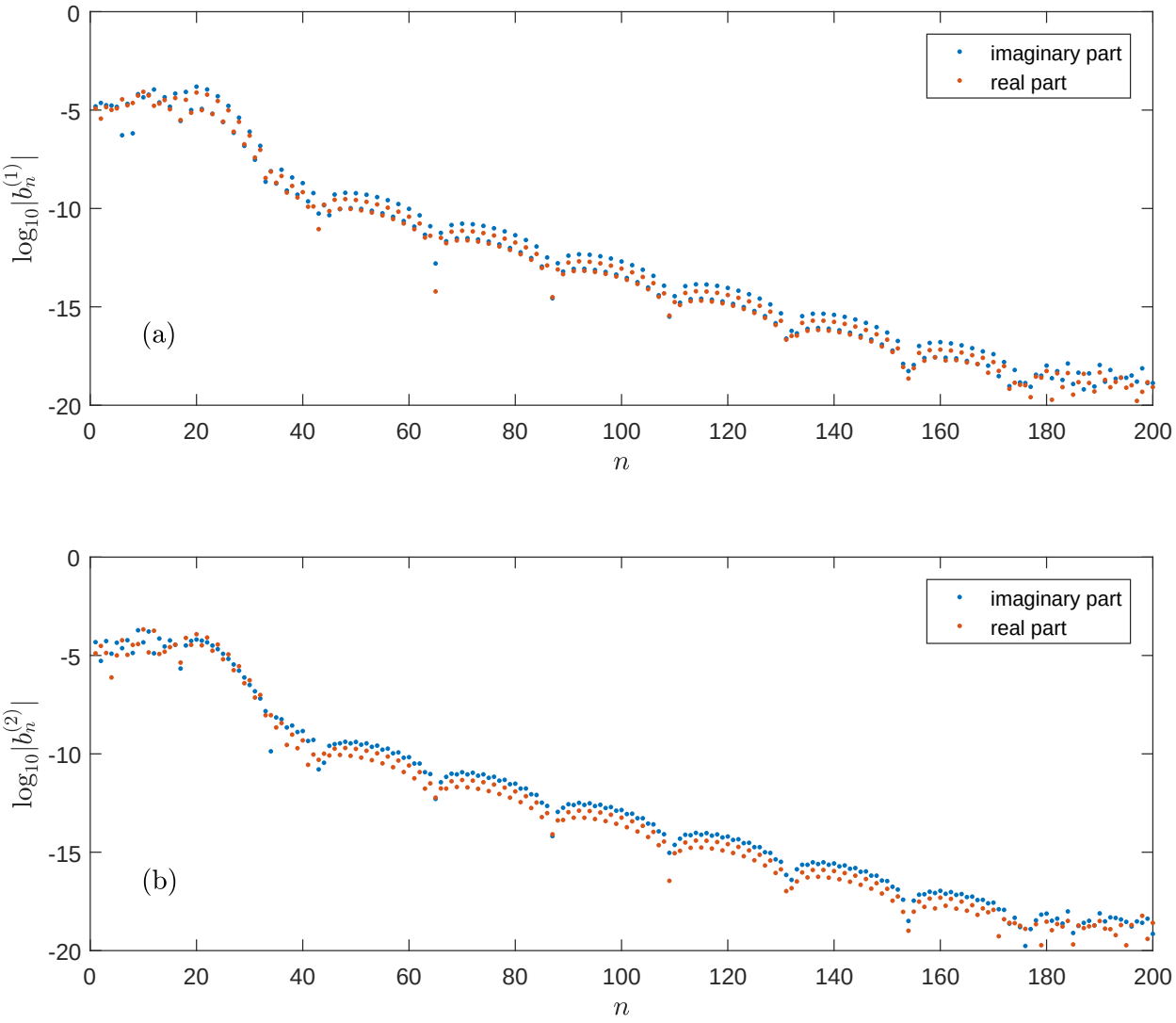

Figure 5.13: Chebyshev series coefficients for $f = 1000$ MHz, $\delta = 5a$ computed using $N = 200$ and $M_1 = M_2 = M_3 = 2^9$.

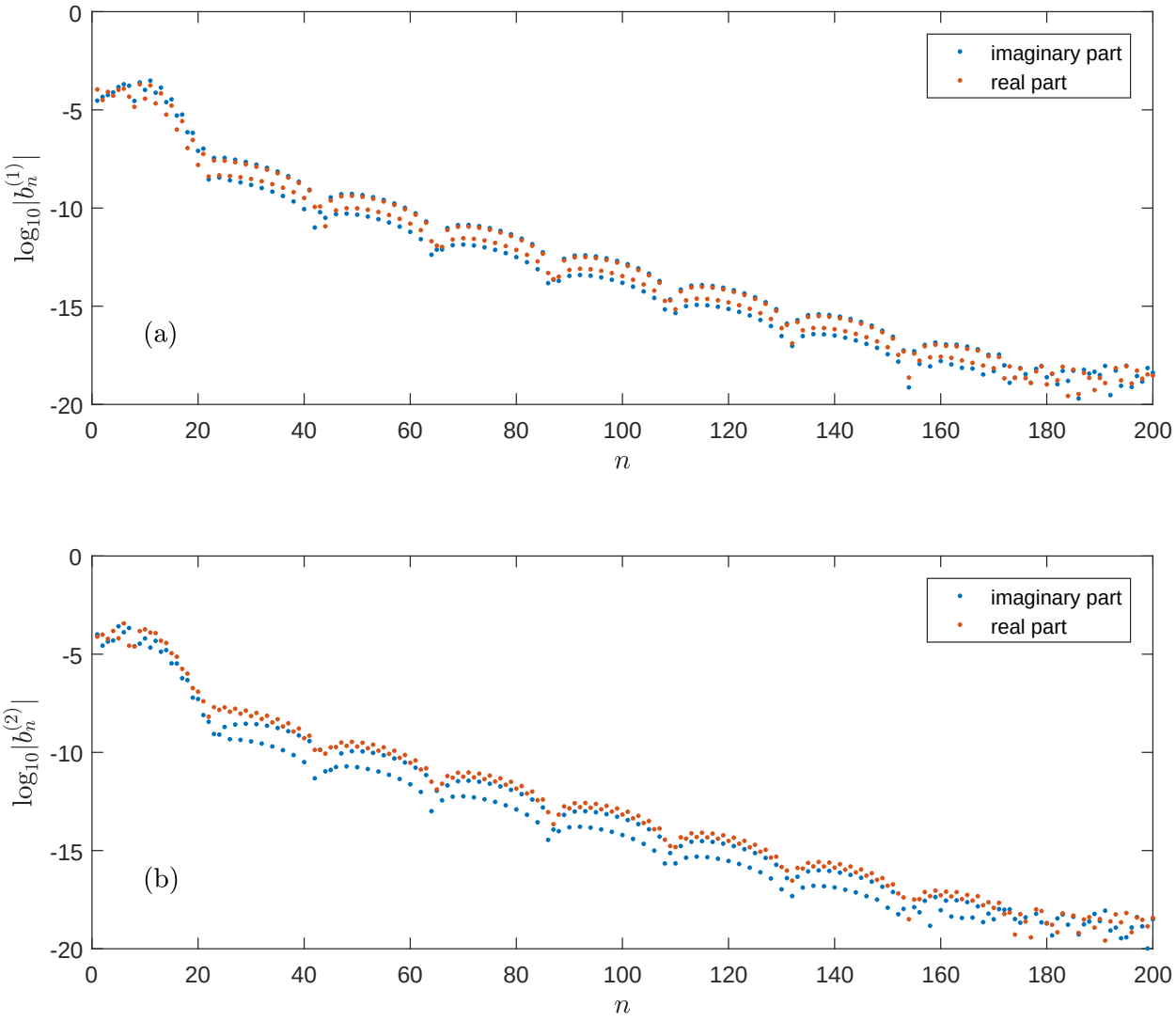

Figure 5.14: Chebyshev series coefficients for $f = 500$ MHz, $\delta = 5a$ computed using $N = 200$ and $M_1 = M_2 = M_3 = 2^8$.

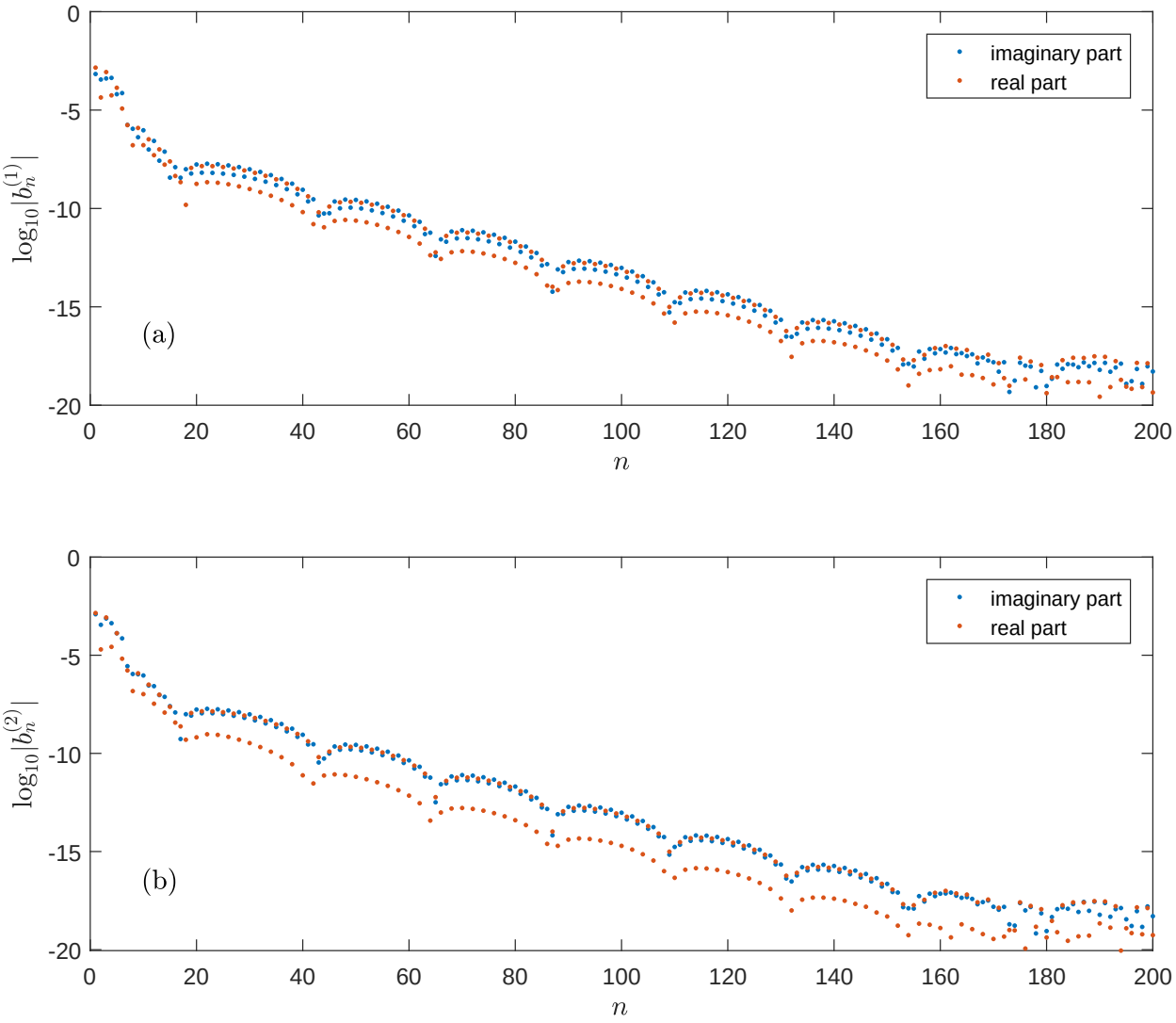

Figure 5.15: Chebyshev series coefficients for $f = 100$ MHz, $\delta = 5a$ computed using $N = 200$ and $M_1 = M_2 = M_3 = 2^8$.

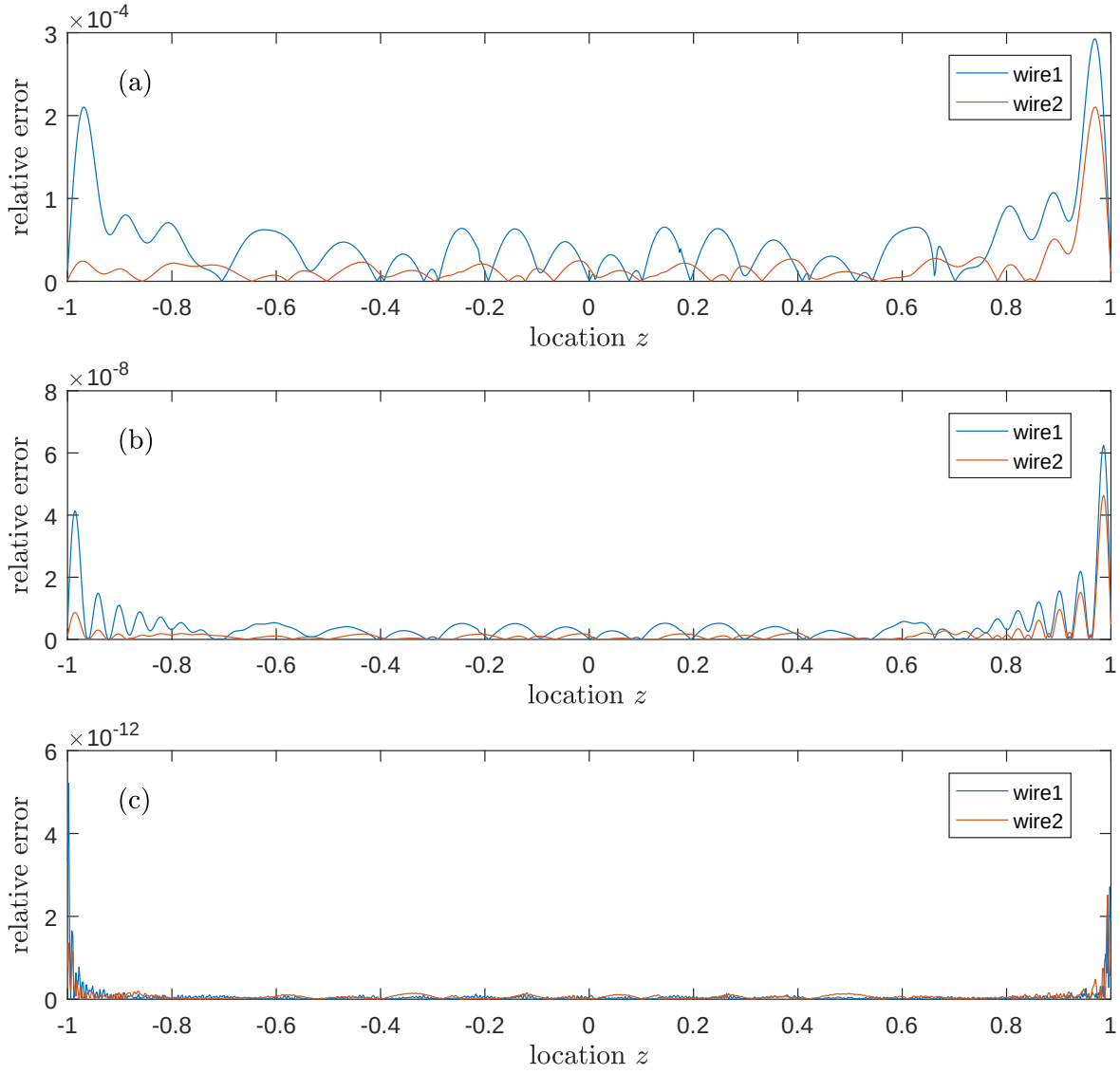

Figure 5.16: Error plots corresponding to case $f = 1000$ MHz, $\delta = 5a$. The data for these plots were computed using $M_1 = M_2 = M_3 = 2^9$ in all cases. The number of Chebyshev modes used for each of the plots was as follows: (a) $N = 40$; (b) $N = 100$; (c) $N = 180$.

6 Conclusions and Future Work

This thesis presents an efficient high order solver to compute the electromagnetic response of an array of parallel straight wires to an incident plane wave. The numerical results presented in Chapter 5 clearly indicate that the solution converges super-algebraically in the number of unknowns retained in the Chebyshev expansion of the the reduced current $I(z)$ on each wire of the array. The code is also extremely fast to execute typically solutions with singe-precision accuracies for the currents are produced in a fraction of a second.

Our solver is enabled by specialized numerical integration techniques which themselves converge super-algebraically in the number of sampling points used, and explicitly treat the case of logarithmically singular integrands. The mathematical basis enabling the numerical integration routines is a new set of quadrature formulas that we derive in this thesis for the first time. We derived quadrature formulas applicable to the cases when the logarithmic singularity lies on the edge of the integration domain, or slightly beyond it. In the former case, our formulas were shown to be an improvement of what was previously available in the literature, Specifically, in reference [11], the same integration weights were produced by an ill-conditioned formula that required symbolic software for accurate evaluation of the quantities (which were subsequently stored in a file to be read in each run). Those same integration weights can now be easily evaluated to full precision using explicit formulas we present. In the case where the logarithmic singularity lies slightly outside the integration domain, we did run into some difficulties. The formulas for the quadrature weights in this case turned out to be very ill-conditioned as a result of a subtractive cancelation. While we still believe this difficulty can be resolved with careful study of the problem as we currently have it formulated.

One improvement that we can easily make to the current implementation is as follows. We note that

for larger array spacings, our quadrature methods were will applying localized integration around the point parametric location $s = s'$ where a near singularity should occur. Our numerical results indicated that the used of such routines were generally not needed for wire spacings greater than 20 radii, at least at moderate and high frequencies. In these cases, the required functions $A_n^{(i,j)}$ for $i \neq j$ in equation (4.1) could be computed for all required indices n simultaneously using a fast cosine transform if the integrand function $\Phi_{i,j}$ is treated as a smooth function, which it is in this case. This simple step may well improve the computing times for larger array spacings by up to 50 percent.

One more difficult improvement to the code would be to allow for non-parallel wires. This is non-trivial since it requires one to first minimize the function $||\mathbf{r}(s) - \mathbf{r}(s')||$ in the two-dimensional parameter space consisting of the square with edges ± 1 in order to determine when to apply our specialized quadrature routines for each different observation point $\mathbf{r}(s)$ considered. The integration routines would need to be generalized to accept more parameters describing the different spatial locations of the wires.

Bibliography

[1] J.A. Kong, *Electromagnetic Wave Theory*, 2nd Ed., Wiley-Interscience, New York, 1990.

[2] J.D. Jackson, *Classical Electrodynamics*, 3rd Ed., Wiley, New York, 1998.

[3] J.A. Stratton, *Electromagnetic Theory*, McGraw-Hill, New York, 1941.

[4] A. Ishimaru, *Electromagnetic Wave Propagation, Radiation, and Scattering*, Prentice-Hall, Englewood Cliffs, 1991.

[5] B.B. Baker and E.T. Copson. *The Mathematical Theory of Huygen's Principle*, 2nd Ed., Clarendon Press, Oxford, 1953.

[6] D.N. Pattanayak and E. Wolf. General form and a new interpretaion of the Ewald-Oseen extinction theorem. *Optics Communications* **6**: 217-220, 1972.

[7] C.-T. Tai. *Dyadic Green's Functions in Electromagnetic Theory*, 2nd Ed., IEEE Press, New York, 1994.

[8] H.C. Pocklington. Electrical oscillations in wires. *Proc. Cambridge Phil. Soc.*, 9:324–332, 1897.

[9] R.W.P. King, *The theory of linear antennas : with charts and tables for practical applications*, Harvard University Press, Cambridge Mass., 1956.

[10] P.J. Davies, D.B. Duncan, and S.A. Funken. Accurate and efficient algorithms for frequency domain scattering from a thin wire. *J. Comput. Phys.*, 168(1):155–183, 2001.

[11] O.P. Bruno and M.C. Haslam. Regularity theory and super-algebraic solvers for wire antenna problems. *SIAM Journal on Scientific Computing*, **29**(4): 1375-1402, 2007.

[12] T. T. Wu. *Introduction to linear antennas.* Inter-University Electronics Series. McGraw-Hill, New York, 1969. In: Antenna Theory Part I. Ed. R.E. Collin and F.J. Zucker.

[13] C.A. Balanis *Antenna Theory: Analysis and Design.* Second Ed., Wiley 1997.

[14] Poggio, A.J. and Miller, E.K., Integral equation solutions of three-dimensional scattering problems. In: Computer Techniques for Electromagnetics, R. Mittra, Ed. Pergamon, 1973.

[15] K.K. Mei. On the integral equation of thin wire antennas. *IEEE Trans. Antennas Propagat.*, AP-13(3):374–378, 1965.

[16] E. Hallén, *Exact treatment of antenna current wave reflection at the end of a tube-shaped cylindrical antenna*, IRE Trans. Antennas Propagation AP-4(3) (1956), pp. 479–491.

[17] D.S. Jones Note on the integral equation for a straight wire antenna. *Proc. IEE-H* **128**(2): 114–116, 1981.

[18] J.C. Mason and D.C. Handscomb. *Chebyshev polynomials.* Chapman & Hall/CRC, Boca Raton, FL, 2003.

[19] T.J. Rivlin. *Chebyshev Polynomials: From Approximation Theory to Algebra and Number Theory.* Pure and Applied Mathematics. John Wiley & Sons Inc., New York, second edition, 1990.

[20] W.H. Press, S.A. Teukolsky, W.T. Vetterling and B.P. Flannery, *Numerical Recipes: The Art of Scientific Computing*, Volume 1, Second Ed., Cambridge University Press, 1992.

[21] D. Colton and R. Kress. *Integral Equation Methods in Scattering Theory.* Wiley-Interscience, New York, 1983.

[22] I. S. Gradshteyn and I. M. Ryzhik. *Table of integrals, series, and products.* Academic Press, San Diego, CA, seventh edition, 2007.

[23] A. Erdélyi, W. Magnus, F. Oberhettinger and F. Tricomi. *Higher Transcendental Functions*, Volume I. McGraw-Hill, New York, 1953.

[24] E.K. Miller. A selective survey of computational electromagnetics. *IEEE Trans Antennas Prop* **36**: 1281-1305, 1988.

[25] L. Tsang, J.A. Kong and K.-H. Ding. *Scattering of Electromagnetic Waves: Theories and Applications* Wiley Interscience, New York, 2000.

[26] L. Tsang, J.A. Kong, K.-H. Ding and C.O. Ao. *Scattering of Electromagnetic Waves: Numerical Simulations.* Wiley Interscience, New York, 2001.

[27] H.M. Srivastava and H.L. Manocha. *A Treatise on Generating Functions.* Halsted Press, New York, 1984.

[28] A. Tucker. *Applied Combinatorics..* Third Edition. Wiley, New York, 1995.

[29] M. Abramowitz and I.A. Stegun, eds., *Handbook of mathematical functions with formulas, graphs, and mathematical tables*, Dover Publications Inc., New York, 1992. Reprint of the 1972 edition.

[30] `http://www.fftw.org/`

[31] C.M. Butler and D.R. Wilton. Analysis of various numerical techniques applied to thin-wire scatterers. *IEEE Trans. Antennas Propagat.*, AP-23(4):534–540, 1975.

[32] N. J. Champagne, D. R. Wilton, and J. D. Rockway, *The analysis of thin wires using higher order elements and basis functions*, IEEE Trans. Antennas Propagat. **54**(12):3815–3821, 2006.

[33] G. Fikioris, *The approximate integral equation for a cylindrical scatterer has no solution*, J. of Electromagn. Waves and Appl. **15**(9): 1153-1159, 2001.

[34] B.P. Rynne, *The well-posedness of the integral equations for thin wire antennas*, IMA J. Appl. Math., 49 (1992), pp. 35–44.

[35] Byrd, P.F., Friedman, M.D., *Handbook of Elliptic Integrals for Engineers and Scientists*, 2nd Ed., Revised, Springer-Verlag, New York, 1971.

[36] L.W. Pearson. A Separation of the logarithmic singularity in the exact kernel of the cylindrical antenna integral equation. *IEEE Trans. Antennas Propagat.*, AP-23(2):256–258, 1975.